

Electronic Thesis and Dissertation Repository

10-30-2019 10:00 AM

Action potential subpopulations in human muscle sympathetic nerve activity: discharge properties and governing mechanisms

Stephen A. Klassen
The University of Western Ontario

Supervisor
Shoemaker, J. Kevin
The University of Western Ontario

Graduate Program in Kinesiology
A thesis submitted in partial fulfillment of the requirements for the degree in Doctor of Philosophy
© Stephen A. Klassen 2019

Follow this and additional works at: <https://ir.lib.uwo.ca/etd>



Part of the [Systems and Integrative Physiology Commons](#)

Recommended Citation

Klassen, Stephen A., "Action potential subpopulations in human muscle sympathetic nerve activity: discharge properties and governing mechanisms" (2019). *Electronic Thesis and Dissertation Repository*. 6624.

<https://ir.lib.uwo.ca/etd/6624>

This Dissertation/Thesis is brought to you for free and open access by Scholarship@Western. It has been accepted for inclusion in Electronic Thesis and Dissertation Repository by an authorized administrator of Scholarship@Western. For more information, please contact wlsadmin@uwo.ca.

Abstract

What discharge properties are expressed by varying-sized sympathetic action potential (AP) subpopulations active under baseline conditions in humans and what are the governing mechanisms? To address this overall question the microneurographic approach was employed to record multi-unit muscle sympathetic nerve activity (MSNA), after which a continuous wavelet transform exposed APs in the recorded neurogram. *Study One* examined the role of the paravertebral ganglia on sympathetic neural discharge patterns. Through trimethaphan infusion under baseline conditions, this study revealed ordered de-recruitment of larger to smaller AP clusters, suggesting that the paravertebral ganglia contribute to the distribution of firing probabilities expressed by differently-sized sympathetic APs. However, the smallest APs were resistant to trimethaphan, suggesting non-nicotinic mechanisms contribute to ganglionic neurotransmission of this specific subpopulation of axons. *Study Two* investigated the synchronization of APs within the cardiac cycle and the role played by the paravertebral ganglia in this process. We observed that under baseline conditions ~30% of total sympathetic APs fired asynchronously between bursts of MSNA and asynchronous discharge frequency was not affected by baroreflex or apneic stress. Thus, asynchronous AP discharge represents a fundamental behaviour within human MSNA. Also, retrospective analysis of asynchronous AP data from Study One demonstrated that non-nicotinic ganglionic mechanisms contributed to some, but not all asynchronous AP discharge. *Study Three* probed the heterogeneity of baroreflex control over the discharge of AP subpopulations. Under baseline conditions, we found a subpopulation of medium-sized APs to express the greatest baroreflex gain, while the smallest and largest APs exhibited minimal baroreflex regulation. During baroreflex stress imposed by lower body negative pressure, the

sympathetic system increases total MSNA by resetting baroreflex control of medium APs to higher levels of activity and increasing the gain to facilitate augmented firing along with recruiting a subpopulation of previously silent larger APs. Overall, these studies provide new knowledge regarding the complex discharge patterns expressed by subpopulations of varying-sized sympathetic APs active at baseline, of which some express augmented firing during baroreflex stress. We also provide insight to the baroreflex and ganglionic mechanisms governing the discharge of these AP subpopulations.

Keywords

action potential; arterial baroreflex; baroreflex gain; microneurography; muscle sympathetic nerve activity; paravertebral ganglia; sympathetic communication strategies; sympathetic nervous system; trimethaphan

Summary for Lay Audience

For humans to survive, blood pressure must be maintained within an optimal range and oxygenated blood flow must be delivered to vital organs such as the brain and the heart. Part of the brain known as the sympathetic nervous system ensures these conditions by sending precise messages along the nerves to communicate with the heart and blood vessels. These messages are made up of electrical signals called action potentials. During periods of stress that change our blood pressure and blood flow — such as the fall in blood pressure that occurs when we stand — the brain changes the message sent to the heart and blood vessels by adjusting the size, number, and timing of action potentials. This message tells the blood vessels to constrict and the heart to beat faster, which increase blood pressure and ensures blood flow to vital organs. This dissertation provided new information regarding the action potential messages used by the sympathetic nervous system to communicate with the blood vessels and identified parts of our nervous system that are important for shaping these messages.

Co-Authorship Statement

Stephen A. Klassen was the first author and J. Kevin Shoemaker was the senior author on all manuscripts. Michael J. Joyner was the co-senior author on Study One. Jacqueline K. Limberg, Sarah E. Baker, Wayne T. Nicholson, and Timothy B. Curry co-authored Study One. M. Erin Moir, Jacqueline K. Limberg, Sarah E. Baker, Wayne T. Nicholson, Timothy B. Curry, and Michael J. Joyner co-authored Study Two. M. Erin Moir co-authored Study Three.

Conception and design: S.A.K., J.K.S., J.K.L., T.B.C., M.J.J.

Data collection: S.A.K., J.K.S., M.E.M., J.K.L., S.E.B.

Data analysis and interpretation: S.A.K., J.K.S., M.E.M., J.K.L., S.E.B., W.T.N., T.B.C., M.J.J.

Manuscript drafting, figures, and revisions: S.A.K. with feedback from all co-authors.

Acknowledgments

We express our sincere thanks to Arlene Fleischhauer and Brad Matuszewski of the Laboratory for Brain and Heart Health/Neurovascular Research Laboratory at Western University for providing administrative and technical support, respectively, in Study One, Study Two, and Study Three.

We gratefully acknowledge the technical, administrative, and clinical support provided by the following research personnel of the Human Integrative Physiology Laboratory at Mayo Clinic (Rochester, MN): Shelly Roberts, Sarah Wolhart, Nancy Meyer, Pam Engrav, Christopher Johnson, Andrew Miller, Zachariah Scruggs, Lauren Newhouse, Gabrielle Dillion, and Humphrey Petersen-Jones. Data collected at Mayo Clinic contributed to Study One and Study Two.

Dedication

Dedicated to Marjorie May Secord.

A big thank you and lots of love to Mom, Dad, Dave, Christine, Ryan, and Callie.

Table of Contents

Abstract.....	ii
Summary for Lay Audience.....	v
Co-Authorship Statement.....	vi
Acknowledgments.....	vii
Dedication.....	viii
Table of Contents.....	ix
List of Tables.....	xiii
List of Figures.....	xiv
List of Abbreviations.....	xv
Chapter 1.....	1
1 Introduction.....	1
1.1 Sympathetic Nervous System.....	4
1.2 Sympathetic Neurocircuitry.....	6
1.2.1 The Baroreflex.....	6
1.2.2 Non-Baroreflex Sympathetic Neurocircuitry.....	8
1.2.3 Sympathetic Preganglionic Neurons.....	10
1.2.4 The Paravertebral Ganglia.....	12
1.2.4.1 Postganglionic Nicotinic Blockade: Trimethaphan.....	15
1.2.5 Sympathetic Postganglionic Neurons.....	15
1.3 The Action Potential.....	17
1.4 Muscle Sympathetic Nerve Activity.....	18
1.4.1 Baroreflex Control of Muscle Sympathetic Nerve Activity.....	28
1.5 Integrated Rationale.....	30
1.6 References.....	34

Chapter 2.....	45
2 The role of the paravertebral ganglia in human sympathetic neural discharge patterns	45
2.1 Introduction.....	45
2.2 Methods.....	47
2.2.1 Ethical Approval.....	47
2.2.2 Participants.....	47
2.2.3 Experimental Procedures	48
2.2.4 Experimental Design.....	48
2.2.5 Experimental Measures and Analysis.....	49
2.2.6 Statistical Analysis.....	51
2.3 Results.....	52
2.4 Discussion.....	65
2.4.1 Conclusion	71
2.5 References.....	72
Chapter 3.....	77
3 Asynchronous action potential discharge in human muscle sympathetic nerve activity	77
3.1 Introduction.....	77
3.2 Methods.....	79
3.2.1 Ethical Approval.....	79
3.2.2 Participants.....	79
3.2.3 Experimental Procedures	79
3.2.4 Experimental Design.....	80
3.2.5 Experimental Measures and Analysis.....	81
3.2.6 Statistical Analysis.....	84
3.3 Results.....	85

3.4 Discussion.....	99
3.4.1 Conclusion	104
3.5 References.....	105
Chapter 4.....	109
4 Baroreflex control of sympathetic action potential subpopulations during orthostatic stress.....	109
4.1 Introduction.....	109
4.2 Methods.....	110
4.2.1 Ethical Approval	110
4.2.2 Sample.....	111
4.2.3 Experimental Procedures and Protocol.....	111
4.2.4 Experimental Measures and Analysis.....	112
4.2.5 Integrated baroreflex threshold and sensitivity.....	114
4.2.6 Action potential baroreflex threshold and sensitivity.....	115
4.2.7 Statistical Analysis.....	115
4.3 Results.....	116
4.4 Discussion.....	127
4.4.1 Conclusion	132
4.5 References.....	133
Chapter 5.....	137
5 General Discussion	137
5.1 Perspectives.....	141
5.2 Conclusion	142
5.3 References.....	144
Appendix: Ethics Approval.....	147
Appendix: Manuscript Permissions	151

Curriculum Vitae 153

List of Tables

Table 3.1	91
Table 4.1	119

List of Figures

Figure 1.1	22
Figure 1.2	26
Figure 2.1	57
Figure 2.2	58
Figure 2.3	59
Figure 2.4	60
Figure 2.5	61
Figure 2.6	63
Figure 2.7	64
Figure 3.1	92
Figure 3.2	93
Figure 3.3	94
Figure 3.4	95
Figure 3.5	96
Figure 3.6	97
Figure 3.7	98
Figure 4.1	120
Figure 4.2	121
Figure 4.3	123
Figure 4.4	124
Figure 4.5	125
Figure 4.6	126

List of Abbreviations

ACh, acetylcholine

AP, action potential

ATP, adenosine triphosphate

α_1 R, alpha-1 adrenergic receptor

α_2 R, alpha-2 adrenergic receptor

APN, apnea

BSL, baseline

BOLD, blood oxygen level dependent

BP, blood pressure

CVLM, caudal ventrolateral medulla

Cl⁻, chloride ion

cAMP, cyclic adenosine monophosphate

ECG, electrocardiogram

EPSP, excitatory postsynaptic potential

GABA, gamma (γ)-aminobutyric acid

HR, heart rate

IP₃, inositol 1,4,5-triphosphate

LBNP, lower body negative pressure

MAP, mean arterial pressure

MSNA, muscle sympathetic nerve activity

NPY, neuropeptide Y

NE, norepinephrine

NTS, nucleus tractus solitarius

PVN, periventricular nucleus

K⁺, potassium ion

RM ANOVA, repeated measures analysis of variance

RVLM, rostral ventrolateral medulla

SNR, signal-to-noise ratio

Na⁺, sodium ion

Chapter 1

1 Introduction

Critical to homeostasis and human survival are the sympathetic messages coordinating circulatory responses to physiological stress (106, 131). These efferent messages result from the integration of feedback signals arising from peripheral receptors and feedforward signals generated centrally into a network of supraspinal nuclei, with further processing by spinal circuits and the paravertebral ganglia (28, 37, 42, 78). Pioneered by Hagbarth and Vallbo in 1968 (49), microneurography provides direct access to the discharge patterns of the population of postganglionic c-fibres innervating the vasculature supplying skeletal muscle in humans — muscle sympathetic nerve activity (MSNA). Due to the low signal-to-noise ratio, early investigations relied on the integrated signal to uncover the fundamental behaviours contained within MSNA: spontaneous bursts of activity expressing time-varying frequency and amplitude (26, 49).

It was not until recent advances in recording techniques and signal processing that the action potentials (AP) underlying the integrated bursts were revealed (81, 98). Among low-threshold APs that are synchronized into bursts under baseline conditions, multiple size-related subpopulations exist, expressing heterogeneous discharge probabilities: medium APs fire within most bursts, while the small and large APs express low within-burst probabilities (110). While burst frequency stems from the quantity of baroreflex-gated periods of synchronized AP discharge, burst size depends on the number and size of synchronized APs (79, 101, 110). To increase total MSNA during physiological stress, the sympathetic system increases the activity of low-threshold APs (79) and recruits a

subpopulation of previously-silent larger and faster conducting APs (6). Thus, low-threshold APs are essential for communicating circulatory adjustments necessary for homeostatic maintenance during baseline conditions and physiological perturbations. However, the discharge properties expressed by subpopulations of low-threshold APs remain incompletely understood and the mechanisms contributing to both differential firing among variously-sized APs under baseline conditions and the increase in emissions during physiological stress remain unclear. Therefore, the **overall objective** of the present dissertation was to investigate the behaviour and governing mechanisms of the low-threshold (i.e., active at baseline) sympathetic AP subpopulations. This dissertation tested the **overall hypothesis** that heterogeneous discharge behaviour exists among varying-sized low-threshold AP subpopulations under baseline conditions and during physiological stress, due to differing regulation within the sympathetic organization. Specific hypotheses tested in this dissertation are as follows:

Study One

The role of the paravertebral ganglia in human sympathetic neural discharge patterns

Tested the hypothesis that the paravertebral ganglia contribute to the discharge behaviours expressed by sympathetic APs active at baseline in humans.

Study Two

Asynchronous action potential discharge within human muscle sympathetic nerve activity

Tested the hypothesis that synchronous and asynchronous discharge exist among sympathetic APs and the ganglia affect AP synchronicity.

Study Three

Baroreflex control of sympathetic action potential subpopulations during orthostatic stress

Tested the hypothesis that during orthostatic stress the baroreflex confers its greatest effect on the gain of medium AP clusters that fire normally with high probability. If so, then the change in position and slope of each AP cluster's baroreflex curve should vary across the distribution of recorded APs.

1.1 Sympathetic Nervous System

The sympathetic nervous system, a division of the autonomic nervous system, maintains homeostasis and supports survival by communicating integrative physiological responses to both spontaneous and stress-imposed deviations in blood pressure and blood flow (17, 24). Key to homeostatic maintenance are rapid alterations in sympathetic discharge destined for the heart and vasculature that enable modifications in cardiac output and vascular resistance (104, 131). While anticipatory feedforward adjustments participate in circulatory regulation, negative feedback circuits represent the critical element underlying short-term sympathetic regulation and circulatory homeostasis (44). According to the homeostat model (44), peripheral receptors initiate feedback reflexes as they ‘monitor’ the internal environment, relaying information centrally regarding blood pressure and volume, the chemical environments of the blood and muscle, and lung stretch, among other signals (37). A network of central nuclei establishes a ‘set-point’ for each physiological variable, such that when sensory nerves communicate a deviation from this level the system adjusts sympathetic outflow to modify effector organ function appropriately to correct the error (44). As such, sympathetic messages directed towards the circulation are goal-oriented and graded to the level of stress (106).

Even the earliest views of integrated physiology predicted that the neural organization of complex organisms reflexively maintain vital properties of the internal environment or *milieu intérieur* in response to the “*colossal forces, often adverse*”, surrounding the body (17). As an example, while not *apparently* colossal, even the gravitational force experienced during standing imposes a redistribution of 500 to 1,000 mL of venous blood to the lower body, primarily in the abdominal cavity and buttocks, that if not

compensated for results in loss of consciousness subsequent to compromised cardiac output, hypotension, and reduced cerebral perfusion (107). However, in a healthy system, reductions in the distension of baroreceptor harbouring vessels linked to falling blood pressure withdraw baroreflex-mediated sympathoinhibition to increase sympathetic outflow to the heart and vasculature (104). Along with the concurrent parasympathetic response, enhanced sympathetic discharge elevates cardiac output by increasing heart rate and myocardial contractile force (12). Simultaneously, elevated sympathetic drive increases vascular resistance to augment blood pressure and venous return by limiting peripheral blood flow (12). Nonetheless, the contemporary understanding of neurocirculatory homeostasis appreciates rhythmic oscillations, in blood pressure for example, produced by an interaction of feedback pathways, even in supine resting conditions (63).

Alteration of sympathetic regulatory mechanisms produces chronically elevated sympathetic outflow which relates to a host of cardiovascular pathologies. Sympathetic outflow directed towards skeletal muscle vasculature (i.e., MSNA) increases with age (116) and while no relationship exists between baseline MSNA and mean arterial pressure in young individuals, these variables express a positive association from about middle-age onwards (87). Accordingly, middle-aged and elderly patients with hypertension commonly display elevated MSNA (46). Interestingly, younger individuals diagnosed with essential hypertension also express high sympathetic activity (46) suggesting deteriorations in the mechanisms buffering MSNA and blood pressure [e.g., inverse relationships between MSNA and cardiac output/vasoconstrictor responsiveness (19, 20)] in normotensive counterparts. Also, consistently elevated MSNA associates

with heart failure (73), coronary artery disease (4), obstructive sleep apnea (108), chronic renal failure (47), and metabolic syndrome (56) among other conditions (46, 104). Thus, despite being an integral component of homeostatic maintenance, deterioration of sympathetic feedback pathways or allostatic modifications shifting the feedback reflex to a new set-point, adversely affects overall health (43).

1.2 Sympathetic Neurocircuitry

The sympathetic neural messages ultimately communicating the appropriate circulatory responses to physiological stress are a product of the central and peripheral organization of the sympathetic nervous system (59). Because the arterial baroreflex has received the bulk of research attention (12, 23), the impact of each nuclei comprising this pathway on sympathetic discharge is established. However, many non-baroreflex processes (and neural behaviours) also warrant discussion as they exist within the sympathetic organization and shape sympathetic outflow (112). The following discourse provides a non-exhaustive overview of the neural architecture of the sympathetic nervous system.

1.2.1 The Baroreflex

Baroreflex regulation of sympathetic and parasympathetic activity ensures maintenance of blood pressure within an optimal narrow range. Two divisions of the baroreflex exist: 1) the arterial (or high-pressure) baroreflex, which relies on baroreceptors located in the carotid sinuses and aortic arch to signal blood pressure changes to the brain; and 2) the cardiopulmonary (or low-pressure) baroreflex, initiated by baroreceptors in the right atrium and ventricle along with pulmonary vessels communicating blood volume and cardiac filling pressures (32, 37). Dispersions in transmural pressure evoking tissue

stretch alter the firing rate of mechanosensitive baroreceptors (58). Overall, the baroreflex ensures negative-feedback such that increased transmural pressure within baroreceptor-harboring regions modulates sympathetic outflow and augments parasympathetic discharge. These neural changes increase total peripheral resistance and cardiac output sufficiently to maintain mean arterial pressure during orthostatic stress, with alterations in resistance representing the primary mechanism (32). Briefly, the fundamental baroreflex neurocircuitry in the brainstem relies on the nucleus tractus solitarius (NTS) which in the pathway subserving parasympathetic regulation, NTS neurons send excitatory projections (releasing glutamate) to the preganglionic parasympathetic neurons in the nucleus ambiguus and the dorsal motor nucleus. In the pathways subserving sympathetic regulation the NTS sends excitatory projections to caudal ventrolateral medulla (CVLM) neurons, which in turn, send inhibitory signals (releasing γ -amino butyric acid; GABA) to pre-sympathetic neurons within the rostral ventrolateral medulla (RVLM) (12, 109). This neural pathway has received the majority of research attention and while it strongly shapes sympathetic discharge behaviour, it does not represent the entirety of the central sympathetic circuitry (8, 23, 105).

The baroreflex primarily defends blood pressure during standing (and as reviewed elsewhere (86, 95), during physical exercise), but in the laboratory orthostatic stress may be imposed by Valsalva's Manoeuvre, head-up tilt, pharmacological infusions (e.g., sodium nitroprusside), or lower body negative pressure (LBNP) (89). LBNP enables investigators to titrate the degree of orthostatic stress, unload all baroreceptor populations, and prevents participant movement, enabling simultaneous microneurographic recordings under closed-loop conditions (89). Once investigators

secure the participant's lower body within an air-tight chamber, chamber decompression to sub-atmospheric pressures induces a redistribution of blood from central regions (i.e., abdomen and thorax) to the venous system of the lower body (i.e., splanchnic circulation, buttocks, thighs, and legs) (136). The magnitude of venous pooling scales to LBNP magnitude. Mild LBNP (e.g., ≤ -20 mmHg) evokes venous pooling sufficient to reduce central venous pressure and unload cardiopulmonary baroreceptors, with negligible impact on stroke volume and cardiac output, leaving arterial baroreceptors unperturbed (68). Interpretations of autonomic responses to mild LBNP should be made with caution however, as Taylor and colleagues (122) observed reduced ascending aortic diameters during -5 mmHg LBNP, suggesting aortic arch baroreceptor unloading even during conditions where pressure is unchanged compared to baseline (70). LBNP greater than approximately -20 mmHg reduces venous return sufficient to modulate stroke volume, cardiac output and pulse pressure (due to reductions in systolic pressure); this stress unloads both cardiopulmonary and arterial baroreceptor populations (68). Cardiopulmonary baroreflex stress increases sympathetic discharge destined for the periphery, whereas arterial baroreflex unloading increases sympathetic discharge directed towards the heart and visceral vascular beds (1).

1.2.2 Non-Baroreflex Sympathetic Neurocircuitry

The collection of pre-sympathetic neurons within the RVLM are vital to the generation of pre- and post-ganglionic discharge based on anatomical evidence of RVLM projections to preganglionic neurons (112) and the consistent observation that destruction of RVLM cells in anaesthetized felines results in a large drop in blood pressure (48). As outlined above, RVLM neurons are integral to the baroreflex neurocircuitry and are strongly

inhibited by the CVLM during baroreflex loading (12). This CVLM inhibitory feature is reduced during baroreflex unloading accompanying orthostatic stress, enabling elevated sympathetic outflow from the RVLM (12, 78). Thus, other neural mechanisms generate the RVLM activity critical for preganglionic sympathetic discharge and ultimately the postganglionic AP behaviour observed in microneurographic recordings.

Researchers have proposed two primary hypotheses to explain RVLM discharge. The *pacemaker theory* suggests that intrinsic depolarization of some RVLM neurons drives sympathetic outflow (25). Using both intracellular and extracellular recordings, Sun and colleagues observed rhythmical pacemaker-like discharge of rat RVLM neurons under conditions where excitatory neurotransmission had been pharmacologically reduced or in the absence of excitatory postsynaptic potentials (EPSP) (114, 115). Alternatively, the *network theory* holds that excitatory and inhibitory synapses arising from several groups of neurons affects RVLM behaviour (23). In support of this concept, Lipski and colleagues found no evidence of rhythmical membrane depolarization of rat RVLM neurons preceding AP discharge, but rather observed EPSPs to drive spiking, indicating excitatory synapsing (75). Indeed, anatomic and functional studies have revealed that the RVLM participates in sympathoexcitatory reflexes (e.g., chemoreflex, metaboreflex) and receives synaptic inputs from a host of neurons beyond the CVLM (many of which form an interconnected network) including the NTS, periaqueductal gray, caudal vestibular nucleus, lateral tegmental field, periventricular nucleus (PVN) and lateral nucleus of the hypothalamus, the mesencephalic locomotor region, the amygdala, medial prefrontal cortex, and insular cortex (8, 23, 128).

The influence of some non-baroreflex sites on sympathetic discharge patterns have been revealed by direct stimulation studies in animals and humans. For example, chemical stimulation of the hypothalamic PVN in anaesthetized rats increased the amplitude but not the frequency of integrated bursts of renal sympathetic nerve activity (83). This effect may be mediated by synapses with the RVLM (8, 22, 138); however, axons arising from some cells within PVN of the hypothalamus also bypass the medulla and synapse directly with spinal sympathetic preganglionic neurons at multiple levels (e.g., preganglionic nerves ultimately supplying the heart and adrenal gland) (11, 23, 61). Similarly, electrical stimulation of the dorsolateral periaqueductal gray via implanted electrodes in humans increased the proportion of larger bursts of integrated MSNA compared to baseline conditions, but did not affect burst frequency (119). Interestingly, in addition to synapsing with the RVLM, periaqueductal gray neurons are also reciprocally connected to the hypothalamus (11), suggesting that the effect seen in humans may have occurred through hypothalamic activation. As discussed below, changes in MSNA burst frequency can be explained by arterial baroreflex regulation while factors affecting burst size — a function of the number and size of synchronously firing APs — remain to be elucidated fully (66, 110, 117).

1.2.3 Sympathetic Preganglionic Neurons

The cell bodies of sympathetic preganglionic neurons reside in the spinal cord, forming clusters primarily located in the intermediolateral cell column, but also in the central autonomic area lying dorsolateral to the central canal, in the intercalated nucleus between the intermediolateral cell column and the central autonomic area, and in the white matter of the dorsolateral funiculus (76, 113). Preganglionic neurons possess dendritic

arborizations broad enough to facilitate connections between neuronal clusters on ipsilateral and contralateral sides of the spinal midline (27, 127), which may contribute to synchronicity among postganglionic APs in each nerve (110) as well as bursting coherence in bilateral limb recordings (30). Also, cell bodies and dendrites of neighbouring preganglionic neurons form electrical synapses known as gap junctions which enable electrically-coupled networks and synchronous firing (28). Large dendritic fields accept both excitatory and inhibitory synapses from supraspinal nuclei which primarily generate their activity, along with sensory inputs emerging from the muscle and skin (23, 76). Importantly, preganglionic activity results from a complex spinal network formed by interneurons receiving input from all sensory nerves and some supraspinal regions (28).

In addition to classic neurotransmitters (e.g., glutamate) synaptic inputs release a variety of peptides [e.g., neuropeptide Y (NPY), substance P, angiotensin II, oxytocin] and catecholamines [e.g., norepinephrine (NE)] that may affect preganglionic excitability (23, 28). Indeed, some feline intermediolateral preganglionic neurons exposed to NE expressed rhythmic oscillations in membrane potential independent of synaptic input suggesting the potential for conditional pacemaker activity (137). Several other studies support the idea that preganglionic neurons or a spinal network contributes to sympathetic discharge recorded from postganglionic nerves. For example, in spinally transected (cervical level) rats, lumbar sympathetic discharge at the 2-6 Hz rhythm was restored following application of an excitatory amino acid, suggesting that supraspinal inputs are necessary for generating sympathetic outflow but some discharge characteristics are generated by preganglionic networks (2). Preganglionic neurons are

myelinated and emerge from the ventral spinal cord via the white ramus (132) and while most project to the ganglion at the same spinal level, others project either rostrally or caudally to synapse at nearby ganglia (113).

1.2.4 The Paravertebral Ganglia

The paravertebral ganglia describe the neural chains running parallel to the vertebrae where c-fibre cell bodies are organized into clusters and receive synaptic input from preganglionic nerves projecting from the spine (84). Through patterns of divergent and convergent synaptic organization the ganglia ensure that central sympathetic messages are faithfully distributed to peripheral targets but may also be integrated and modified accordingly (42). The ganglia amplify the distribution of the centrally arising message through divergent connections, which describes the synaptic phenomenon where each preganglionic neuron synapses with multiple postganglionic neurons (41, 59). While the pattern of divergence varies between ganglia and the volume of target tissue, estimates suggest that one preganglionic neuron synapses with a pool of about 100 postganglionic neurons in humans (31). Theoretically, divergence may contribute to synchronized discharge among postganglionic nerves as multiple c-fibres can be depolarized by the same input signal. Also, the recruitment of one previously-silent preganglionic neuron may represent a simple strategy for increasing the number of synchronously firing postganglionic nerves.

Convergence defines the pre-to-postganglionic nerve organization where each postganglionic neuron receives inputs from multiple preganglionic axons (84). This feature enables the ganglia to serve as an additional juncture for integration rather than strictly relaying information. Each postganglionic cell body receives between 2 and 15

preganglionic inputs (94). However, among preganglionic inputs to a single postganglionic nerve, the strength or ability to evoke postganglionic discharge varies and may be classified as primary (strong) or accessory (weak) inputs (59). While earlier studies indicated that postganglionic firing resulted only from the activity of primary inputs, recent studies including those performed *in vivo* in mammals have revealed that integration of convergent accessory inputs augments the firing rate of the postganglionic nerve beyond that evoked invariably by the primary input (13, 65, 96). For example, evidence suggests that postganglionic APs may be evoked by a pair of accessory inputs firing near simultaneously or a single accessory input firing twice in rapid succession (55, 65). Intriguingly, there also exists a subpopulation of accessory inputs whose strength fluctuates over time but often generates sufficient depolarization to drive postganglionic firing (13, 96). Synaptic convergence may contribute to the complexity of sympathetic c-fibre discharge as the number of preganglionic synapses scales with dendritic surface area, which relates to neuronal size (41). Therefore, larger neurons are expected to receive a greater number of preganglionic synapses (excitatory and inhibitory), potentially from different subpopulations of spinal nerves.

Pre-to-postganglionic transmission occurs mainly via cholinergic mechanisms at the ganglia. AP arrival at the preganglionic axon terminals initiates an intracellular cascade resulting in acetylcholine (ACh) release into the synaptic cleft (45). ACh molecules surviving breakdown by acetylcholinesterase in the cleft may bind to nicotinic receptors located on the dendritic and somatic surfaces of the postganglionic neuron (N_N nicotinic receptors) (129). These nicotinic receptors are ligand-gated ion channels that undergo conformational changes upon ACh binding, enabling channel opening and sodium (Na^+)

influx (45). Depolarization of the cell body, known as a postsynaptic potential, is responsible for generating an AP but only if this depolarization or the sum of the postsynaptic potentials reaches the threshold for AP initiation (~ -50 mV) (92).

Postsynaptic potentials arising from cation influx are known as EPSPs but inhibitory postsynaptic potentials also exist, reducing the likelihood of AP generation (92). While nicotinic receptors represent the primary mechanism for postganglionic firing, ACh may also bind muscarinic receptors which are expressed on some postganglionic neurons (59, 129). Unlike nicotinic mechanisms, muscarinic receptor binding by ACh results in a slower EPSP due to the G-protein coupled structure and required intracellular signaling cascade to initiate postsynaptic potentials (132).

The paravertebral ganglia also exist as a site for non-cholinergic neurotransmission.

Many preganglionic neurons contain chemical co-transmitters that are released with ACh and postganglionic synaptic targets expressing the appropriate receptor. According to the neurochemical coding hypothesis (41, 84), co-transmitter release varies by neuron and links to the functional sub-type of pre-and-postganglionic nerves (39). Many co-transmitters have now been identified including (but not limited to): adenosine, adenosine tri-phosphate (ATP), dopamine, GABA, nitric oxide, NPY, and substance P (28, 132).

Co-transmitter release represents a further option for postganglionic activation or inhibition; however, in many cases this appears to occur through slow postsynaptic potentials which affect postganglionic activity directly along with facilitating or modulating depolarization by fast EPSPs (52, 84, 129). Also, due to their position outside the blood-brain barrier (132), the ganglia are exposed to a variety of circulating

substances (e.g., angiotensin II) that may affect neurotransmitter release or postganglionic excitability in a similar manner (18, 38).

1.2.4.1 Postganglionic Nicotinic Blockade: Trimethaphan

In humans and lower animals, ganglionic neurotransmission via nicotinic mechanisms can be abolished through pharmacological intervention. Trimethaphan camsylate (Arfornad) is a selective nondepolarizing competitive antagonist of postganglionic nicotinic receptors (97). The onset of nicotinic blockade occurs within 1 to 5 minutes and lasts about 10 minutes (26, 126). Administration occurs by intravenous infusion with doses starting at 0.5 – 1 mg/min. Clinically, trimethaphan was used for blood pressure management during surgery but was discontinued and now the remaining supply exists for physiological research (135). Nicotinic ganglionic blockade may be verified by negligible (< 5 bpm) heart rate responses to Valsava's Manoeuvre or by the absence of integrated MSNA bursts in microneurographic studies (7, 9). Importantly, nicotinic blockade via trimethaphan infusion revealed the efferent nature of MSNA (26) and insight to sympathetic circulatory control in humans (21, 62).

1.2.5 Sympathetic Postganglionic Neurons

Sympathetic postganglionic neurons exit the paravertebral ganglia via the gray ramus, projecting towards cardiovascular end-targets. Microneurographic recordings for the studies comprising this dissertation were made from the peroneal (also called the fibular) nerve, a branch of the sciatic nerve arising from the lumbosacral plexus (4th lumbar segment to 3rd sacral segment) (123). Tyrosine-hydroxylase (i.e., enzyme for catecholamine synthesis) stained postganglionic axons obtained from the peroneal nerve of human cadavers revealed that these nerves do not form their own fascicles but are

organized in bundles among myelinated nerves ranging in number from 1 to about 45 axons (median: 5 axons) (124). Sympathetic c-fibres range in size from 0.5 to 2 μm (124), supporting the observation of varying-sized APs (confirmed by conduction velocities) within human multi-unit recordings (106). This dissertation focuses on the postganglionic axons within the peroneal nerve that are directed to vascular smooth muscle supplying skeletal muscle. Postganglionic c-fibres traverse arteries as they branch, forming a plexus within the adventitia and interface the smooth muscle via bulging varicosities containing synaptic vesicles then continue on and form varicosities distally (133). This organization, referred to as *synapse en passant*, enables a single postganglionic nerve to innervate a large volume of the vasculature (132). Size variability among postganglionic c-fibres may confer graded vasoconstrictor control as larger neurons innervate a larger vascular field in guinea pigs (40).

Fundamentally, AP arrival at the varicosity depolarizes the cellular membrane opening voltage-gated calcium channels to initiate calcium influx, which causes vesicular exocytosis and neurotransmitter release (132). Briefly, the primary neurotransmitters released by sympathetic nerve varicosities are NE, NPY, and ATP (133). The major source of vasoconstriction for NE results from binding postsynaptic alpha-1 ($\alpha_1\text{R}$) and alpha-2 ($\alpha_2\text{R}$) adrenergic receptors on the smooth muscle (104). For NPY and ATP, the receptors primarily mediating vasoconstriction are the NPY Y1R and P2X₁ receptors, respectively (104). $\alpha_1\text{R}$ activation results in calcium release from the sarcoplasmic reticulum via Gq-protein related phospholipase C production, subsequent inositol 1,4,5-trisphosphate (IP3) production and sarcoplasmic IP3 receptor binding (90).

Neurotransmitter binding of NPY Y1R and $\alpha_2\text{R}$ inhibit cyclic adenosine monophosphate

(cAMP) production via Gi-protein related attenuation of adenylyl cyclase activity (133). A reduction in cAMP activates myosin light chain kinase which phosphorylates myosin light chain to cause vasoconstriction. Last, P2X₁ receptors are inotropic and activation enables calcium influx, cellular depolarization and vasoconstriction (118).

1.3 The Action Potential

The AP represents the fundamental neural signal enabling the sympathetic system to communicate with the circulation. The prototypical AP arising from an unmyelinated sympathetic c-fibre axon has a triphasic shape lasting one to two milliseconds in duration that represents phases of membrane depolarization, repolarization and hyperpolarization, and the return to resting membrane potential (54). APs are commonly described from the perspective of intracellular preparations such as those revealing the first AP recordings from the giant axons of squid by Hodgkin and Huxley (53, 54). Due to the relative abundance of potassium ions (K⁺) in the intracellular fluid, and relative abundance of Na⁺ and chloride ions (Cl⁻) in the extracellular fluid along with the large concentration of open resting K⁺ channels which facilitate K⁺ diffusion, most axons express a resting membrane potential of about -60 to -70 mV (10, 92).

Changes in the permeability of these ions facilitated by voltage-gated Na⁺ and K⁺ channels underlie AP generation. At the resting membrane potential, voltage-gated Na⁺ channels are closed and passive spread of the AP depolarization at an upstream adjacent axonal segment initiates channel opening leading to inward Na⁺ diffusion and rapid depolarization of this region (i.e., the intracellular fluid becomes more positive resulting in an AP upstroke) (77). Voltage-gated Na⁺ channels close at peak depolarization and

remain inactivated for several milliseconds contributing to the refractory period of the axonal segment which ensures orthodromic AP conduction (10). Cell depolarization triggers transient voltage-gated K^+ channel opening leading to K^+ efflux causing repolarization (i.e., the intracellular fluid becomes negative resulting in an AP downstroke) and hyperpolarization (i.e., the intracellular fluid transiently becomes more negative than the resting membrane potential) then returns to the resting membrane potential (92). The AP hyperpolarization phase also produces a refractory stage, contributing to orthodromic conduction (77). Because the tip of the microelectrode used in microneurographic recordings is up to 10-fold larger in diameter than c-fibre axons (124), recordings in humans yield extracellular sympathetic APs, which express the reciprocal waveform to that described above (81, 98)

1.4 Muscle Sympathetic Nerve Activity

MSNA, postganglionic c-fibre discharge directed towards the skeletal muscle vasculature, represents a critical neural avenue for homeostasis. In humans, the microneurographic technique enables continuous MSNA recordings from superficial nerves (49). Briefly, microneurography involves inserting a tungsten microelectrode trans-dermally into a peripheral nerve and delicately manipulating the electrode to position its tip, and recording field, near a discharging bundle of postganglionic axons (106, 125). Populations of varying-sized postganglionic nerves depolarize synchronously, or at about the same time, due to strong phasic baroreflex-inhibition accompanying pressure variations across the cardiac cycle (26). This bursty behaviour represents a cardinal feature of MSNA.

Consistent with the first microneurographic recordings by Hagbarth and Vallbo (49), MSNA is commonly measured at the multi-unit level, capturing the activity of a population of c-fibres rather than individual nerves. Due to the low signal-to-noise ratio of sympathetic recordings, after signal amplification (50,000 to 100,000x) and filtering (700 – 2,000 Hz band-pass), researchers often derive metrics of sympathetic activity from the integrated neurogram (51, 134). Inspection of the integrated neurogram reveals bursts of MSNA that vary in size and occurrence under baseline conditions (49, 130). Integrated bursts typically express latencies, i.e., the time from the R-wave corresponding to the systolic pulse terminating the burst to the burst peak, between about 1.2 and 1.5 seconds (35) and stems from all components of the sympathetic organization with most influence arising from the conduction velocity of unmyelinated postganglionic nerves (~1.1 m/s) (34, 35). Because burst size stems, in part, from the proximity of the recording electrode to a c-fibre bundle and micro-electrode position can vary across an experiment, many studies have solely examined burst frequency (51). While the strong intra-individual repeatability over months confers utility to this metric (36, 67), the singular focus on burst occurrence exposes insight to baroreflex mechanisms but conceals additional, broader properties of the sympathetic nervous system (106). Based on the observation that burst size was inversely related to its latency (130): that is, larger bursts expressed faster conduction velocities than smaller bursts, Wallin and colleagues suspected that modifiable central synaptic delays and/or subpopulations of larger and faster-conducting axons may exist. This early hypothesis suggested that provided microelectrode position remains stable, burst size (or amplitude) may reflect the number and size of synchronously discharging postganglionic axons.

Advances in the microneurographic technique, high quality recordings, and signal processing strategies have enabled access to the actual sympathetic neural signal — the AP (80, 104, 106). Macefield and colleagues were the first to reveal the firing properties of individual vasoconstrictor fibres in humans (81). Reductions in the recording field accompanying high impedance electrodes (e.g., 10 vs. 3 M Ω) enabled this group to track the activity of APs arising from one (i.e., single-unit) or a few axons in close proximity to the microelectrode tip. An important consideration with this technique remains that a single-unit may be generated by two close-proximity axons with identical morphology, though investigators suspect this describes a low-probability occurrence (80). This technique exposed that in healthy participants, individual c-fibres fire in few cardiac cycles (~30 %) and most often they fire only once in an integrated burst but can fire more than 4 times in a burst (81). During an end-expiratory apnea, single-units fired in a greater proportion of cardiac cycles and expressed an increased probability of firing more than once per burst (79). However, multiple within-burst firing could not explain fully the increase in integrated burst size, furthering the hypothesis that recruitment of previously-silent larger and faster conducting axons may represent the primary mechanism for augmented burst size (79).

To test the hypothesis that a subpopulation of previously silent, larger and faster conducting sympathetic axons are recruited during physiological stress requires APs to be detected and extracted from the multi-unit neurogram. Two wavelet denoising techniques (16, 29, 98) and a mixed separation template-matching model (120) have been designed to interrogate the multi-unit signal; however, most research has employed the wavelet model constructed from real human muscle sympathetic APs (98, 110) and therefore the

present dissertation will focus on this technique and related outcomes. Briefly, this technique relies on a mother wavelet that was based on the mean AP template constructed from real human muscle sympathetic APs (98). Using a continuous transform of the filtered neurogram, the approach identifies the exact location of individual APs and extracts them from the surrounding noise (98). Using a 32-point K-means approach families of similarly-shaped APs are clustered based on their overall shape, primarily reflecting the peak-to-peak amplitude (98). Subsequently, APs can be organized into bins (i.e., clusters) manually or based on Scott's rule (102). When used to compare multi-unit data obtained during a baseline condition and a period of physiological stress, this approach enables investigators to make inferences regarding the recruitment of previously-silent larger APs (i.e., high-threshold) or the enhanced firing of previously-active APs (i.e., low-threshold), provided a constant micro-electrode position. Also, this method exposes the temporal characteristics of individual APs: relative to adjacent APs, the beginning of an integrated burst, and the R-wave associated with the systolic pressure inhibiting the coinciding burst (98). Figure 1.1 provides an overview of wavelet method for AP detection.

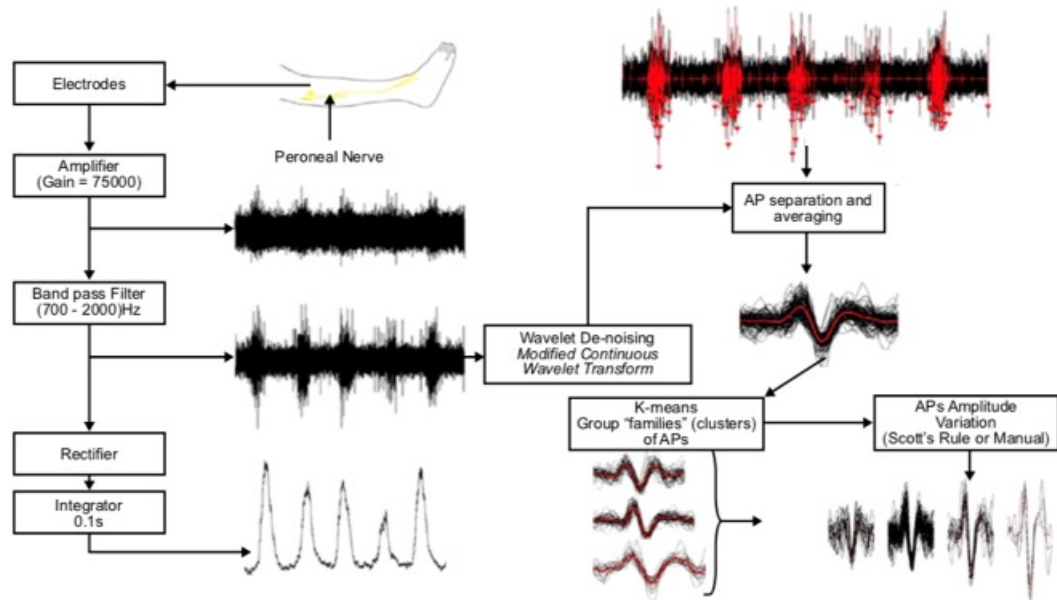


Figure 1.1 Overview of the stages involved in extracting sympathetic action potentials (AP) from the filtered neurogram using the continuous wavelet transform (98) including signal processing, clustering, and binning.

The wavelet approach has illustrated diverse behaviours expressed by the varying-sized APs firing within the sympathetic multi-unit neurogram under baseline conditions and during periods of physiological stress (103, 104, 106). These complex patterns of AP activity — defined broadly as sympathetic communication strategies — are tailored to the magnitude and form of stress and employed by the sympathetic nervous system to communicate the circulatory adjustments necessary for homeostatic maintenance (106). Among APs firing synchronously to form bursts, multiple size-related subpopulations exist expressing heterogeneous discharge and recruitment characteristics that contribute to fluctuations in burst size and occurrence over time. The firing probability of APs active at baseline (i.e., low-threshold APs) varies by size to resemble an inverted ‘U’ shaped distribution as medium APs fire in most bursts, while the small and large APs discharge less often (74, 101).

During diverse forms of physiological stress, two key AP patterns elevate total MSNA. First, the sympathetic system utilizes a rate-coding strategy which defines the increased firing of previously-active AP subpopulations achieved via a greater occurrence of synchronized bursts of AP discharge and a greater propensity for multiple firing within each burst of activity (79, 110). Because the wavelet approach does not track APs arising from single fibres over time, rate-coding from this perspective refers to an increase in the firing probability of similarly-sized APs (i.e., clusters) already active at baseline. Second, during stress the sympathetic system utilizes a population-coding strategy which describes the recruitment of larger and faster-conducting AP clusters that were not active at baseline. These strategies appear to be reflex non-specific as they have been observed during a host of stressors targeting the chemoreflex (3, 6, 88, 110), baroreflex (6, 74, 99–

101), and metaboreflex (5) among other forms of physiological stress such as apnea (4, 69). Fig. 1.2 provides an overview of the varying-sized AP subpopulations contained within the filtered neurogram.

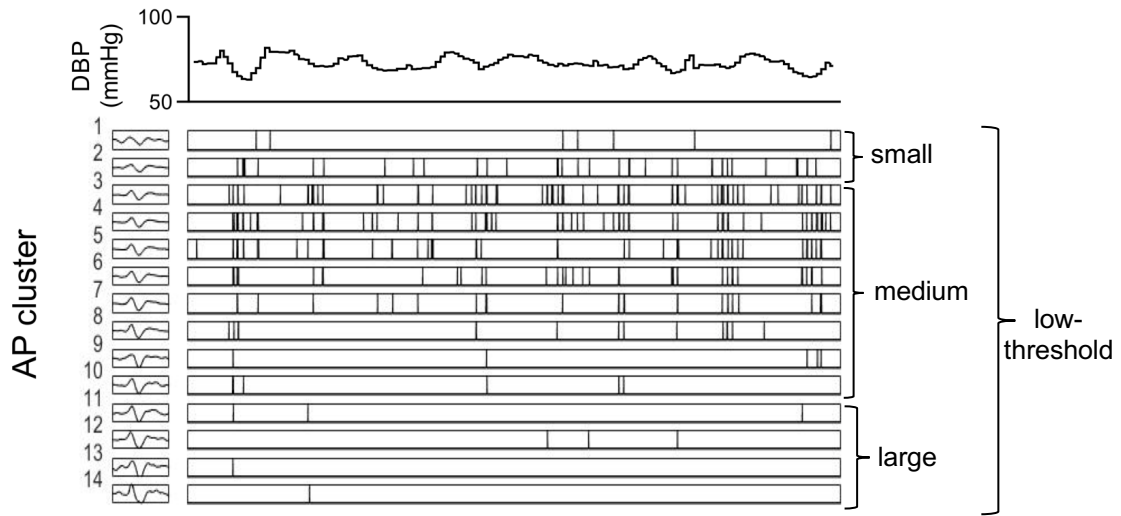
Not all APs previously-active at baseline appear to increase firing rates with physiological stress, however. During the hypotensive phase of a sodium nitroprusside bolus infusion, Limberg and colleagues (74) found the cluster of the smallest APs extracted using the wavelet technique to express a paradoxical reduction in firing probability, while medium clusters fired more often and a subpopulation of larger and faster-conducting APs were recruited. Studies from laboratories employing high impedance electrodes to examine a few active APs provide evidence consistent with this phenomenon. In a sample of young and middle-aged healthy individuals, Millar and colleagues identified a subpopulation of APs that fired less often during modest LBNP (-10 mmHg) and moderate rhythmic handgrip exercise (40 % max effort) (57, 85). While the different microneurographic techniques preclude direct comparisons between studies, these observations suggest that a subpopulation of sympathetic APs, perhaps arising from the smallest postganglionic axons, may be inhibited during periods of sympathetic arousal such as simulated orthostatic stress or physical exercise. If so, this feature aligns with the de-recruitment or reduced firing of low-threshold motor neurons during periods of high-threshold neuron activation as observed in decerebrate cats (64). This concept remains to be studied directly for postganglionic sympathetic c-fibres.

The AP cluster latency represents a critical criterion for making inferences regarding axonal size within the microneurographic recording field (110). In a similar manner to measuring burst latency, AP latency represents the time from the R-wave associated with

AP occurrence and the negative peak of the AP waveform (99). According to cable theory, axonal size should be proportional to its conduction velocity and AP amplitude (91, 121). Importantly, when regressing AP cluster latency against AP cluster size an exponential decay relationship emerges consistently for AP data obtained at baseline and physiological stress, indicating that larger APs arise from larger axons that express faster conduction velocities (6, 69, 100, 110). This evidence argues against the notion that larger APs reflect depolarization of axons closer to the microelectrode tip.

The temporal behaviour of AP discharge represents an additional strategy for modifying MSNA. At baseline, Macefield and colleagues (81) reported considerable variation in latency of single sympathetic axons, providing additional support for the idea that variable synaptic delays exist in the central sympathetic organization. During both Valsalva's Manoeuvre and apnea, all AP clusters express reduced latency (4, 6, 69, 100). Based on the observation that AP latency was reduced during isometric handgrip but returned to baseline values in the subsequent period of circulatory occlusion suggests that the central command mechanism related to perceptual effort may contribute to this phenomenon (5). In contrast, severe baroreflex stress in the absence of perceptual stress such as that imposed by -80 mmHg LBNP prolongs the latency of all AP clusters (6, 99). The mechanisms shaping AP latency also appear chronically modifiable as exposure to 60-days of head-down bed rest increased the latency of all APs firing at baseline and during apneic stress (69).

Baseline



-80 mmHg LBNP

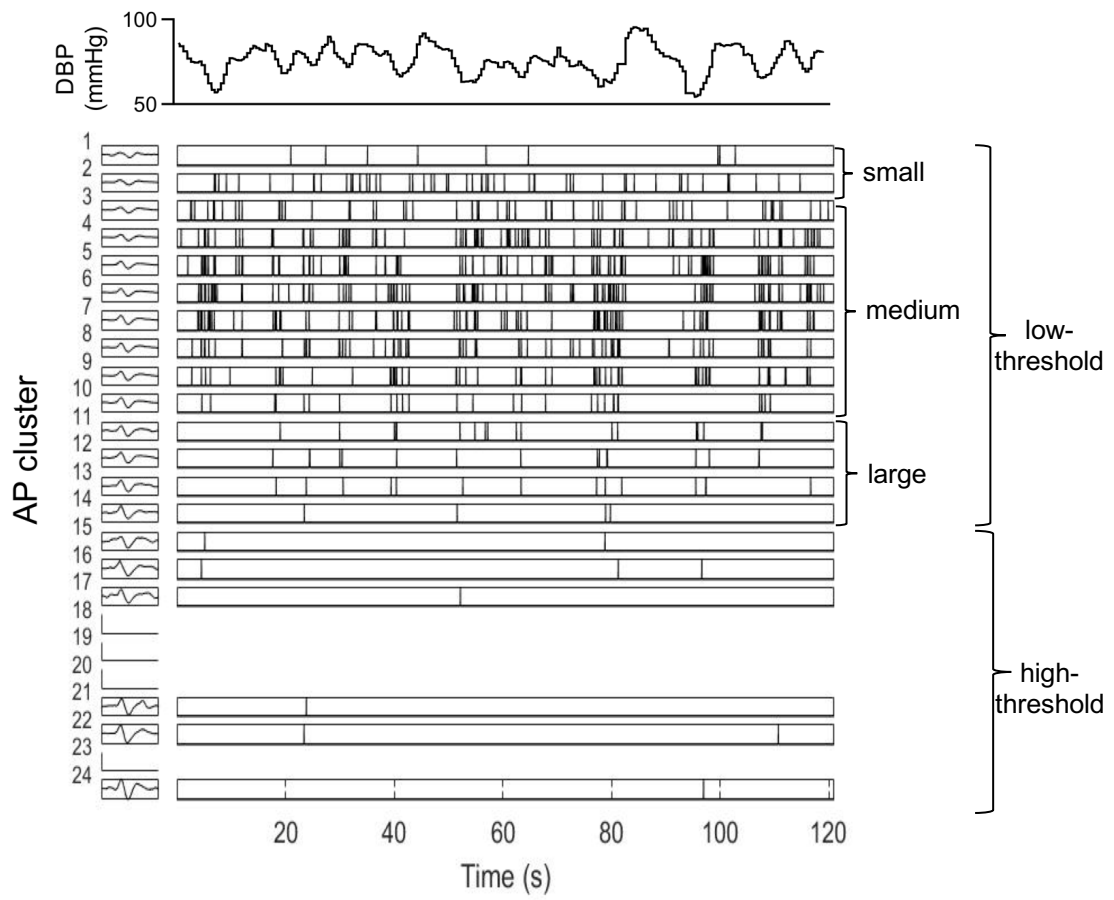


Figure 1.2 Data from a single participant providing an overview of the discharge characteristics associated with the varying-sized sympathetic action potential (AP) subpopulations. Low-threshold APs are active under baseline conditions and are comprised by three fundamental subpopulations small, medium, and large, as highlighted on the right (see text for details). During physiological stress such as -80mmHg lower body negative pressure (LBNP), some low-threshold APs increase their firing rate. Also, a subpopulation of high-threshold larger APs are recruited during physiological stress. Each panel illustrates AP discharge over time as a function of their diastolic blood pressure (DBP; top) and cluster (left). AP cluster refers to all APs of similar morphology and are normalized between conditions to ensure within-participant comparisons (e.g., cluster 1 represents the same-sized APs at BSL and LBNP). (Previous page).

1.4.1 Baroreflex Control of Muscle Sympathetic Nerve Activity

As mentioned, pulse-rhythmic input from arterial baroreceptors shapes the bursty behaviour of MSNA and contributes to the time-varying outflow of sympathetic discharge (33). Arterial baroreflex control of MSNA can be derived by measuring baroreflex gain, the strength of the relationship between baroreflex-mediated MSNA changes and spontaneous blood pressure oscillations. Sundlöf and Wallin (116) designed this strategy to examine baroreflex-mediated alterations in integrated burst probability (i.e., baroreflex threshold analysis) and integrated burst amplitude (i.e., baroreflex sensitivity analysis) for given changes in blood pressure. Commonly, baroreflex threshold analysis involves grouping diastolic blood pressure into bins (e.g., 1 or 2 mmHg bin width) and calculating the percentage of heartbeats per diastolic bin that were associated with an integrated burst (50, 66, 101). The slope of the linear relationship between burst probability and diastolic blood pressure represents baroreflex threshold gain.

Alternatively, baroreflex sensitivity examines the slope of the linear relationship between amplitude of each burst and its corresponding diastolic blood pressure (50).

Comparison of baroreflex threshold and sensitivity measures by Kienbaum and colleagues (66) demonstrated stronger baroreflex threshold than sensitivity slopes in each participant during baseline. This finding spurred the baroreflex-gating hypothesis stating that the baroreflex gates whether or not a burst will fire but other central neural processes influence the size (i.e., AP content) of each burst. This notion aligns with the observation that the severity of LBNP was positively related to the change in burst frequency from baseline, while no relationship existed with the change in burst amplitude (117). In

contrast, some forms of chemoreflex stress preferentially augment burst size over burst frequency (82, 111).

To explain the observations regarding differential baroreflex regulation of burst occurrence versus size, Salmanpour and Shoemaker (2012) studied the baroreflex control of AP discharge by regressing AP firing probability of each cluster against diastolic blood pressure (i.e., baroreflex threshold analysis). During baseline conditions this approach revealed that the gain of baroreflex control over AP discharge linearly decreases with increasing AP cluster size indicating that the arterial baroreflex strongly governs small-to-medium AP discharge but exerts weak control over larger AP cluster firing. Thus, the baroreflex strongly governs burst occurrence because it affects medium AP firing, which occur in most bursts. Alternatively, burst amplitude is only minimally affected by the arterial baroreflex because larger AP clusters express weak slopes and fire less often. Also, because burst amplitude represents both the size and number of synchronously firing APs (110), Salmanpour and Shoemaker (2012) examined the relationship between the number of unique AP clusters per burst and the diastolic blood pressure associated with that burst (i.e., baroreflex sensitivity analysis). This method also revealed weak slopes, suggesting the baroreflex does not strongly govern within-burst AP content (101). Together, the observation that larger AP clusters fire less often, express weak baroreflex slopes but contribute more to integrated burst size, and that the baroreflex weakly controls the number of AP clusters per burst, results in minimal baroreflex control over burst amplitude. Consistent with these data are the repeated findings that baroreflex stress (i.e., imposed by LBNP or sodium nitroprusside) weakly

recruits subpopulations of larger and faster conducting APs, at least until severe levels of baroreflex unloading in some individuals (6, 74, 99).

1.5 Integrated Rationale

As illustrated in the discourse above, single- and multi-fibre microneurographic recordings have revealed an array of intricate behaviours contained within the sympathetic discharge directed towards the circulation supplying skeletal muscle (80, 106). Fundamentally, the complexity of sympathetic neural emissions stems from the heterogenous firing probabilities expressed by sized-related AP subpopulations. Of APs synchronized into bursts under baseline conditions (i.e., low-threshold APs), medium APs fire in most bursts, whereas the small and large APs fire less often (101, 110). These low-threshold APs are critical for communicating with the vasculature and supporting homeostasis in humans under baseline conditions. Given that postganglionic emissions reflect the central and peripheral organization of the sympathetic system (59), heterogenous discharge behaviours among AP subpopulations suggest differential regulatory mechanisms. While the arterial baroreflex governs the behaviour of some low-threshold APs during baseline (101), other neural mechanisms affecting AP patterns remain to be investigated.

To maintain homeostasis during physiological stress the sympathetic system employs two key strategies to increase total MSNA. First, the sympathetic system increases the firing rate of previously-active APs, then during severe stress, the system recruits a subpopulation of latent larger and faster-conducting APs (5, 99). Recently, research efforts have been dedicated to understanding the discharge patterns and reflex mechanisms governing larger previously-silent (i.e., high-threshold) sympathetic APs (3,

4, 6), yet the AP subpopulations expressing heterogeneous discharge under baseline conditions and augmented firing probabilities during physiological stress have received less attention.

Therefore, the present dissertation proposed the **overall objective** to investigate the behaviour and mechanisms governing the low-threshold (i.e., active at baseline) sympathetic AP subpopulations. This dissertation tested the **overall hypothesis** that heterogeneous discharge behaviour exists among varying-sized low-threshold AP subpopulations under baseline conditions and during physiological stress, due to differing regulation within the sympathetic organization. While each study addresses the overall objective and hypothesis in a specific way, the following discourse highlights the logical succession of studies that emerged with our observations.

At the paravertebral ganglia, patterns of divergent and convergent pre- to postganglionic innervation amplify distribution and confer complexity to the discharge of varying-sized sympathetic c-fibres (42, 84), respectively. In fact, synaptic convergence appears to vary by sympathetic postganglionic neuron size in lower animals (93, 94), a feature which may produce AP size-related firing characteristics. Therefore, **Study One** (71) tested the **hypothesis** that the paravertebral ganglia contribute to the discharge behaviour of sympathetic APs active at baseline in humans. Two novel findings emerged from this study: 1) Trimethaphan infusion produced ordered AP de-recruitment whereby the large APs firing with low probability during baseline were abolished first, followed by the reduced discharge probability of smaller APs; 2) Although trimethaphan infusion blocked integrated bursts of MSNA, we observed the smallest APs to express trimethaphan-resistance and fire in an asynchronous manner. We interpret these observations to suggest

that the ganglia contribute to the heterogeneous discharge patterns among varying-sized APs due to differential patterns of ganglionic synaptic input. Also, we hypothesize that the trimethaphan-resistant property of smaller APs reflects non-nicotinic mechanisms (60), which participate in neurotransmission at the human sympathetic ganglia.

The primary characterization of MSNA to date focuses on pulse-rhythmic bursts formed by the synchronized discharge of varying-sized APs (49, 110). But observations made in Study One (71) and studies in lower animals (14, 15) suggest that some sympathetic c-fibres may express non-burst forming asynchronous discharge, and that the ganglia may participate in this behaviour (15). Therefore, **Study Two** (72) tested the **hypothesis** that synchronous and asynchronous discharge exist among sympathetic APs and the ganglia affect AP synchronicity. By studying all APs rather than just those within identified bursts, we found that: 1) At baseline, ~30% of total sympathetic AP discharge fired asynchronously, between bursts; 2) The probability of asynchronous discharge was related inversely to AP cluster size and the asynchronous AP discharge frequency was not affected by baroreflex or apneic stress; 3) While the largest asynchronously firing AP clusters present at baseline were blocked by trimethaphan infusion, the smaller asynchronous APs persisted to fire. We interpret these findings to suggest that the fundamental behaviour of MSNA contains between-burst asynchronous AP discharge, which accounts for a considerable amount of baseline activity, and the ganglia contribute to some, but not all asynchronous AP firing.

Pulse-rhythmic arterial baroreceptor input synchronizes APs into bursts (33) and of the APs organized into these bursts, arterial baroreflex control relates inversely to AP cluster size under baseline conditions (101). However, our understanding of baroreflex AP

control remains unclear given that Study Two found ~30% of total APs to fire asynchronously outside baroreflex-gated bursts at baseline, with the smallest APs expressing the greatest proportion of asynchronous discharge (72). Combined with the finding that the baroreflex primarily relies on augmenting the firing probability of previously-active APs to maintain blood pressure during orthostatic stress (99), these observations warrant an investigation into the heterogeneity of baroreflex control over AP discharge. Accordingly, **Study Three** tested the **hypothesis** that the baroreflex exerts the strongest gain over medium-sized APs that fire with high probability under baseline conditions, and the change in position and slope of each clusters baroreflex curve accompanying orthostatic stress should vary across the distribution of recorded APs. Here, by studying all active APs, we found that medium APs expressed the greatest baroreflex gain while the smallest and largest clusters expressed lesser gains during baseline conditions. On going from baseline to baroreflex stress, the baroreflex gain for each AP cluster was modified differently: the medium AP slopes increased, while the slopes for the small and large APs present at baseline exhibited a reduction and no change, respectively. Also, the larger AP clusters that were silent at baseline but recruited during orthostatic stress expressed weak baroreflex gains. From these findings we infer that resetting the activity upwards and augmenting the gain of a discrete group of medium APs already active at baseline, as well as the recruitment of a non-baroreflex high-threshold subpopulation, elevates sympathetic discharge during baroreflex stress in humans.

1.6 References

1. **Abboud FM, Eckberg DL, Johannsen UJ, Mark AL.** Carotid and cardiopulmonary baroreceptor control of splanchnic and forearm vascular resistance during venous pooling in man. *J Physiol* 286: 173–184, 1979.
2. **Allen AM, Adams JM, Guyenet PG.** Role of the spinal cord in generating the 2- to 6-Hz rhythm in rat sympathetic outflow. *Am J Physiol Integr Comp Physiol* 264: R938–R945, 1993.
3. **Badrov MB, Barak OF, Mijacika T, Shoemaker LN, Borrell LJ, Lojpur M, Drvis I, Dujic Z, Shoemaker JK.** 50 Years of Microneurography: Insights into Neural Mechanisms in Humans: Ventilation inhibits sympathetic action potential recruitment even during severe chemoreflex stress. *J Neurophysiol* 118: 2914, 2017.
4. **Badrov MB, Lalande S, Olver TD, Suskin N, Shoemaker JK.** Effects of aging and coronary artery disease on sympathetic neural recruitment strategies during end-inspiratory and end-expiratory apnea. *Am J Physiol Circ Physiol* 311: H1040–H1050, 2016.
5. **Badrov MB, Olver TD, Shoemaker JK.** Central vs. peripheral determinants of sympathetic neural recruitment: insights from static handgrip exercise and postexercise circulatory occlusion. *Am J Physiol Integr Comp Physiol* 311: R1013–R1021, 2016.
6. **Badrov MB, Usselman CW, Shoemaker JK.** Sympathetic neural recruitment strategies: responses to severe chemoreflex and baroreflex stress [Online]. *Am J Physiol Integr Comp Physiol* 309: R160–R168, 2015.
7. **Baker SE, Limberg JK, Dillon GA, Curry TB, Joyner MJ, Nicholson WT.** Aging Alters the Relative Contributions of the Sympathetic and Parasympathetic Nervous System to Blood Pressure Control in Women. *Hypertension* 72: 1236–1242, 2018.
8. **Barman SM, Yates BJ.** Deciphering the Neural Control of Sympathetic Nerve Activity: Status Report and Directions for Future Research. *Front Neurosci* 11: 730, 2017.
9. **Barnes JN, Hart EC, Curry TB, Nicholson WT, Eisenach JH, Wallin BG, Charkoudian N, Joyner MJ.** Aging enhances autonomic support of blood pressure in women. *Hypertension* 63: 303–308, 2014.
10. **Barnett MW, Larkman PM.** The action potential. *Pract Neurol* 7: 192–197, 2007.
11. **Benarroch EE.** Paraventricular nucleus, stress response, and cardiovascular disease. *Clin Auton Res* 15: 254–263, 2005.

12. **Benarroch EE.** The arterial baroreflex: functional organization and involvement in neurologic disease. *Neurology* 71: 1733–1738, 2008.
13. **Bratton B, Davies P, Jänig W, McAllen R.** Ganglionic transmission in a vasomotor pathway studied in vivo. *J Physiol* 588: 1647–1659, 2010.
14. **Brown AM.** Cardiac sympathetic adrenergic pathways in which synaptic transmission is blocked by atropine sulfate. *J Physiol* 191: 271–288, 1967.
15. **Brown AM.** Sympathetic ganglionic transmission and the cardiovascular changes of the defense reaction in the cat. *Circ Res* 24: 843–849, 1969.
16. **Brychta RJ, Shiavi R, Robertson D, Diedrich A.** Spike detection in human muscle sympathetic nerve activity using the kurtosis of stationary wavelet transform coefficients. *J Neurosci Methods* 160: 359–367, 2007.
17. **Cannon WB.** Organization for physiological homeostasis. *Physiol Rev* 9: 399–431, 1929.
18. **Castrén E, Kurihara M, Gutkind JS, Saavedra JM.** Specific angiotensin II binding sites in the rat stellate and superior cervical ganglia. *Brain Res* 422: 347–351, 1987.
19. **Charkoudian N, Joyner MJ, Johnson CP, Eisenach JH, Dietz NM, Wallin BG.** Balance between cardiac output and sympathetic nerve activity in resting humans: role in arterial pressure regulation. *J Physiol* 568: 315–321, 2005.
20. **Charkoudian N, Joyner MJ, Sokolnicki LA, Johnson CP, Eisenach JH, Dietz NM, Curry TB, Wallin BG.** Vascular adrenergic responsiveness is inversely related to tonic activity of sympathetic vasoconstrictor nerves in humans. *J Physiol* 572: 821–827, 2006.
21. **Christou DD, Jones PP, Jordan J, Diedrich A, Robertson D, Seals DR.** Women have lower tonic autonomic support of arterial blood pressure and less effective baroreflex buffering than men. *Circulation* 111: 494–498, 2005.
22. **Coote JH, Yang Z, Pyner S, Deering J.** Control of sympathetic outflows by the hypothalamic paraventricular nucleus. *Clin Exp Pharmacol Physiol* 25: 461–463, 1998.
23. **Dampney RA.** Functional organization of central pathways regulating the cardiovascular system. *Physiol Rev* 74: 323–364, 1994.
24. **Dampney RAL, Coleman MJ, Fontes MAP, Hirooka Y, Horiuchi J, Li Y, Polson JW, Potts PD, Tagawa T.** Central mechanisms underlying short- and long-term regulation of the cardiovascular system. *Clin Exp Pharmacol Physiol* 29: 261–268, 2002.

25. **Dampney RAL, Tagawa T, Horiuchi J, Fontes M, Polson JW.** What drives the tonic activity of presympathetic neurons in the rostral ventrolateral medulla? *Clin Exp Pharmacol Physiol* 27: 1049–1053, 2000.
26. **Delius W, Hagbarth K, Hongell A, Wallin BG.** General characteristics of sympathetic activity in human muscle nerves [Online]. *Acta Physiol Scand* 84: 65–81, 1972.
27. **Dembowsky K, Czachurski J, Seller H.** Morphology of sympathetic preganglionic neurons in the thoracic spinal cord of the cat: an intracellular horseradish peroxidase study. *J Comp Neurol* 238: 453–465, 1985.
28. **Deuchars SA, K. Lall V.** Sympathetic preganglionic neurons: properties and inputs. *Compr Physiol* 5: 829–869, 2011.
29. **Diedrich A, Charoensuk W, Brychta RJ, Ertl AC, Shiavi R.** Analysis of raw microneurographic recordings based on wavelet de-noising technique and classification algorithm: wavelet analysis in microneurography. *IEEE Trans Biomed Eng* 50: 41–50, 2003.
30. **Diedrich A, Porta A, Barbic F, Brychta RJ, Bonizzi P, Diedrich L, Cerutti S, Robertson D, Furlan R.** Lateralization of expression of neural sympathetic activity to the vessels and effects of carotid baroreceptor stimulation. *Am J Physiol Circ Physiol* 296: H1758–H1765, 2009.
31. **Ebbesson SOE.** Quantitative studies of superior cervical sympathetic ganglia in a variety of primates including man. I. The ratio of preganglionic fibers to ganglionic neurons. *J Morphol* 124: 117–131, 1968.
32. **Fadel PJ, Ogoh S, Keller DM, Raven PB.** Recent insights into carotid baroreflex function in humans using the variable pressure neck chamber [Online]. *Exp Physiol* 88: 671–680, 2003. <http://ep.physoc.org/content/88/6/671.full.pdf>.
33. **Fagius JAN, Wallin BG, Sundlof G, Christer N, Englesson S.** Sympathetic outflow in man after anaesthesia of the glossopharyngeal and vagus nerves. *Brain* 108: 423–438, 1985.
34. **Fagius J, Sundlöf G, Wallin BG.** Variation of sympathetic reflex latency in man. *J Auton Nerv Syst* 21: 157–165, 1987.
35. **Fagius J, Wallin BG.** Sympathetic reflex latencies and conduction velocities in normal man. *J Neurol Sci* 47: 433–448, 1980.
36. **Fagius J, Wallin BG.** Long-term variability and reproducibility of resting human muscle nerve sympathetic activity at rest, as reassessed after a decade. *Clin Auton Res* 3: 201–205, 1993.
37. **Fisher JP, Young CN, Fadel PJ.** Autonomic adjustments to exercise in humans.

- Compr Physiol* 5: 475–512, 2011.
38. **Floras JS.** Sympathoinhibitory effects of atrial natriuretic factor in normal humans. *Circulation* 81: 1860–1873, 1990.
 39. **Gibbins IL.** Vasomotor, pilomotor and secretomotor neurons distinguished by size and neuropeptide content in superior cervical ganglia of mice. *J Auton Nerv Syst* 34: 171–183, 1991.
 40. **Gibbins IL, Hoffmann B, Morris JL.** Peripheral fields of sympathetic vasoconstrictor neurons in guinea pigs. *Neurosci Lett* 248: 89–92, 1998.
 41. **Gibbins IL, Jobling P, Messenger JP, Teo EH, Morris JL.** Neuronal morphology and the synaptic organisation of sympathetic ganglia. *J Auton Nerv Syst* 81: 104–109, 2000.
 42. **Gibbins IL, Morris JL.** Structure of peripheral synapses: autonomic ganglia. *Cell Tissue Res* 326: 205–220, 2006.
 43. **Goldstein DS.** How does homeostasis happen? Integrative physiological, systems biological, and evolutionary perspectives. *Am J Physiol Integr Comp Physiol* 316: R301–R317, 2019.
 44. **Goldstein DS, Kopin IJ.** Homeostatic systems, biocybernetics, and autonomic neuroscience. *Auton Neurosci* 208: 15–28, 2017.
 45. **Goodman LS.** *Goodman and Gilman's the pharmacological basis of therapeutics.* McGraw-Hill New York, 1996.
 46. **Grassi G, Mark A, Esler M.** The sympathetic nervous system alterations in human hypertension. *Circ Res* 116: 976–990, 2015.
 47. **Grassi G, Quarti-Trevano F, Seravalle G, Arenare F, Volpe M, Furiani S, Dell'Oro R, Mancina G.** Early sympathetic activation in the initial clinical stages of chronic renal failure. *Hypertension* 57: 846–851, 2011.
 48. **Guertzenstein PG, Silver A.** Fall in blood pressure produced from discrete regions of the ventral surface of the medulla by glycine and lesions. *J Physiol* 242: 489–503, 1974.
 49. **Hagbarth K, Vallbo ÅB.** Pulse and respiratory grouping of sympathetic impulses in human muscle nerves. *Acta Physiol Scand* 74: 96–108, 1968.
 50. **Hart EC, Joyner MJ, Wallin BG, Karlsson T, Curry TB, Charkoudian N.** Baroreflex control of muscle sympathetic nerve activity: a nonpharmacological measure of baroreflex sensitivity [Online]. *Am J Physiol Circ Physiol* 298: H816–H822, 2010.

51. **Hart ECJ, Head GA, Carter JR, Wallin G, May CN, Hamza SM, Hall JE, Charkoudian N, Osborn JW.** Recording sympathetic nerve activity in conscious humans and other mammals: guidelines and the road to standardization. *Am J Physiol Circ Physiol* 312: H1031–H1051, 2017.
52. **Hartzell HC.** Mechanisms of slow postsynaptic potentials. *Nature* 291: 539, 1981.
53. **Hodgkin AL, Huxley AF.** Action potentials recorded from inside a nerve fibre. *Nature* 144: 710, 1939.
54. **Hodgkin AL, Huxley AF.** Resting and action potentials in single nerve fibres. *J Physiol* 104: 176–195, 1945.
55. **Horn JP, Kullmann PHM.** Dynamic clamp analysis of synaptic integration in sympathetic ganglia. *Neurophysiology* 39: 423, 2007.
56. **Huggett RJ, Burns J, Mackintosh AF, Mary DASG.** Sympathetic neural activation in nondiabetic metabolic syndrome and its further augmentation by hypertension. *Hypertension* 44: 847–852, 2004.
57. **Incognito A V, Doherty CJ, Nardone M, Lee JB, Notay K, Seed JD, Millar PJ.** Evidence for differential control of muscle sympathetic single units during mild sympathoexcitation in young healthy humans. *Am J Physiol Circ Physiol* 316: H13–H23, 2018.
58. **James JEA.** The effects of changes of extramural, “intrathoracic”, pressure on aortic arch baroreceptors. *J Physiol* 214: 89–103, 1971.
59. **Janig W.** Pre- and postganglionic vasoconstrictor neurons: differentiation, types, and discharge properties. *Annu Rev Physiol* 50: 525–539, 1988.
60. **Jänig W, Krauspe R, Wiedersatz G.** Reflex activation of postganglionic vasoconstrictor neurones supplying skeletal muscle by stimulation of arterial chemoreceptors via non-nicotinic synaptic mechanisms in sympathetic ganglia. *Pflügers Arch* 396: 95–100, 1983.
61. **Jansen ASP, Van Nguyen X, Karpitskiy V, Mettenleiter TC, Loewy AD.** Central command neurons of the sympathetic nervous system: basis of the fight-or-flight response. *Science (80-)* 270: 644–646, 1995.
62. **Jones PP, Shapiro LF, Keisling GA, Jordan J, Shannon JR, Quaife RA, Seals DR.** Altered autonomic support of arterial blood pressure with age in healthy men. *Circulation* 104: 2424–2429, 2001.
63. **Julien C.** The enigma of Mayer waves: facts and models. *Cardiovasc Res* 70: 12–21, 2006.
64. **Kanda K, Burke RE, Walmsley B.** Differential control of fast and slow twitch

- motor units in the decerebrate cat. *Exp Brain Res* 29: 57–74, 1977.
65. **Karila P, Horn JP.** Secondary nicotinic synapses on sympathetic B neurons and their putative role in ganglionic amplification of activity. *J Neurosci* 20: 908–918, 2000.
 66. **Kienbaum P, Karlsson T, Sverrisdottir YB, Elam M, Wallin BG.** Two sites for modulation of human sympathetic activity by arterial baroreceptors? *J Physiol* 531: 861–869, 2001.
 67. **Kimmerly DS, O’leary DD, Shoemaker JK.** Test–retest repeatability of muscle sympathetic nerve activity: influence of data analysis and head-up tilt [Online]. *Auton Neurosci* 114: 61–71, 2004.
 68. **Kimmerly DS, Shoemaker JK.** Hypovolemia and neurovascular control during orthostatic stress [Online]. *Am J Physiol Circ Physiol* 282: H645–H655, 2002.
 69. **Klassen SA, De Abreu S, Greaves DK, Kimmerly DS, Arbeille P, Denise P, Hughson RL, Normand H, Shoemaker JK.** Long-duration bed rest modifies sympathetic neural recruitment strategies in males and females. *J Appl Physiol* 124: 769–779, 2017.
 70. **Klassen SA, Chirico D, Dempster KS, Shoemaker JK, O’Leary DD.** The role of aortic arch vascular mechanics in cardiovascular baroreflex sensitivity. *Am J Physiol Integr Comp Physiol* 311: R24–R32, 2016.
 71. **Klassen SA, Limberg JK, Baker SE, Nicholson WT, Curry TB, Joyner MJ, Shoemaker JK.** The role of the paravertebral ganglia in human sympathetic neural discharge patterns. *J Physiol* 596: 4497–4510, 2018.
 72. **Klassen SA, Moir ME, Limberg JK, Baker SE, Nicholson WT, Curry TB, Joyner MJ, Shoemaker JK.** Asynchronous action potential discharge in human muscle sympathetic nerve activity [Online]. *Am. J. Physiol. Circ. Physiol.* <https://doi.org/10.1152/ajpheart.00258>. 2019.
 73. **Leimbach Jr WN, Wallin BG, Victor RG, Aylward PE, Sundlöf G, Mark AL.** Direct evidence from intraneural recordings for increased central sympathetic outflow in patients with heart failure. *Circulation* 73: 913–919, 1986.
 74. **Limberg JK, Ott EP, Holbein WW, Baker SE, Curry TB, Nicholson WT, Joyner MJ, Shoemaker JK.** Pharmacological Assessment of the Contribution of the Arterial Baroreflex to Sympathetic Discharge Patterns in Healthy Humans. *J Neurophysiol.* 119: 2166-2175, 2018.
 75. **Lipski J, Kanjhan R, Kruszevska B, Rong W.** Properties of presympathetic neurones in the rostral ventrolateral medulla in the rat: an intracellular study" in vivo'. *J Physiol* 490: 729–744, 1996.

76. **Llewellyn-Smith IJ.** Anatomy of synaptic circuits controlling the activity of sympathetic preganglionic neurons. *J Chem Neuroanat* 38: 231–239, 2009.
77. **Lodish H, Berk A, Zipursky SL, Matsudaira P, Baltimore D, Darnell J.** The action potential and conduction of electric impulses. In: *Molecular Cell Biology. 4th edition.* WH Freeman, 2000.
78. **Macefield VG, Henderson LA.** “Real-time” imaging of cortical and subcortical sites of cardiovascular control: concurrent recordings of sympathetic nerve activity and fMRI in awake subjects. *J Neurophysiol* 116: 1199–1207, 2016.
79. **Macefield VG, Wallin BG.** Firing properties of single vasoconstrictor neurones in human subjects with high levels of muscle sympathetic activity. *J Physiol* 516: 293–301, 1999.
80. **Macefield VG, Wallin BG.** Physiological and pathophysiological firing properties of single postganglionic sympathetic neurons in humans. *J Neurophysiol* 119: 944–956, 2017.
81. **Macefield VG, Wallin BG, Vallbo AB.** The discharge behaviour of single vasoconstrictor motoneurons in human muscle nerves. *J Physiol* 481: 799–809, 1994.
82. **Malpas SC, Bendle RD, Head GA, Ricketts JH.** Frequency and amplitude of sympathetic discharges by baroreflexes during hypoxia in conscious rabbits. *Am J Physiol Circ Physiol* 271: H2563–H2574, 1996.
83. **Malpas SC, Coote JH.** Role of vasopressin in sympathetic response to paraventricular nucleus stimulation in anesthetized rats. *Am J Physiol Integr Comp Physiol* 266: R228–R236, 1994.
84. **McLachlan EM.** Transmission of signals through sympathetic ganglia—modulation, integration or simply distribution? *Acta Physiol* 177: 227–235, 2003.
85. **Millar PJ, Murai H, Morris BL, Floras JS.** Microneurographic evidence in healthy middle-aged humans for a sympathoexcitatory reflex activated by atrial pressure. *Am J Physiol Circ Physiol* 305: H931–H938, 2013.
86. **Mueller PJ, Clifford PS, Crandall CG, Smith SA, Fadel PJ.** Integration of central and peripheral regulation of the circulation during exercise: acute and chronic adaptations. *Compr Physiol* 8: 103–151, 2011.
87. **Narkiewicz K, Phillips BG, Kato M, Hering D, Bieniaszewski L, Somers VK.** Gender-selective interaction between aging, blood pressure, and sympathetic nerve activity. *Hypertension* 45: 522–525, 2005.
88. **Ott EP, Baker SE, Holbein WW, Shoemaker JK, Limberg JK.** Effect of varying chemoreflex stress on sympathetic neural recruitment strategies during

- apnea. *J. Neurophysiol.* doi.org/10.1152/jn.00319.2019.
89. **Parati G, Di Rienzo M, Mancia G.** How to measure baroreflex sensitivity: from the cardiovascular laboratory to daily life. *J Hypertens* 18: 7–19, 2000.
 90. **Piasek MT, Soltis EE, Piasek MM, Macmillan LB.** α -Adrenoceptors and vascular regulation: molecular, pharmacologic and clinical correlates. *Pharmacol Ther* 72: 215–241, 1996.
 91. **Pumphrey RJ, Young JZ.** The rates of conduction of nerve fibres of various diameters in cephalopods. *J Exp Biol* 15: 453–466, 1938.
 92. **Purves D, Augustine GJ, Fitzpatrick D, Katz LC, Lamantia A-S, McNamara JO, Williams SM.** Neuroscience. 2nd. *Sunderland, MA Sinauer Assoc.* 2001.
 93. **Purves D, Lichtman JW.** Geometrical differences among homologous neurons in mammals. *Science (80-)* 228: 298–302, 1985.
 94. **Purves D, Rubin E, Snider WD, Lichtman J.** Relation of animal size to convergence, divergence, and neuronal number in peripheral sympathetic pathways. *J Neurosci* 6: 158–163, 1986.
 95. **Raven PB, Young BE, Fadel PJ.** Arterial Baroreflex Resetting During Exercise in Humans: Underlying Signaling Mechanisms. *Exerc Sport Sci Rev* 47: 129–141, 2019.
 96. **Rimmer K, Horn JP.** Weak and straddling secondary nicotinic synapses can drive firing in rat sympathetic neurons and thereby contribute to ganglionic amplification. *Front Neurol* 1, 2010.
 97. **Van Rossum JM.** Classification and molecular pharmacology of ganglionic blocking agents: Part II Mode of action of competitive and non-competitive ganglionic blocking agents. *Int J Neuropharmacol* 1: 403–421, 1962.
 98. **Salmanpour A, Brown LJ, Shoemaker JK.** Spike detection in human muscle sympathetic nerve activity using a matched wavelet approach [Online]. *J Neurosci Methods* 193: 343–355, 2010.
 99. **Salmanpour A, Brown LJ, Steinback CD, Usselman CW, Goswami R, Shoemaker JK.** Relationship between size and latency of action potentials in human muscle sympathetic nerve activity [Online]. *J Neurophysiol* 105: 2830–2842, 2011.
 100. **Salmanpour A, Frances MF, Goswami R, Shoemaker JK.** Sympathetic neural recruitment patterns during the Valsalva maneuver. In: *2011 Annual International Conference of the IEEE Engineering in Medicine and Biology Society.* IEEE, 2011, p. 6951–6954.

101. **Salmanpour A, Shoemaker JK.** Baroreflex mechanisms regulating the occurrence of neural spikes in human muscle sympathetic nerve activity [Online]. *J Neurophysiol* 107: 3409–3416, 2012.
102. **Scott DW.** On optimal and data-based histograms. *Biometrika* 66: 605–610, 1979.
103. **Shoemaker JK.** Recruitment strategies in efferent sympathetic nerve activity. *Clin Auton Res* 27: 369–378, 2017.
104. **Shoemaker JK, Badrov MB, Al-Khazraji BK, Jackson DN.** Neural Control of Vascular Function in Skeletal Muscle. *Compr Physiol* 6: 303–329, 2016.
105. **Shoemaker JK, Goswami R.** Forebrain neurocircuitry associated with human reflex cardiovascular control. *Front Physiol* 6, 2015.
106. **Shoemaker JK, Klassen SA, Badrov MB, Fadel PJ.** Fifty years of microneurography: learning the language of the peripheral sympathetic nervous system in humans. *J Neurophysiol* 119: 1731–1744, 2018.
107. **Smit AAJ, Halliwill JR, Low PA, Wieling W.** Pathophysiological basis of orthostatic hypotension in autonomic failure. *J Physiol* 519: 1–10, 1999.
108. **Somers VK, Dyken ME, Clary MP, Abboud FM.** Sympathetic neural mechanisms in obstructive sleep apnea. *J Clin Invest* 96: 1897–1904, 1995.
109. **Spyer KM.** Annual review prize lecture. Central nervous mechanisms contributing to cardiovascular control. *J Physiol* 474: 1–19, 1994.
110. **Steinback CD, Salmanpour A, Breskovic T, Dujic Z, Shoemaker JK.** Sympathetic neural activation: an ordered affair. *J Physiol* 588: 4825–4836, 2010.
111. **Steinback CD, Salzer D, Medeiros PJ, Kowalchuk J, Shoemaker JK.** Hypercapnic vs. hypoxic control of cardiovascular, cardiovagal, and sympathetic function. *Am J Physiol Integr Comp Physiol* 296: R402–R410, 2009.
112. **Strack AM, Sawyer WB, Hughes JH, Platt KB, Loewy AD.** A general pattern of CNS innervation of the sympathetic outflow demonstrated by transneuronal pseudorabies viral infections. *Brain Res* 491: 156–162, 1989.
113. **Strack AM, Sawyer WB, Marubio LM, Loewy AD.** Spinal origin of sympathetic preganglionic neurons in the rat. *Brain Res* 455: 187–191, 1988.
114. **Sun M-K, Hackett JT, Guyenet PG.** Sympathoexcitatory neurons of rostral ventrolateral medulla exhibit pacemaker properties in the presence of a glutamate-receptor antagonist. *Brain Res* 438: 23–40, 1988.
115. **Sun M-K, Young BS, Hackett JT, Guyenet PG.** Reticulospinal pacemaker neurons of the rat rostral ventrolateral medulla with putative sympathoexcitatory

- function: an intracellular study in vitro. *Brain Res* 442: 229–239, 1988.
116. **Sundlöf G, Wallin BG.** Human muscle nerve sympathetic activity at rest. Relationship to blood pressure and age. *J Physiol* 274: 621–637, 1978.
 117. **Sundlöf G, Wallin BG.** Effect of lower body negative pressure on human muscle nerve sympathetic activity. *J Physiol* 278: 525–532, 1978.
 118. **Surprenant A, North RA.** Signaling at purinergic P2X receptors. *Annu Rev Physiol* 71: 333–359, 2009.
 119. **Sverrisdóttir YB, Rundqvist B, Johannsson G, Elam M.** Sympathetic Neural Burst Amplitude Distribution A More Specific Indicator of Sympathoexcitation in Human Heart Failure [Online]. *Circulation* 102: 2076–2081, 2000.
 120. **Tan CO, Taylor JA, Ler ASH, Cohen MA.** Detection of multifiber neuronal firings: a mixture separation model applied to sympathetic recordings. *IEEE Trans Biomed Eng* 56: 147–158, 2009.
 121. **Tasaki I, Matsumoto G.** On the cable theory of nerve conduction. *Bull Math Biol* 64: 1069, 2002.
 122. **Taylor JA, Halliwill JR, Brown TE, Hayano J, Eckberg DL.** “Non-hypotensive” hypovolaemia reduces ascending aortic dimensions in humans. *J Physiol* 483: 289–298, 1995.
 123. **Tomaszewski KA, Graves MJ, Henry BM, Popieluszko P, Roy J, Pękala PA, Hsieh WC, Vikse J, Walocha JA.** Surgical anatomy of the sciatic nerve: A meta-analysis. *J Orthop Res* 34: 1820–1827, 2016.
 124. **Tompkins RPR, Melling CWJ, Wilson TD, Bates BD, Shoemaker JK.** Arrangement of sympathetic fibers within the human common peroneal nerve: implications for microneurography [Online]. *J Appl Physiol* 115: 1553–1561, 2013.
 125. **Vallbo ÅB, Hagbarth K-E, Wallin BG.** Microneurography: how the technique developed and its role in the investigation of the sympathetic nervous system [Online]. *J Appl Physiol* 96: 1262–1269, 2004.
 126. **Varon J, Marik PE.** The diagnosis and management of hypertensive crises. *Chest* 118: 214–227, 2000.
 127. **Vera PL, Hurwitz BE, Schneiderman N.** Sympathoadrenal preganglionic neurons in the adult rabbit send their dendrites into the contralateral hemicord. *J Auton Nerv Syst* 30: 193–198, 1990.
 128. **Verberne AJM, Owens NC.** Cortical modulation of the cardiovascular system. *Prog Neurobiol* 54: 149–168, 1998.

129. **Volle RL.** Modification by drugs of synaptic mechanisms in autonomic ganglia. *Pharmacol Rev* 18: 839–869, 1966.
130. **Wallin BG, Burke D, Gandevia S.** Coupling between variations in strength and baroreflex latency of sympathetic discharges in human muscle nerves. *J Physiol* 474: 331, 1994.
131. **Wallin BG, Charkoudian N.** Sympathetic neural control of integrated cardiovascular function: insights from measurement of human sympathetic nerve activity. *Muscle Nerve* 36: 595–614, 2007.
132. **Wehrwein EA, Orer HS, Barman SM.** Overview of the anatomy, physiology, and pharmacology of the autonomic nervous system. *Compr. Physiol.* 6: 1239–1278, 2011.
133. **Westcott EB, Segal SS.** Perivascular innervation: a multiplicity of roles in vasomotor control and myoendothelial signaling. *Microcirculation* 20: 217–238, 2013.
134. **White DW, Shoemaker JK, Raven PB.** Methods and considerations for the analysis and standardization of assessing muscle sympathetic nerve activity in humans [Online]. *Auton Neurosci* 193: 12–21, 2015.
135. **Wilkins BW, Hesse C, Charkoudian N, Nicholson WT, Sviggum HP, Moyer TP, Joyner MJ, Eisenach JH.** Autonomic cardiovascular control during a novel pharmacologic alternative to ganglionic blockade. *Clin Pharmacol Ther* 83: 692–701, 2008.
136. **Wolthuis RA, Bergman SA, Nicogossian AE.** Physiological effects of locally applied reduced pressure in man [Online]. *Physiol Rev* 54: 566–595, 1974.
137. **Yoshimura M, Polosa C, Nishi S.** Noradrenaline induces rhythmic bursting in sympathetic preganglionic neurons. *Brain Res* 420: 147–151, 1987.
138. **Zhou J-J, Ma H-J, Shao J-Y, Pan H-L, Li D-P.** Impaired hypothalamic regulation of sympathetic outflow in primary hypertension. *Neurosci Bull* 35: 124–132, 2019.

Chapter 2

2 The role of the paravertebral ganglia in human sympathetic neural discharge patterns

Published in The Journal of physiology: 596(18), 4497-4510, 2018.

2.1 Introduction

The ganglia determine the extent to which the sympathetic nervous system communicates central intentions to the peripheral vasculature supplying skeletal muscle (13). The ganglia participate in spatial amplification of efferent sympathetic outflow through synaptic divergence of a distribution of primary “strong” synapses (19, 35). Also, patterns of pre-to-postganglionic convergent innervation have been observed in rodent and amphibian models (41, 52). As the degree of convergence appears to scale with neuron size in mammals (39, 40), it would be expected to add greater complexity to the temporal and spatial summation of excitatory post-synaptic potentials (EPSP).

The synchronization of differently-sized action potentials (AP) into bursts of activity represents a fundamental characteristic of sympathetic activity, readily observed in neurograms of sympathetic nerve activity directed towards the vasculature of skeletal muscle (MSNA). Furthermore, multi-unit and single-unit recordings of axonal firing patterns within MSNA bursts have revealed additional layers of complexity regarding communication strategies contained within the sympathetic neural signal in humans (31, 47, 51). For instance, under baseline conditions, recruited axons fire with relatively low probability [e.g., 21% of cardiac cycles (32)]. In addition, multi-unit AP recordings show that as a population, firing probabilities of differently-sized APs (probably not the same axon) tend to vary with AP size in an inverted “U” manner, such that the smallest AP

clusters and largest AP clusters express low within-burst probabilities whereas moderately-sized AP clusters are expressed frequently, with some occurring in every burst (28, 45, 54). Furthermore, acute homeostatic challenges (e.g., apneic, metabolic, and orthostatic stress) reveal an orderly recruitment strategy where the sympathetic system expresses options of increasing the firing probability of already-active APs and, in high stress, recruitment of a subpopulation of latent, larger and faster-conducting APs (2, 43, 54). Further, the timing of a recruited AP may be modified by synaptic delays (11, 61): a feature which we hypothesize to be mediated in part, by perceptual mechanisms (3, 26, 44). These ordered patterns of postganglionic AP behaviour and recruitment infer heterogeneous regulation of sympathetic neurons. However, the neural sites within reflex arcs and/or descending sympathetic pathways that exert influence over these discharge patterns remain uncertain.

Even at the level of the integrated sympathetic signal, the neural circuitry involved in MSNA control remains unclear. While the brainstem network forming the arterial baroreflex represents perhaps the most thoroughly studied site of sympathetic regulation, contributing to the pulse-synchronous “bursty” nature of the signal (53), evidence also points towards baroreflex-independent pathways as a source of MSNA patterns, especially fluctuations in burst amplitude, which are dependent on AP content (23, 33). For example, supra-medullary sites are involved in regulating sympathetic outflow (4, 15, 25, 48, 57), including the variability in burst size (56). To date, however, few investigations have studied the contribution of other, non-baroreflex sites within the sympathetic system, to patterns of sympathetic discharge, such as spinal (55) or ganglionic mechanisms.

This study tested the hypothesis that the paravertebral ganglia contribute to ordered patterns of sympathetic AP discharge at baseline in humans. To address this hypothesis, we examined the impact of paravertebral ganglionic blockade (via intravenous trimethaphan camsylate) on multifibre recordings with microneurography at the peroneal nerve in female participants.

2.2 Methods

2.2.1 Ethical Approval

All procedures were approved by the Mayo Clinic Institutional Review Board (No. 09-008548) and the study conformed to the standards set by the Declaration of Helsinki, except for registration in a database. All participants provided written, informed consent after receiving verbal and written instructions outlining the experimental protocol.

2.2.2 Participants

This study evaluated data from seven healthy females (37 ± 5 years, 165 ± 2 cm, 60 ± 4 kg, 22 ± 1 kg/m², 25 ± 3 % body fat). On a separate day prior to the testing session, participants performed health screening to determine that all fit study inclusion/exclusion criteria: non-smoker, systolic blood pressure (BP) <150 mmHg, diastolic BP <95 mmHg, body mass index <30 kg/m², and no history of diabetes or cardiovascular diseases. All participants provided a negative pregnancy test result within 48 h. Pre-menopausal women ($n = 5$) were tested in the early follicular stage of the menstrual cycle (days 2-6 of menses) or the placebo phase for young women on oral contraceptives ($n = 2$, participant identifiers TM59 and TM63, both taking levonorgestrel and ethinyl estradiol). No other

participants were taking medications. Two participants were post-menopausal ($n = 2$, participant identifiers TM32 and TM50, 7 and 6 years since last menses, respectively).

2.2.3 Experimental Procedures

Participants arrived at the laboratory after an overnight fast and refraining from heavy exercise, caffeine, and alcohol for 24 h before the study. Participants assumed the supine position for instrumentation and data collection. After local anesthetic with 2% lidocaine, a 5-cm 20-gauge arterial catheter was placed in the brachial artery of the non-dominant arm, using aseptic technique. The catheter was connected to a pressure transducer, positioned at heart level to record continuous arterial BP. A 3-lead electrocardiogram (ECG) recorded continuous heart rate (HR). Research personnel placed an intravenous catheter in the contralateral arm for drug infusion.

2.2.4 Experimental Design

Data were collected during baseline and the trimethaphan camsylate infusion (1-7 mg/min; Cambridge Laboratories, Wallsend, United Kingdom). Trimethaphan infusion rate was adjusted over time, though this varied across participants. During the trimethaphan infusion, once cessation of integrated MSNA burst activity occurred, participants were instructed to perform a 20 s Valsalva's Manoeuvre with an expiratory mouth pressure of 40 mmHg. After discontinuation of the study and de-instrumentation, subjects remained in the Clinical Research Unit for ≥ 2 hours for observation.

Data analysis was conducted for four study conditions: 1) 5-min baseline (309 ± 28 s), 2) minute-by-minute of the trimethaphan infusion where integrated sympathetic bursts *were visible* and AP analysis could be performed [note that the last "minute" was 89 ± 17 s to

provide a suitable number of bursts for analysis], 3) two minutes (120 ± 0 s) of the trimethaphan infusion where sympathetic bursts *were not visible*, and 4) a Valsalva's Manoeuvre performed during the trimethaphan infusion where sympathetic bursts *were not visible* (23 ± 7 s).

2.2.5 Experimental Measures and Analysis

Efferent multiunit MSNA was measured from postganglionic C-fibres in the peroneal nerve by microneurography (14) as detailed recently (26). Integrated bursts of MSNA were analyzed if they were pulse-synchronous, had a signal-to-noise ratio of at least 2:1 relative to the previous period of neural silence, and expressed characteristic rising and falling slopes. MSNA bursts were inspected for consistent amplitude to rule out shifts in microelectrode position.

At the integrated level, sympathetic activity was quantified as burst frequency (bursts/min) and burst incidence (bursts/100 heartbeats). Burst amplitude (AU) was measured in volts and normalized to the max burst amplitude at baseline, which was given a value of 100. Total MSNA (AU/min) was measured as the product of burst frequency and amplitude. Sympathetic burst latency was measured as the mean time interval (s) from the preceding ECG R-wave, to the peak of the corresponding MSNA burst in the integrated neurogram (12).

Postganglionic sympathetic APs were detected and extracted from the filtered raw MSNA signal using a continuous wavelet transform, which has been described in detail previously (42). At baseline and during trimethaphan infusion where integrated bursts were visible, APs were only extracted if they occurred within an integrated burst (i.e.,

0.8s around the peak of the burst). Alternatively, during trimethaphan infusion where integrated bursts were no longer visible, any AP that occurred was extracted. With both techniques, extracted APs were ordered based on peak-to-peak amplitude, and histogram analysis was performed to separate APs into amplitude-based clusters. Cluster bin widths for baseline data were automatically defined based on Scott's rule which balanced bin width, data bias and variance to minimize the integrated mean square error (46). Thus, the number of total clusters at baseline varied by participant. AP data collected during the different periods of the trimethaphan infusion (i.e., MSNA bursting period, non-bursting period, and Valsalva's Manoeuvre) were normalized to baseline for each participant to ensure that bin width, maximum bin centre, and the total number of bins would be identical across conditions. APs that were not detected during trimethaphan were considered de-recruited from baseline. The signal-to-noise ratio was determined as the amplitude of the negative peak of the mean AP over the standard deviation of the background noise. Based on our previous simulations, the signal-to-noise ratio of the multi-unit AP signal obtained at baseline (4.2 ± 0.7) and during trimethaphan (4.2 ± 0.5) was expected to produce a correct detection rate of $> 90\%$ and a false positive rate of $< 3\%$ (42).

AP indices included AP frequency (APs/minute), incidence (APs/100 beats), and the mean AP content per integrated burst. Also, the number of total clusters detected and the number of active clusters per integrated burst were assessed. AP latency was determined as the time delay from the R-wave of the preceding cardiac cycle to the negative peak of the AP (44). AP cluster latency was determined as the mean latency of all APs within a cluster. AP cluster firing probability distributions were constructed to evaluate the firing

probability of each sympathetic AP cluster at baseline and the final minute of bursting activity during the trimethaphan infusion. To do so, we divided the number of times an AP cluster fired by the total number of bursts that occurred in a given condition, multiplied by 100%. A probability of 100% indicates that the cluster fired once in every integrated burst, whereas a probability of less than, or greater than, 100% indicates that the cluster was not active in every burst, or occasionally fired more than once per burst, respectively.

HR and BP were collected at 1,000 Hz. The mean values for HR and mean arterial pressure (MAP) were calculated for all conditions. All signals were sampled using PowerLab (ADInstruments; Castle Hill, New South Wales, Australia) and stored on a computer for subsequent analysis. Researchers were not blinded during analysis.

2.2.6 Statistical Analysis

This study tested the hypothesis that the ganglia contribute to patterns of postganglionic sympathetic AP discharge at baseline in humans. All data are presented as mean \pm SD. Due to the inter-individual variability in magnitude and time course of the nicotinic blockade, minute-by-minute changes in all sympathetic indices with trimethaphan infusion were not evaluated statistically. Accordingly, paired sample *t*-tests were employed to assess differences between: 1) baseline versus the last minute of bursting activity during the trimethaphan infusion, and 2) the non-bursting period of the trimethaphan infusion versus the responses to Valsalva's Manoeuvre. For AP clusters expressing trimethaphan-resistance, a repeated-measures analysis of variance (RM ANOVA) assessed changes in AP incidence across baseline, the last minute of the trimethaphan infusion with visible bursts, and the period of the trimethaphan infusion

without visible bursts. Linear regression was performed to assess the relationship between normalized integrated burst amplitude and AP content per burst. Statistical analysis was performed using SPSS (v 23, SPSS Inc., Chicago, IL). Tests were two tailed with $\alpha = 0.05$. Each unique symbol represents the same participant's data across figures depicting individual data.

2.3 Results

Fig. 2.1 illustrates one participant's response to trimethaphan infusion, particularly the reductions in integrated bursting activity (Fig. 2.1 A1) and the discharge patterns of sympathetic AP clusters during drug infusion (Fig. 2.1 A2). These results compare baseline to the last minute of visible bursting activity that was suitable for AP analysis during the trimethaphan infusion, unless specified otherwise. The mean time from infusion start to burst cessation was 523 ± 242 s. At this time, the infusion rate was 2 ± 1 mg/min. Trimethaphan infusion was associated with an increase in HR (baseline versus final minute of trimethaphan condition with MSNA bursts: 57 ± 11 to 66 ± 12 bpm, $P < 0.01$) and a reduction in MAP (97 ± 7 to 90 ± 7 mmHg, $P < 0.01$) compared to baseline (Fig. 2.2). Relative to baseline, trimethaphan elicited a progressive reduction in total sympathetic outflow (833 ± 458 to 157 ± 120 AU/min, $P < 0.01$), characterized by fewer integrated bursts (burst frequency: 17 ± 9 to 5 ± 4 bursts/min, $P = 0.01$; burst incidence: 30 ± 14 to 9 ± 8 bursts/100beats, $P < 0.01$) with decaying amplitude (49 ± 3 to 31 ± 3 AU, $P < 0.01$) (Fig. 2.3). Underlying trimethaphan-mediated attenuations in the integrated MSNA signal were reductions in AP frequency (104 ± 65 to 17 ± 17 AP/min, $P = 0.01$) and incidence (186 ± 101 to 29 ± 31 AP/100beats, $P < 0.01$) as well as attenuated AP

content per integrated burst (7 ± 2 to 3 ± 1 AP/burst, $P < 0.01$) (Fig. 2.4). When detected APs were binned according to peak-to-peak amplitude, the total number of active AP clusters was reduced with trimethaphan (14 ± 3 to 8 ± 2 , $P < 0.01$), resulting in fewer unique clusters firing per burst (4 ± 1 to 3 ± 1 clusters/burst, $P < 0.01$) (Fig. 2.4).

Trimethaphan infusion did not affect the latency of MSNA bursts (1.25 ± 0.05 to 1.22 ± 0.05) or APs (1.18 ± 0.06 to 1.16 ± 0.07 s) (both $P > 0.12$).

Closer analysis of the within-burst AP cluster firing patterns revealed a distribution of firing probabilities that scaled to AP cluster size in an inverted “U” manner. At baseline, moderately-sized clusters fired with high probability (i.e., approximately every burst), whereas the smallest AP clusters and largest AP clusters expressed low within-burst probabilities across all participants. In the last minute of visible bursting activity during the trimethaphan infusion, participants demonstrated a reduction in the firing probability of the majority of AP clusters with the largest AP clusters (range: 4 to 10 largest clusters) ceasing to fire, moderately-sized cluster firing displaying moderate declines in probability, and generally no change in the activity of smaller clusters. Firing probability distributions for each participant (Fig. 2.5A) enable visualization of the between-subject variability in active cluster number and the extent of large cluster de-recruitment with trimethaphan, whereas, the group averaged normalized distributions (Fig. 2.5B) show a similar pattern of reduced cluster firing probability with trimethaphan but allow statistical comparisons between baseline and trimethaphan.

At baseline, AP cluster latency decreased as a function of normalized cluster number (i.e., as peak-to-peak AP cluster amplitude increased) ($R^2 = 0.67$, $P < 0.01$). Because

trimethaphan abolished the firing of the largest clusters, the AP cluster latency-size relationship was examined for the entire condition (i.e., from infusion start until the last minute of visible bursting activity) and was not restricted to the final minute of bursting activity. Here, the same general pattern was observed, but did not reach significance ($R^2 = 0.28$, $P = 0.11$). The mean AP cluster latency-size responses were fitted using an exponential decay function (Fig. 2.6). These relationships support the concept that AP cluster size scaled to the diameter of sympathetic C-fibres within the recording field of the micro-electrode.

At baseline, linear regression indicated moderate-to-strong relationships between relative integrated burst size and the number of APs per burst ($y = 0.14 \pm 0.05x - 0.37 \pm 0.55$, $r^2 = 0.57 \pm 0.17$, all $P < 0.01$), normalized integrated burst amplitude and AP clusters per burst ($y = 0.05 \pm 0.02x + 1.64 \pm 0.31$, $r^2 = 0.37 \pm 0.21$, all $P < 0.01$), and the number of AP clusters per burst and the number of APs per burst ($y = 0.33 \pm 0.05x + 1.78 \pm 0.13$, $r^2 = 0.60 \pm 0.13$, all $P < 0.01$). In the last minute of visible bursting activity during the trimethaphan infusion, the same fundamental relationships were observed, though these were not significant in all participants (integrated burst size vs. the number of APs per burst: $y = 0.12 \pm 0.08x + 0.02 \pm 3.3$, $r^2 = 0.30 \pm 0.25$, $P < 0.05$ in $n = 3$ of 7 participants, normalized integrated burst amplitude vs. AP clusters per burst: $y = 0.04 \pm 0.05x + 1.65 \pm 2.0$, $r^2 = 0.19 \pm 0.16$, $P < 0.05$ in $n = 2$ of 7 participants, and the number of AP clusters per burst vs. the number of APs per burst: $y = 0.36 \pm 0.25x + 1.28 \pm 0.62$, $r^2 = 0.56 \pm 0.33$, $P < 0.05$ in $n = 5$ of 7 participants). Figure 2.7 illustrates these relationships for one participant.

During the period of the trimethaphan infusion where integrated bursts were no longer visible (120 ± 0 s, 80 ± 6 bpm, MAP: 87 ± 12 mmHg), we observed the discharge of a population of trimethaphan-resistant APs. In all seven individuals, these APs were the smallest 6 ± 2 sympathetic AP clusters (range: 4 – 8 AP clusters) present at baseline, firing in an asynchronous pattern (i.e., visual inspection showed no apparent baroreflex-mediated pulse rhythmicity) with a frequency of 38 ± 32 AP/min (49 ± 41 AP/100beats) (Figure 1 B1 and B2). Compared to baseline (118 ± 61 APs/100beats), trimethaphan-resistant clusters (i.e., not clusters de-recruited by trimethaphan), demonstrated reduced incidence in the last minute of visible bursts during trimethaphan infusion (26 ± 24 APs/100beats, simple-effects paired *t*-test: $P < 0.01$) as well as during the period of the trimethaphan infusion without visible bursts (49 ± 41 APs/100beats, simple-effects paired *t*-test: $P < 0.05$; RM ANOVA: $P < 0.05$). There were no differences in the incidence of trimethaphan resistant clusters between the final minute of visible bursts during trimethaphan and the period of the trimethaphan without visible bursts (simple-effects paired *t*-test: $P > 0.3$).

While trimethaphan infusion continued, research personnel instructed participants to perform a Valsalva's Manoeuvre. Valsalva's Manoeuvre (28 ± 9 and 24 ± 7 mmHg reduction in MAP and PP, respectively, from baseline to phase II, both $P < 0.01$) failed to elicit integrated MSNA bursts in six of seven participants. When examining the data from the six individuals with absent MSNA responses to Valsalva's Manoeuvre only, compared to the period of the trimethaphan infusion where trimethaphan-resistant APs were observed, but integrated bursts were not visible (38 ± 32 AP/min; 49 ± 41 APs/100beats), the Valsalva's Manoeuvre did not increase the firing frequency of

trimethaphan-resistant APs (49 ± 32 AP/min, 60 ± 42 AP/100beats; both $P > 0.30$, both $d \leq 0.21$, $n = 6$), nor were additional larger APs recruited (6 ± 1 clusters, $P = 0.30$, $n = 6$).

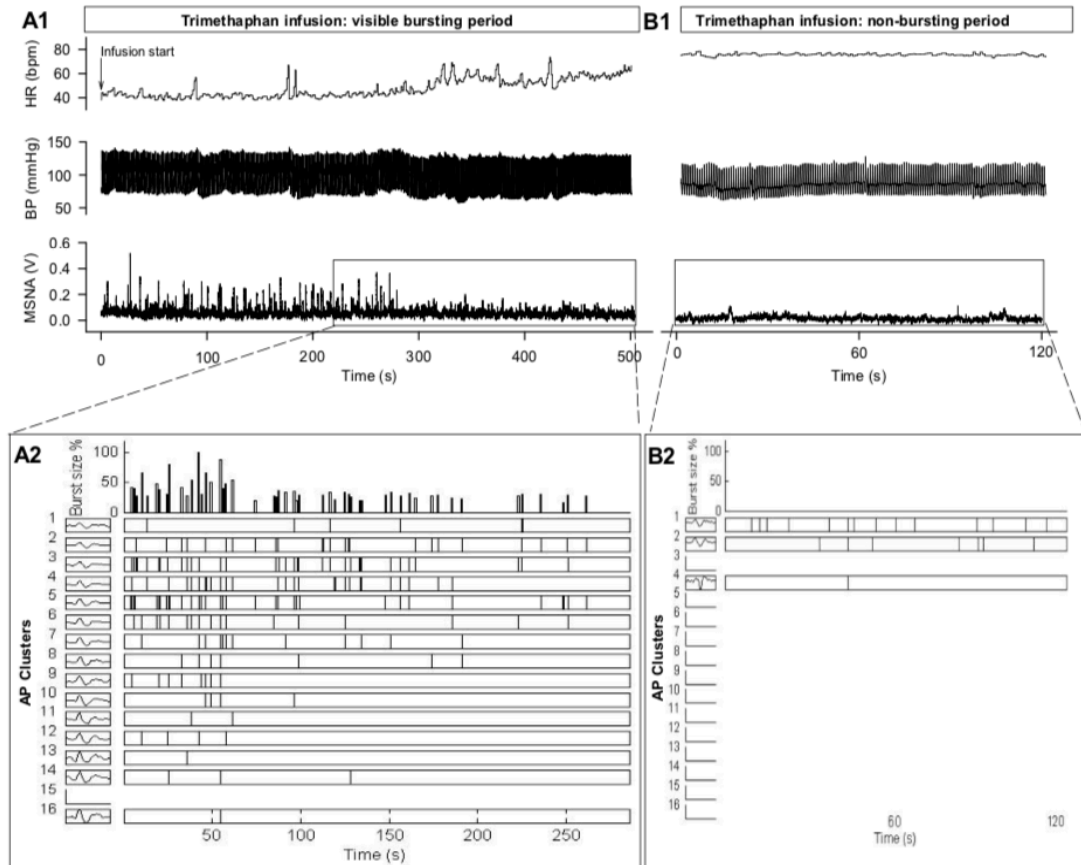


Figure 2.1 Representative recordings of heart rate (HR), blood pressure (BP), and the integrated muscle sympathetic nerve activity (MSNA) neurogram from one individual. Data were collected during the trimethaphan infusion where integrated MSNA bursts were detected (A1) and during the trimethaphan infusion where integrated MSNA bursts were no longer visible (B1). The associated pattern of action potential (AP) activity during the trimethaphan infusion where integrated MSNA bursts were detected (A2) and during the trimethaphan infusion where integrated MSNA bursts were no longer visible (B2) is illustrated. *A2*: AP occurrence within each burst as a function of their cluster (illustrated along the left). Cluster refers to all APs of similar morphology. *B2*: Because no bursts were detected, all AP activity was extracted and presented as a function of their cluster. APs extracted during trimethaphan infusion were normalized to baseline.

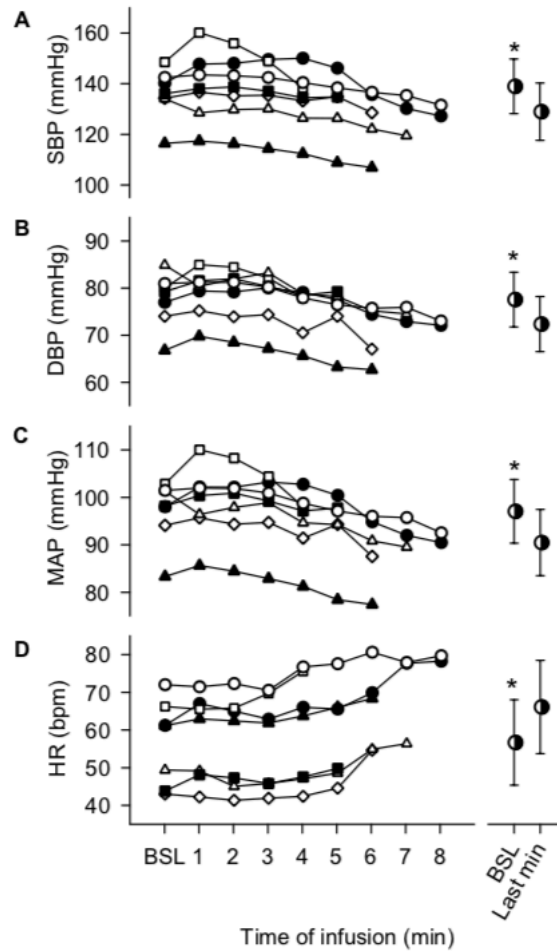


Figure 2.2 Systolic (SBP; A), diastolic (DBP; B), mean arterial pressure (MAP; C), and heart rate (HR; D) at baseline (BSL) and during each minute of the trimethaphan infusion where integrated sympathetic bursts were visible. Minute-by-minute data are presented by line graphs with each unique symbol representing the same participant's data across figures depicting individual data. Mean \pm SD for BSL and the last minute of detectable integrated sympathetic bursting activity during the trimethaphan infusion (Last min) are represented by half-filled circles and error bars. *, indicates significantly different from Last min, $P < 0.01$.

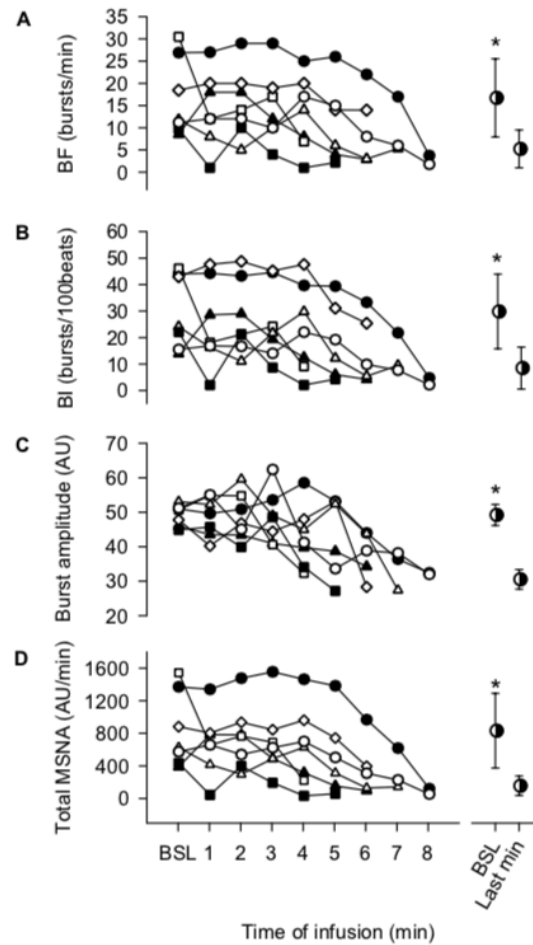


Figure 2.3 Integrated muscle sympathetic nerve activity (MSNA) burst frequency (BF; A), burst incidence (BI; B), normalized burst amplitude (C), and total activity (D) at baseline (BSL) and during each minute of the trimethaphan infusion where integrated sympathetic bursts were visible. Minute-by-minute data are presented by line graphs with each unique symbol representing the same participant's data across figures depicting individual data. Mean \pm SD for baseline and the last minute of detectable integrated sympathetic bursting activity during the trimethaphan infusion (Last min) are represented by half-filled circles and error bars. *, indicates significantly different from Last min, $P < 0.01$.

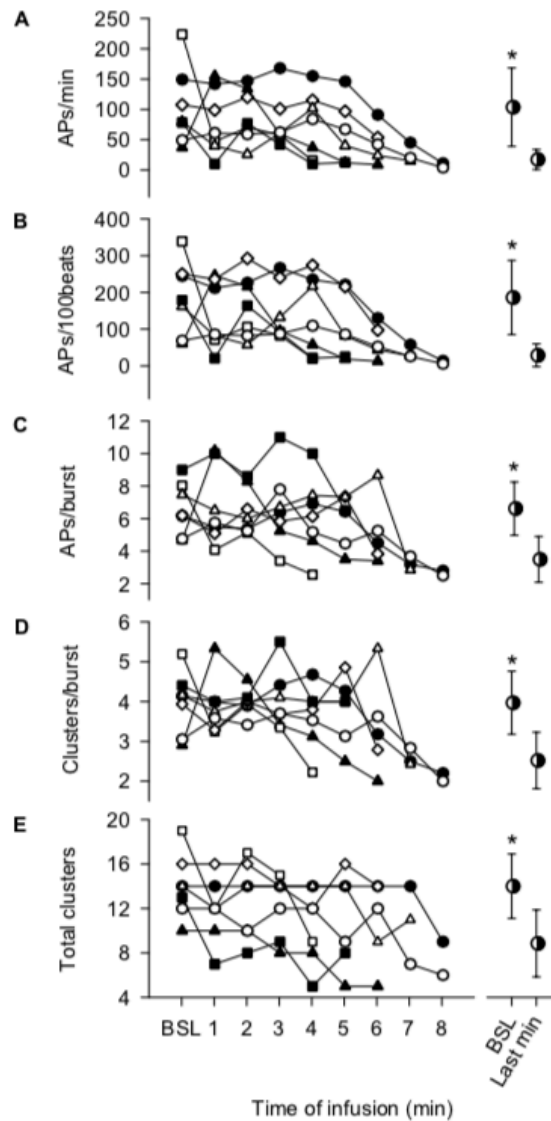


Figure 2.4 Sympathetic action potential (AP) frequency (A), AP incidence (B), APs per burst (C), AP clusters per burst (D), and total AP clusters (E) at baseline (BSL) and during each minute of the trimethaphan infusion during the period where integrated sympathetic bursts were visible. Minute-by-minute data are presented by line graphs with each unique symbol representing the same participant's data across figures depicting individual data. Mean \pm SD for baseline and the last minute of detectable integrated sympathetic bursting activity during the trimethaphan infusion (Last min) are represented by half-filled circles and error bars. *, indicates significantly different from Last min, $P < 0.01$.

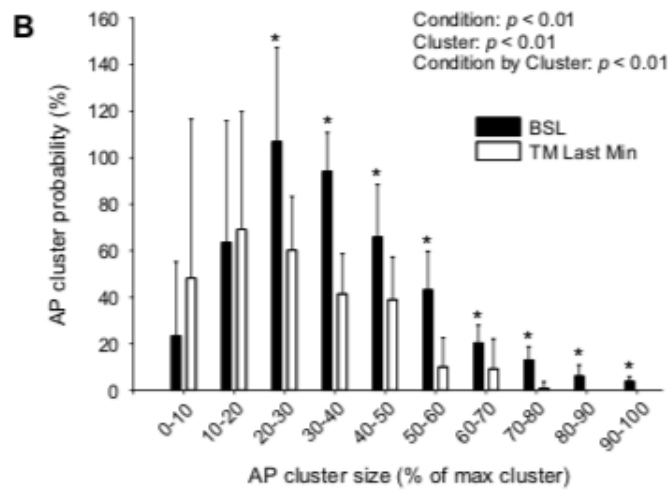
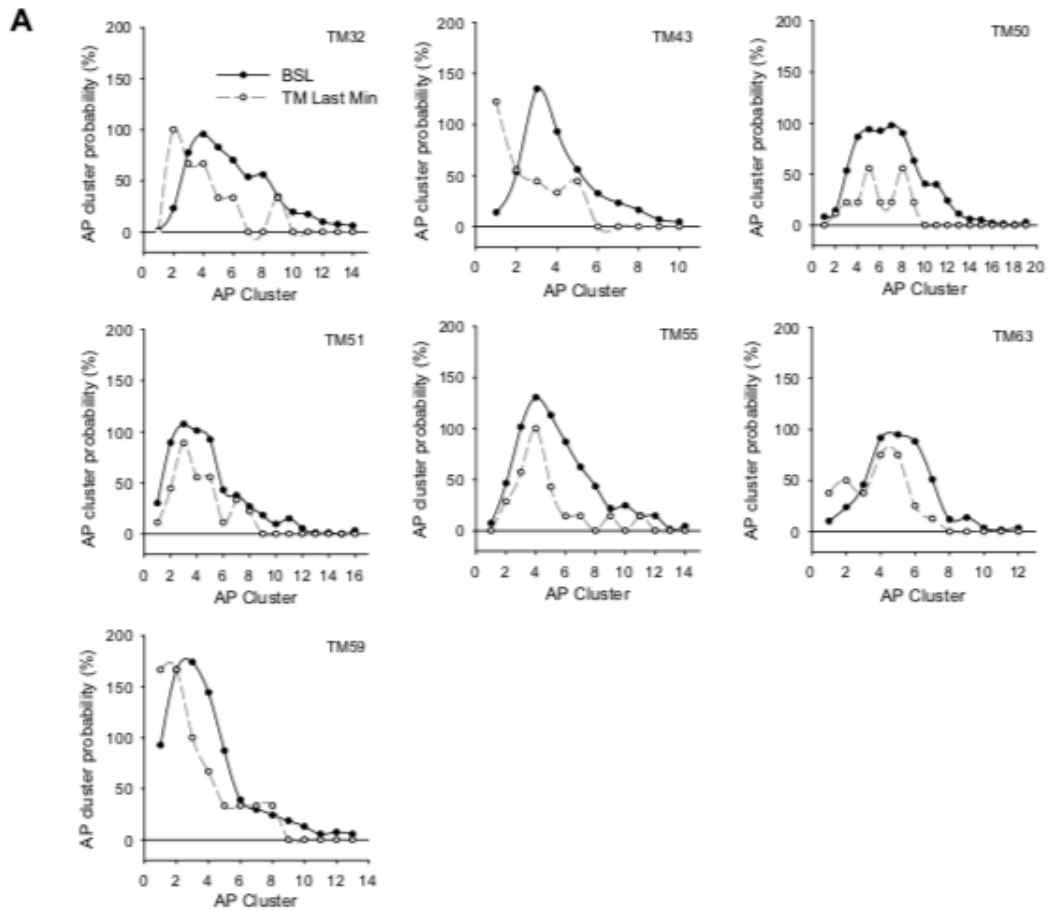


Figure 2.5 Sympathetic action potential (AP) cluster probability distributions for each participant at baseline (BSL) and the last minute of visible integrated sympathetic bursting activity during the trimethaphan infusion (TM Last Min) (A). Group averaged sympathetic AP probability distributions for BSL and TM Last Min with AP clusters normalized to the largest cluster at baseline (B). For both individual and group averaged figures a probability of 100% indicates that the cluster fired once in every integrated burst, whereas a probability of less than or greater than 100% indicates that the cluster occasionally fired more than once per burst or was not active in every burst, respectively. *, indicates significantly different from TM Last Min within cluster, $P < 0.01$. (Previous page).

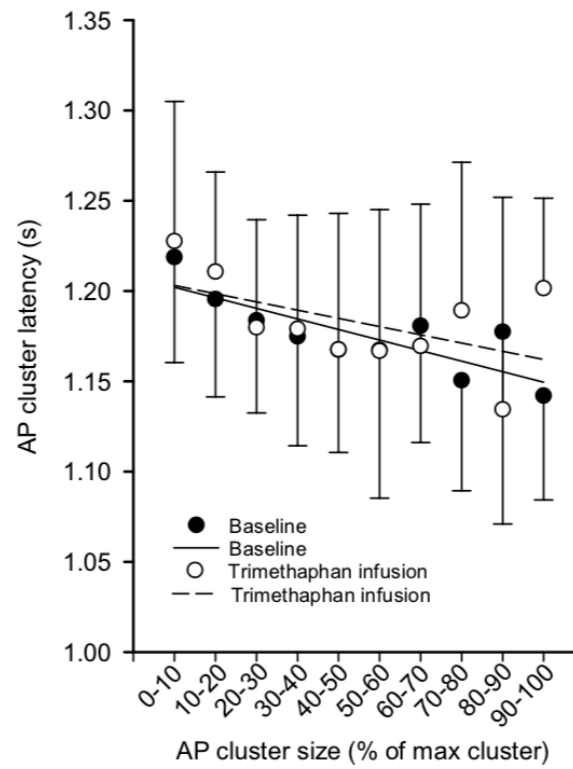


Figure 2.6 Action potential (AP) cluster latency as a function of AP cluster size at baseline (BSL) and during the entire trimethaphan infusion. The decrease in cluster latency as a function of amplitude was fit with an exponential decay function. Data presented are group mean (SD).

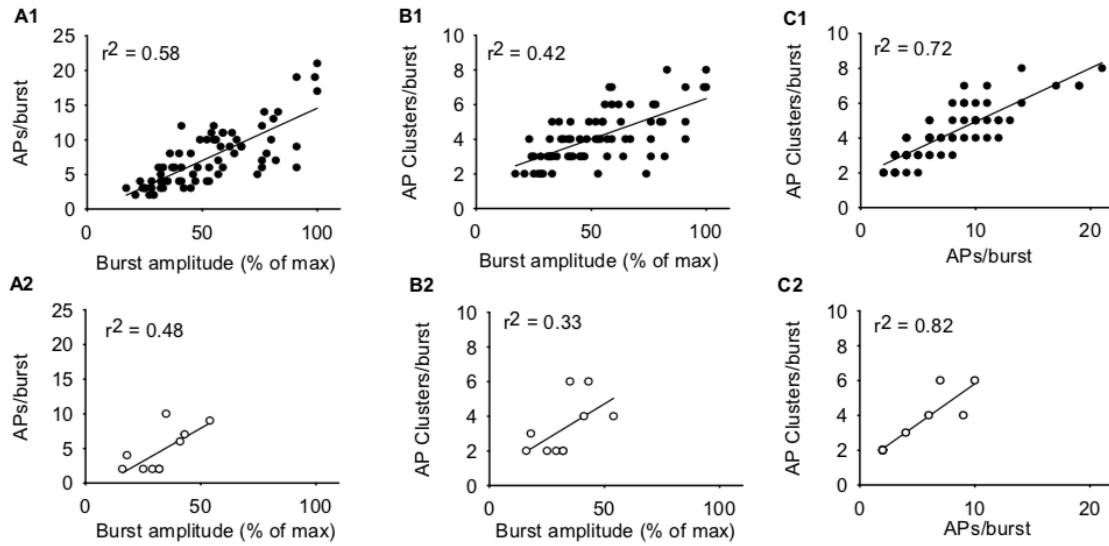


Figure 2.7 The number of sympathetic action potentials (AP) per burst as a function of relative integrated burst amplitude (normalized to the largest burst at baseline and during the trimethaphan infusion) at baseline (A1) and the last minute of detectable integrated sympathetic bursting activity during the trimethaphan infusion (A2). The number of unique sympathetic AP clusters per burst as a function of relative integrated burst amplitude at baseline (B1) and the last minute of detectable integrated sympathetic bursting activity during the trimethaphan infusion (B2). The number of unique AP clusters per sympathetic burst as a function of the number of APs per burst at baseline (C1) and the last minute of detectable integrated sympathetic bursting activity during the trimethaphan infusion. Data presented are from one individual.

2.4 Discussion

The current study provides new evidence regarding the role of the paravertebral ganglia in the emission patterns of sympathetic postganglionic nerves directed towards the skeletal muscle vasculature. First, we demonstrate that blockade of nicotinic receptors at the ganglia elicited an ordered pattern of AP de-recruitment beginning with larger APs that fire with lower probability under baseline conditions, followed by the progressive decreased probability of smaller APs. Second, following trimethaphan-mediated cessation of integrated MSNA bursts, small AP clusters persisted to fire in an asynchronous pattern. Also, Valsalva's Manoeuvre did not increase the firing rate of these persistent AP clusters, or elicit recruitment of larger APs that had previously been inhibited by trimethaphan. We interpret these observations to suggest: 1) the paravertebral ganglia contribute to the heterogeneity in the firing probabilities of differently-sized postganglionic sympathetic APs active under baseline conditions, and 2) the presence of non-synchronized APs that express resistance to blockade with trimethaphan.

Variations in integrated burst amplitude reflect the number and size of APs synchronized to fire at about the same time (37, 43). Varying sized APs express a heterogeneity of firing probabilities, such that, compared to moderately-sized APs, larger and smaller APs contribute to considerably fewer bursts, while a subpopulation of even larger APs are recruited during severe stress (45, 54). Focusing on baseline data only, ganglionic blockade in the current study produced an ordered pattern of de-recruitment where larger APs were inhibited, reducing burst size, followed by blockade of most small AP clusters, rendering integrated bursts from being detected. As these data were collected as part of a

larger study, waiting for metabolism of trimethaphan and subsequent return of MSNA signal was not possible. Therefore, we cannot rule out the possibility that reductions in burst size and AP cluster firing as well as the cessation of bursts following blockade were attributed to changes in microelectrode position. However, this is unlikely given the observation that small AP clusters were present through the entire study and no changes in background signal intensity were observed.

Whereas trimethaphan exerted early effects on larger AP clusters, our previous studies suggest that these clusters must express a higher threshold for recruitment (54). Also, based on replicated evidence that larger AP clusters express faster conduction velocity (26, 43) we expect that larger AP clusters reflect neurons with larger axons. Together, these observations indicate that the larger AP clusters express a higher threshold for recruitment and also a higher sensitivity for de-recruitment through a post-junctional nicotinic mechanism. These data indicate that the ganglia participate in the recruitment probability of larger AP clusters. Furthermore, the observation that medium-sized APs exhibited moderate reductions in firing probability but were still active in the final minute of MSNA bursting during trimethaphan infusion suggests that the ganglia express some differential organization for postganglionic recruitment by neuron size.

We speculate that this pattern of recruitment and de-recruitment may reflect a scaling of preganglionic synaptic input strength at the ganglia. However, the neural mechanisms mediating such a preganglionic effect are not known. To our knowledge, beyond the investigations using ganglionic blockade as a model of the circulation under negligible autonomic control (21, 34) or delineating the origins of the integrated sympathetic signal (10), no previous study has examined the role of the ganglia in human sympathetic AP

discharge. While earlier studies in animals may provide some insight to the mechanisms (e.g., ganglionic convergence) contributing to the present observations, the focus on compound APs or single-unit recordings in these investigations (5, 17, 22, 38, 41, 52) prevent direct comparisons with the current observations. Interestingly, compared to moderately-sized APs that express strong baroreflex modulation, larger APs are weakly associated with fluctuations in diastolic BP, suggesting that additional sites of control beyond the arterial baroreflex participate in the regulation of the larger, low probability APs (45). Similar conclusions have been drawn based on the observation that burst occurrence, but not size, was related to diastolic BP in humans (23), causing this latter group, and others (33) to speculate on sites outside of the baroreflex pathways that affect burst size (analogous to large AP cluster recruitment). Consistent with this idea, both magnetic resonance imaging and electroencephalographic studies suggest the involvement of neural regions beyond the baroreflex brainstem nuclei in the regulation of MSNA (15, 24, 27, 56). In this conjecture, the strength of preganglionic inputs to postganglionic neurons possessing larger diameter axons, would reflect a subpopulation of descending neural signals from higher cortical sites that are not under direct baroreflex regulation.

The second major observation of the current study was a population of smaller AP clusters that persisted to fire in an asynchronous manner, without consistent baroreflex rhythmicity, following blockade of nicotinic receptors. To our knowledge, this phenomenon has not been reported previously in humans. While these APs may not have been sympathetic, this is unlikely as they exhibited similar morphological characteristics to the smaller AP clusters that were synchronized to fire within bursts at baseline and

during the trimethaphan infusion when integrated bursts were visible. This observation also suggests that these clusters did not represent a new population of APs recruited following trimethaphan. Also, an incomplete ganglionic blockade likely did not produce these APs as, in six of seven individuals, Valsalva's Manoeuvre performed during the non-bursting period of trimethaphan infusion failed to elicit the recruitment of larger AP clusters or integrated bursts (44). From these data, we surmise that they represent spontaneous firing of postganglionic axons that normally receive cardiac entrainment via descending baroreflex inputs and/or are controlled by non-nicotinic synaptic mechanisms at the human paravertebral ganglia. Previous studies have documented spontaneous neuronal activity within the medullary sites governing sympathetic discharge (9) and while this evidence raises the possibility of spontaneous postganglionic spiking, this idea has not been tested. Alternatively, detailed studies in feline and rodent models showed persistent postganglionic activity during nicotinic blockade, illustrating the contribution of non-nicotinic mechanisms to ganglionic signaling (16, 20, 60). Also, ganglionic exposure to muscarinic agonists appears to enhance postganglionic nerve activity across several studies (7, 60). Janig et al. (1983) further showed that chemoreflex-induced discharge was evident in some, but not all postganglionic neurons during combined nicotinic and muscarinic (atropine) blockade. In the bullfrog, peptide neurotransmitters (including substance P and a peptide resembling luteinizing hormone releasing hormone) contribute to postganglionic EPSPs (18). Thus, the most direct explanation of the trimethaphan resistant AP clusters in the current observations is that they represent a population of neurons with non-nicotinic synaptic mechanisms.

The purpose of non-nicotinic ganglionic neurotransmission remains unclear. This feature does highlight the complex nature of sympathetic neuronal recruitment. Interestingly, repetitive preganglionic nerve stimulation exposes two phases of postganglionic activity in vertebrates: These phases are a rapid onset, high frequency discharge mediated by nicotinic receptor actions, and a delayed, low frequency firing pattern evoked by muscarinic and peptidergic mechanisms (18, 20, 60). The purpose and mechanism(s) supporting the trimethaphan-resistance of the smallest AP clusters remains unknown, although the observation may be consistent with the conjecture that the ganglia also participate in axonal size-related recruitment patterns. It is noted, however, that baroreflex unloading via mild (36) and moderate-to-severe lower body suction (3, 43), or sodium nitroprusside infusion (28), result in a paradoxical decrease in the firing of some APs including smaller clusters, supporting the notion that complex mechanisms may regulate small AP patterns.

An additional explanation for the trimethaphan-resistant AP clusters is that they do not represent sympathetic C-fibre spiking. We believe this scenario is improbable for three reasons. First, they likely were not produced by sensory axons sensitive to metabolite accumulation, stretch, or pain because participants remained still, abstained from exercise 24 hours prior to testing, and did not report any discomfort throughout the protocol. Second, trimethaphan-resistant APs were unlikely to represent Type I/II proprioceptive fibre activity, as the myelination of these nerves produces wider APs with prominent positive-going depolarization (29, 59), which are distinct from the sympathetic C-fibre APs detected by the wavelet model used here (42). Third, we do not suspect that these APs represent false positive detections by the wavelet de-noising method because the

signal-to-noise ratio for these APs in the trimethaphan period was 4.2 ± 0.7 , a high level that produces a false detection rate of $< 3\%$ (42).

Some methodological considerations exist for the present study. First, this study did not employ a randomized, placebo control arm alongside the trimethaphan condition. However, in healthy individuals under normal conditions of supine rest, complete abolishment of MSNA bursts during protracted periods of falling BP would be highly unlikely. Second, this investigation only studied pre- and post-menopausal females. Both sex and female reproductive hormones are known to affect resting sympathetic outflow as well as total MSNA responses to diverse forms of physiological stress (49, 58). However, these recruitment strategies appear to be fundamental properties of the human sympathetic nervous system (31, 47) that are simply modified by sex hormones, age and/or health status (1, 30). Consistent with this notion, the two post-menopausal participants (participant identifiers TM32 and TM50) exhibited greater baseline MSNA (due to a burst incidence mechanism rather than the AP content per burst) than pre-menopausal females (TM32, TM50 vs. pre-menopausal mean \pm SD: 44, 46 vs. 24 ± 12 bursts/100beats; 245, 339 vs. 144 ± 80 AP/100beats; 6, 8 vs. 6 ± 2 AP/burst). Despite the larger effect of trimethaphan on MSNA burst incidence in post-menopausal females versus pre-menopausal counterparts (Δ 39, Δ 37 vs. Δ 15 ± 3 bursts/100 beats, Δ 231, Δ 319 vs. Δ 110 ± 51 AP/100beats, Δ 3, Δ 5 vs. Δ 3 ± 1 APs/burst), the ordered pattern of trimethaphan-mediated AP de-recruitment was consistent between groups (Fig. 2.5A). Third, Valsalva's Manoeuvre was used to test adequacy of the blockade based clinically on heart and BP responses. We recognize that additional manoeuvres before blockade would have enabled a prospective analysis of reflex AP recruitment as well. Nonetheless,

Valsalva's Manoeuvre produces a robust AP recruitment stimulus under baseline conditions in healthy individuals (44, 50) such that the lack of any recruitment post blockade indicates a severe impairment of the ganglionic sympathetic transmission.

2.4.1 Conclusion

The current study provides new evidence regarding the role of the paravertebral ganglia in human MSNA regulation. Specifically, the organization of the ganglia may contribute, in part, to the distribution of firing probabilities exhibited by differently-sized APs at rest and the recruitment of previously silent, larger and faster-conducting sympathetic neurons during homeostatic stress. Interestingly, our observations also suggest that a population of postganglionic neurons with non-nicotinic synaptic mechanisms may exist within the human sympathetic nervous system. These findings offer new information regarding the neural sites which regulate sympathetic emission patterns fundamental to the maintenance of homeostasis and may contribute to chronic adaptations in sympathetic discharge in aging and disease.

2.5 References

1. **Badrov MB, Lalande S, Olver TD, Suskin N, Shoemaker JK.** Effects of aging and coronary artery disease on sympathetic neural recruitment strategies during end-inspiratory and end-expiratory apnea. *Am J Physiol Circ Physiol* 311: H1040–H1050, 2016.
2. **Badrov MB, Olver TD, Shoemaker JK.** Central vs. peripheral determinants of sympathetic neural recruitment: insights from static handgrip exercise and postexercise circulatory occlusion. *Am J Physiol Integr Comp Physiol* 311: R1013–R1021, 2016.
3. **Badrov MB, Usselman CW, Shoemaker JK.** Sympathetic neural recruitment strategies: responses to severe chemoreflex and baroreflex stress. *Am J Physiol Integr Comp Physiol* 309: R160–R168, 2015.
4. **Barman SM, Yates BJ.** Deciphering the Neural Control of Sympathetic Nerve Activity: Status Report and Directions for Future Research. *Front Neurosci* 11: 730, 2017.
5. **Bratton B, Davies P, Jänig W, McAllen R.** Ganglionic transmission in a vasomotor pathway studied in vivo. *J Physiol* 588: 1647–1659, 2010.
6. **Breskovic T, Steinback CD, Salmanpour A, Shoemaker JK, Dujic Z.** Recruitment pattern of sympathetic neurons during breath-holding at different lung volumes in apnea divers and controls. *Auton Neurosci* 164: 74–81, 2011.
7. **Brown DA, Fatherazi S, Garthwaite J, White RD.** Muscarinic receptors in rat sympathetic ganglia. *Br J Pharmacol* 70: 577–592, 1980.
8. **Christou DD, Jones PP, Jordan J, Diedrich A, Robertson D, Seals DR.** Women have lower tonic autonomic support of arterial blood pressure and less effective baroreflex buffering than men. *Circulation* 111: 494–498, 2005.
9. **Dampney RA.** Functional organization of central pathways regulating the cardiovascular system. *Physiol Rev* 74: 323–364, 1994.
10. **Delius W, Hagbarth K, Hongell A, Wallin BG.** General characteristics of sympathetic activity in human muscle nerves. *Acta Physiol Scand* 84: 65–81, 1972.
11. **Fagius J, Sundlöf G, Wallin BG.** Variation of sympathetic reflex latency in man. *J Auton Nerv Syst* 21: 157–165, 1987.
12. **Fagius J, Wallin BG.** Sympathetic reflex latencies and conduction velocities in normal man. *J Neurol Sci* 47: 433–448, 1980.
13. **Gibbins IL, Morris JL.** Structure of peripheral synapses: autonomic ganglia. *Cell Tissue Res* 326: 205–220, 2006.

14. **Hagbarth K, Vallbo ÅB.** Pulse and respiratory grouping of sympathetic impulses in human muscle nerves. *Acta Physiol Scand* 74: 96–108, 1968.
15. **Henderson LA, James C, Macefield VG.** Identification of sites of sympathetic outflow during concurrent recordings of sympathetic nerve activity and fMRI. *Anat Rec* 295: 1396–1403, 2012.
16. **Hoffmeister B, Hussels W, Jänig W.** Long-lasting discharge of postganglionic neurones to skin and muscle of the cat's hindlimb after repetitive activation of preganglionic axons in the lumbar sympathetic trunk. *Pflügers Arch* 376: 15–20, 1978.
17. **Horn JP, Kullmann PHM.** Dynamic clamp analysis of synaptic integration in sympathetic ganglia. *Neurophysiology* 39: 423, 2007.
18. **Jan LY, Jan YN.** Peptidergic transmission in sympathetic ganglia of the frog. *J Physiol* 327: 219–246, 1982.
19. **Jänig W, Häbler H.** Neurophysiological analysis of target-related sympathetic pathways—from animal to human: Similarities and differences. *Acta Physiol* 177: 255–274, 2003.
20. **Jänig W, Krauspe R, Wiedersatz G.** Reflex activation of postganglionic vasoconstrictor neurones supplying skeletal muscle by stimulation of arterial chemoreceptors via non-nicotinic synaptic mechanisms in sympathetic ganglia. *Pflügers Arch* 396: 95–100, 1983.
21. **Jones PP, Shapiro LF, Keisling GA, Jordan J, Shannon JR, Quaife RA, Seals DR.** Altered autonomic support of arterial blood pressure with age in healthy men. *Circulation* 104: 2424–2429, 2001.
22. **Karila P, Horn JP.** Secondary nicotinic synapses on sympathetic B neurons and their putative role in ganglionic amplification of activity. *J Neurosci* 20: 908–918, 2000.
23. **Kienbaum P, Karlsson T, Sverrisdottir YB, Elam M, Wallin BG.** Two sites for modulation of human sympathetic activity by arterial baroreceptors? *J Physiol* 531: 861–869, 2001.
24. **Kimmerly DS, O'Leary DD, Menon RS, Gati JS, Shoemaker JK.** Cortical regions associated with autonomic cardiovascular regulation during lower body negative pressure in humans. *J Physiol* 569: 331–345, 2005.
25. **Kimmerly DS, Wong SW, Salzer D, Menon R, Shoemaker JK.** Forebrain regions associated with postexercise differences in autonomic and cardiovascular function during baroreceptor unloading [Online]. *Am J Physiol Circ Physiol* 293: H299–H306, 2007.

26. **Klassen SA, De Abreu S, Greaves DK, Kimmerly DS, Arbeille P, Denise P, Hughson RL, Normand H, Shoemaker JK.** Long-duration bed rest modifies sympathetic neural recruitment strategies in males and females. *J Appl Physiol* 124: 769–779, 2017.
27. **Kobuch S, Fazalbhoy A, Brown R, Macefield VG, Henderson LA.** Muscle sympathetic nerve activity-coupled changes in brain activity during sustained muscle pain. *Brain Behav* 8, 2018.
28. **Limberg JK, Ott EP, Holbein WW, Baker SE, Curry TB, Nicholson WT, Joyner MJ, Shoemaker JK.** Pharmacological Assessment of the Contribution of the Arterial Baroreflex to Sympathetic Discharge Patterns in Healthy Humans. *J Neurophysiol.* 19: 2166-2175, 2018.
29. **Macefield VG, Knellwolf TP.** Functional Properties of Human Muscle Spindles. *J. Neurophysiol.* 120: 452-467, 2018.
30. **Macefield VG, Rundqvist B, Sverrisdottir YB, Wallin BG, Elam M.** Firing properties of single muscle vasoconstrictor neurons in the sympathoexcitation associated with congestive heart failure. *Circulation* 100: 1708–1713, 1999.
31. **Macefield VG, Wallin BG.** Physiological and pathophysiological firing properties of single postganglionic sympathetic neurons in humans. *J Neurophysiol* 119: 944–956, 2017.
32. **Macefield VG, Wallin BG, Vallbo AB.** The discharge behaviour of single vasoconstrictor motoneurons in human muscle nerves. *J Physiol* 481: 799–809, 1994.
33. **Malpas SC.** A new model for the generation of sympathetic nerve activity. *Clin Exp Pharmacol Physiol* 22: 11–16, 1995.
34. **Marinos A, Gamboa A, Celedonio JE, Preheim BA, Okamoto LE, Ramirez CE, Arnold AC, Diedrich A, Biaggioni I, Shibao CA.** Hypertension in Obese Black Women is Not Caused by Increased Sympathetic Vascular Tone. *J Am Heart Assoc* 6: e006971, 2017.
35. **McLachlan EM.** Transmission of signals through sympathetic ganglia—modulation, integration or simply distribution? *Acta Physiol* 177: 227–235, 2003.
36. **Millar PJ, Murai H, Morris BL, Floras JS.** Microneurographic evidence in healthy middle-aged humans for a sympathoexcitatory reflex activated by atrial pressure. *Am J Physiol Circ Physiol* 305: H931–H938, 2013.
37. **Ninomiya I, Malpas SC, Matsukawa K, Shindo T, Akiyama T.** The amplitude of synchronized cardiac sympathetic nerve activity reflects the number of activated pre-and postganglionic fibers in anesthetized cats. *J Auton Nerv Syst* 45: 139–147, 1993.

38. **Obrador S, Odoriz JB.** Transmission through a lumbar sympathetic ganglion. *J Physiol* 86: 269–276, 1936.
39. **Purves D, Lichtman JW.** Geometrical differences among homologous neurons in mammals. *Science (80-)* 228: 298–302, 1985.
40. **Purves D, Rubin E, Snider WD, Lichtman J.** Relation of animal size to convergence, divergence, and neuronal number in peripheral sympathetic pathways. *J Neurosci* 6: 158–163, 1986.
41. **Rimmer K, Horn JP.** Weak and straddling secondary nicotinic synapses can drive firing in rat sympathetic neurons and thereby contribute to ganglionic amplification. *Front Neurol* 1, 2010.
42. **Salmanpour A, Brown LJ, Shoemaker JK.** Spike detection in human muscle sympathetic nerve activity using a matched wavelet approach. *J Neurosci Methods* 193: 343–355, 2010.
43. **Shoemaker JK.** Relationship between size and latency of action potentials in human muscle sympathetic nerve activity. *J Neurophysiol* 105: 2830–2842, 2011.
44. **Salmanpour A, Frances MF, Goswami R, Shoemaker JK.** Sympathetic neural recruitment patterns during the Valsalva maneuver. In: *2011 Annual International Conference of the IEEE Engineering in Medicine and Biology Society*. IEEE, 2011, p. 6951–6954.
45. **Salmanpour A, Shoemaker JK.** Baroreflex mechanisms regulating the occurrence of neural spikes in human muscle sympathetic nerve activity. *J Neurophysiol* 107: 3409–3416, 2012.
46. **Scott DW.** On optimal and data-based histograms. *Biometrika* 66: 605–610, 1979.
47. **Shoemaker JK, Badrov MB, Al-Khazraji BK, Jackson DN.** Neural Control of Vascular Function in Skeletal Muscle. *Compr Physiol* 6: 303–329, 2016.
48. **Shoemaker JK, Goswami R.** Forebrain neurocircuitry associated with human reflex cardiovascular control. *Front Physiol* 6, 2015.
49. **Shoemaker JK, Hogeman CS, Khan M, Kimmerly DS, Sinoway LI.** Gender affects sympathetic and hemodynamic response to postural stress. *Am J Physiol Circ Physiol* 281: H2028–H2035, 2001.
50. **Shoemaker JK, Hogeman CS, Sinoway LI.** Sympathetic responses to Valsalva’s manoeuvre following bed rest. *Can J Appl Physiol* 28: 342–355, 2003.
51. **Shoemaker JK, Klassen SA, Badrov MB, Fadel PJ.** Fifty years of microneurography: learning the language of the peripheral sympathetic nervous system in humans. *J Neurophysiol* 119: 1731–1744, 2018.

52. **Springer MG, Kullmann PHM, Horn JP.** Virtual leak channels modulate firing dynamics and synaptic integration in rat sympathetic neurons: implications for ganglionic transmission in vivo. *J Physiol* 593: 803–823, 2015.
53. **Spyer KM.** Annual review prize lecture. Central nervous mechanisms contributing to cardiovascular control. *J Physiol* 474: 1–19, 1994.
54. **Steinback CD, Salmanpour A, Breskovic T, Dujic Z, Shoemaker JK.** Sympathetic neural activation: an ordered affair. *J Physiol* 588: 4825–4836, 2010.
55. **Stjernberg L, Blumberg H, Wallin BG.** Sympathetic activity in man after spinal cord injury: outflow to muscle below the lesion. *Brain* 109: 695–715, 1986.
56. **Tank J, Diedrich A, Hale N, Niaz FE, Furlan R, Robertson RM, Mosqueda-Garcia R.** Relationship between blood pressure, sleep K-complexes, and muscle sympathetic nerve activity in humans. *Am J Physiol Integr Comp Physiol* 285: R208–R214, 2003.
57. **Taylor KS, Millar PJ, Murai H, Haruki N, Kimmerly DS, Bradley TD, Floras JS.** Cortical Autonomic Network Grey Matter and Sympathetic Nerve Activity in Obstructive Sleep Apnea. *Sleep* 41. 2017.
58. **Usselman CW, Gimon TI, Nielson CA, Luchyshyn TA, Coverdale NS, Van Uum SHM, Shoemaker JK.** Menstrual cycle and sex effects on sympathetic responses to acute chemoreflex stress. *Am J Physiol Circ Physiol* 308: H664–H671, 2015.
59. **Vallbo AB, Hagbarth KE, Torebjork HE, Wallin BG.** Somatosensory, proprioceptive, and sympathetic activity in human peripheral nerves. *Physiol Rev* 59: 919–957, 1979.
60. **Volle RL.** Modification by drugs of synaptic mechanisms in autonomic ganglia. *Pharmacol Rev* 18: 839–869, 1966.
61. **Wallin BG, Burke D, Gandevia S.** Coupling between variations in strength and baroreflex latency of sympathetic discharges in human muscle nerves. *J Physiol* 474: 331, 1994.

Chapter 3

3 Asynchronous action potential discharge in human muscle sympathetic nerve activity

Published online ahead of print in Am J Physiol Heart Circ Physiol.

doi: 10.1152/ajpheart.00258.2019

3.1 Introduction

The sympathetic nervous system achieves homeostatic adjustments to physiological stress by eliciting coordinated circulatory responses that are tailored to the magnitude and form of that stress (31). Microneurographic studies of action potentials (AP) emanating from postganglionic sympathetic c-fibres directed towards the muscle vasculature have revealed many fundamental neural patterns for circulatory control (26, 37). The primary characterization of muscle sympathetic nerve activity (MSNA) focuses on pulse-rhythmic bursts formed by the synchronized discharge of varying-sized APs entrained to the cardiac cycle by the arterial baroreflex (9, 16, 38). Among APs synchronized into bursts, multiple size-related subpopulations exist, expressing non-uniform patterns of discharge and recruitment that generate the variability in MSNA burst size and occurrence over time (23, 37).

However, studies in humans (24, 34) and lower mammals (10, 19, 22) suggest that sympathetic c-fibres may express non-burst forming asynchronous discharge.

Specifically, in healthy humans, we identified a subpopulation of smaller sympathetic APs active under baseline conditions that persisted to fire when trimethaphan had abolished integrated bursts. These persistent APs exhibited weak cardiac-rhythmicity, producing asynchronous discharge (24). In anesthetized cats, both reflex physiological stress (22) and electrical stimulation of upstream nerves (e.g., hypothalamic or

preganglionic) (11, 19) produced a rapid burst of synchronized postganglionic nerve activity followed by asynchronous neural discharge. Interestingly, the initial burst of synchronous APs was abolished by nicotinic blockade, whereas the asynchronously firing APs were often blocked by muscarinic antagonists (10, 11, 19, 22), suggesting that non-nicotinic ganglionic mechanisms contribute to asynchronous behaviour. While the abovementioned evidence points towards asynchronous sympathetic nerve discharge, this behavior has remained unexplored in humans due to a methodological approach of signal integration (17) and/or the focus on single- or multi-unit AP activity that occurs within bursts (36). Studying APs that fire at approximately the same time to form bursts as well as the APs that express asynchronous behaviour (observed between bursts) in humans will improve our understanding of sympathetic neural messaging directed towards the circulation.

Therefore, the present study tested the hypothesis that synchronous and asynchronous discharge (i.e., APs firing within and between bursts, respectively) exist among human muscle sympathetic APs, and that the ganglia affect synchronicity within the sympathetic nervous system. Experiment One quantified AP synchronicity at baseline (BSL) and during both baroreflex and apneic stress in eight healthy males and females. Experiment Two examined the impact of nicotinic blockade at the paravertebral ganglia (via trimethaphan camsylate) on AP synchronicity in a separate sample of healthy female participants.

3.2 Methods

3.2.1 Ethical Approval

All procedures were approved by the research ethics boards at the University of Western Ontario (No. 108026) and Mayo Clinic (No. 09-008548). The study conforms to the *Declaration of Helsinki*, except for registration in a database. Participants provided informed written consent following oral and written explanation of the experimental procedures and measures.

3.2.2 Participants

Experiment One tested eight healthy individuals ($n = 4$ females, 26 ± 3 years, 170 ± 7 cm, 69 ± 13 kg), while Experiment Two tested seven healthy females (37 ± 5 years, 165 ± 2 cm, 60 ± 4 kg). Prior to the testing session the participants performed health screening to ensure they met the inclusion/exclusion criteria: non-smoker and no prior diagnosis of cardiovascular disease, diabetes, hypertension, or neurological disorder. Experiment One did not control for oral contraceptive use or stage of menstrual cycle at time of testing. As reported previously (24), $n = 5$ females in Experiment Two were pre-menopausal and tested during the early follicular stage or placebo stage for oral contraceptive users ($n = 2$, both taking levonorgestrel and ethinyl estradiol). Participants were not on any other medications. Two female participants in Experiment Two were post-menopausal (6 and 7 years since last menses).

3.2.3 Experimental Procedures

Participants in Experiment One arrived at the Laboratory for Brain and Heart Health at the University of Western Ontario for testing after a 4-hour fast and abstaining from

vigorous exercise, alcohol, and caffeine for 12-hours prior to the study. Following measurement of height and weight, participants assumed the supine position for instrumentation and data collection. Participants were sealed in a lower body negative pressure (LBNP) chamber distal to the iliac crest. LBNP chamber pressure was measured with a pressure sensor (MLT0670, ADInstruments; Castle Hill, New South Wales, Australia) calibrated with a manual sphygmomanometer. A strain gauge (Model 1132 Pneumotrace II, UFI, Morro Bay, CA) enabled investigators to discriminate end-expiratory apnea (APN) from spontaneous breathing. Continuous arterial blood pressure (BP) was measured via finger photoplethysmography and the Modelflow algorithm (41) was used to obtain brachial BP, stroke volume, and cardiac output (Finometer; Finapres Medical Systems, Amsterdam, The Netherlands). Heart rate (HR) was quantified using a three-lead electrocardiogram (ECG). Participants were familiarized with -40 mmHg LBNP and at least one APN prior to data collection. Data collection began following at least 30-min in the supine position. Procedures for Experiment Two, performed in the Human Integrative Physiology Laboratory at Mayo Clinic (Rochester, MN), have been described previously (24).

3.2.4 Experimental Design

Experiment One data were collected during: at least 5-min BSL, 3-5 minutes of -10 mmHg LBNP, 3-5 minutes of -40 mmHg LBNP, and APN. Experimental interventions were performed in a randomized order, though -10 mmHg was always performed before -40 mmHg. Bouts of LBNP and the APN were followed by at least 3-min with the lower body chamber at ambient pressure prior to the next experimental intervention. Data

analysis was performed on 190 ± 36 s of BSL, 116 ± 33 s of -10 mmHg LBNP, 109 ± 23 s of -40 mmHg LBNP, and 30 ± 7 s of APN.

Experiment Two data were collected during BSL and a trimethaphan camsylate infusion (1–7 mg/min; Cambridge Laboratories, Wallsend, UK). These data were obtained through a retrospective analysis of data reported earlier in an investigation studying the impact of ganglionic blockade on *synchronous* AP de-recruitment (24). Here, we focus on the patterns of *asynchronous* APs. Trimethaphan infusion rate was adjusted over time, and variably across participants until ganglionic blockade was achieved. In this study, ganglionic blockade was defined as participants exhibiting no visible integrated MSNA bursts and < 5 bpm change in HR from BSL during phase II of Valsalva's Manoeuvre. Data analysis was performed on 181 ± 1 s at BSL, the last 86 ± 16 s with *visible* integrated bursts during the trimethaphan infusion, and 120 ± 0 s of the trimethaphan infusion where integrated bursts were *not visible*. Additional information regarding this experimental design is available elsewhere (24).

3.2.5 Experimental Measures and Analysis

Continuous postganglionic muscle sympathetic c-fibre discharge was measured by microneurography at the peroneal nerve using the same equipment and settings in each experiment (16). MSNA recordings were confirmed by the absence of skin paresthesia and an increase in bursting discharge upon voluntary APN, but not during arousal to a loud noise (40). Postganglionic sympathetic activity was recorded with a nerve traffic analyzer (662C-3; Bioengineering University of Iowa, Iowa City, IA). The neural signal was pre-amplified with a gain of 1,000 (using preamplifier and isolation amplifier; gains of 100 and 10, respectively), then further amplified with a gain of 75 (using a variable

gain amplifier). Neural activity was then band-pass filtered (bandwidth of 700–2,000 Hz) before being rectified and integrated (using a leaky integrator; 0.1-s time constant). The filtered and integrated microneurographic signals were sampled at 10,000 Hz while all other signals were sampled at 1,000 Hz. Data were collected using LabChart 8 and PowerLab systems (ADInstruments; Castle Hill, New South Wales, Australia) then saved for offline analysis.

Prior to analysis, integrated and filtered MSNA signals were time adjusted for the conduction delay, which was derived from the burst latency (see below) of several varying-sized integrated bursts. Integrated MSNA bursts were included in the analysis if they aligned with an R-wave and exhibited a 2:1 ratio relative to the previous period of between-burst signal. Integrated MSNA burst occurrence was quantified as burst frequency (bursts/min) and burst incidence (bursts/100beats). Burst amplitude (AU) was measured in volts and normalized to the largest burst at BSL. The product of burst frequency and normalized amplitude yielded a metric of total MSNA (AU/min). Burst latency (s) was the time difference between the ECG R-wave and the peak of the corresponding integrated burst.

In both experiments, muscle sympathetic APs in the filtered neurogram were detected using a continuous wavelet transform, described in detail previously (32). Throughout all study conditions any detected APs were extracted, regardless of their temporal coherence with an integrated MSNA burst. For each condition all extracted APs were ordered based on peak-to-peak amplitude then assigned to a bin (i.e., cluster) following Scott's rule which balances bin width, data bias, and variance to minimize integrated mean square error (35). Consequently, the number of bins varies across participants and conditions. To

resolve this, AP bin properties were normalized for each participant to ensure that minimal bin width (value selected from the condition with the smallest bins), total number of bins (value selected from the condition with the greatest number of bins), and maximum bin centre (value selected from the condition with the greatest maximal bin centre) were identical across conditions. This allowed us to detect whether APs were recruited or de-recruited from BSL during physiological stress or ganglionic blockade, respectively, and to compare the behaviour of each cluster between conditions.

Following binning, APs were determined to be firing synchronously or asynchronously based on the following criteria (Fig. 3.1): An AP was considered to fire synchronously 1) if its occurrence corresponded with a burst (as defined above) in the integrated MSNA signal (i.e., within ± 0.4 s of the burst peak), or 2) despite no visible integrated burst, if it was one of ≥ 2 *visible* APs in the filtered microneurographic signal firing within ± 0.4 s of an ECG R-wave (after adjusting for the conduction delay). All other APs were considered to fire asynchronously. For HR > 75 bpm the window for synchronous AP detection was reduced to one-half the R-R interval. This approach will necessarily underestimate the occurrence of those asynchronous APs that also occur during a burst period (either spontaneously or through some synchronization process).

The signal-to-noise ratio (SNR) was determined as the amplitude of the negative peak of the mean AP over the standard deviation of the background noise around each AP. In Experiment One the SNR values at BSL (4.0 ± 0.4), -10 mmHg LBNP (4.1 ± 0.4), -40 mmHg LBNP (4.1 ± 0.4), and end-expiratory apnea (4.2 ± 0.5) enabled a correct detection rate of >95% and a false positive rate of <3% (32). As reported previously (24),

in Experiment Two the SNR at BSL and the trimethaphan infusion were 4.2 ± 0.7 and 4.2 ± 0.5 , respectively.

Asynchronous APs were quantified by AP frequency (AP/min) and total AP clusters. The time between bursts of synchronized APs was used to calculate the asynchronous AP frequency. Synchronous APs were quantified by AP frequency (AP/min), incidence (AP/100beats), the number of APs per integrated burst, the number of unique AP clusters per burst and total AP clusters. For synchronous APs, latency was determined as the time difference from the R-wave of the preceding cardiac cycle to the negative peak of the AP (33). Synchronous AP cluster latency was determined as the mean latency of all APs within a cluster. The relationship between synchronous AP cluster latency and cluster size was fitted with an exponential decay function. The probability of asynchronous AP activity (%) was quantified for *each AP cluster* by taking the number of asynchronous APs that fired in a given condition divided by the total number of active APs (asynchronous and synchronous) within each cluster, multiplied by 100%. Distributions of asynchronous firing across clusters were constructed. The total probability of asynchronous AP activity (%) was calculated as the number of asynchronously firing APs *regardless of cluster* divided by the total number of active APs (asynchronous and synchronous), multiplied by 100%.

3.2.6 Statistical Analysis

In Experiment One, a repeated-measures analysis of variance (RM ANOVA) assessed the effect of study conditions (i.e., BSL, -10 mmHg LBNP, -40 mmHg LBNP, and APN) on AP patterns. For Experiment Two, RM ANOVAs evaluated differences in asynchronous AP discharge between BSL, the last minute of the trimethaphan infusion, and the period

of the trimethaphan infusion without visible bursts. For both experiments, post-hoc t -tests with a Holm-Bonferroni (20) correction were employed for significant RM ANOVAs to expose which conditions were different from BSL. The relationship between the probability of asynchronous firing or asynchronous AP frequency and normalized cluster size was fitted with a logarithmic function. Bland-Altman agreement analysis assessed the repeatability of asynchronous discharge across different segments at BSL. Statistical analyses were performed with SPSS Statistics (v 25, IBM Corp., Armonk, NY, USA). Tests were two tailed with $\alpha = 0.05$. Data are reported as mean \pm standard deviation unless stated otherwise.

3.3 Results

Experiment One: Quantifying AP synchronicity during baseline, baroreflex, and apneic stress

Analyses were performed on a total of 607 ± 294 APs (183 ± 99 asynchronous APs), 490 ± 260 APs (114 ± 59 asynchronous APs), 753 ± 369 APs (107 ± 67 asynchronous APs), and 197 ± 79 APs (24 ± 14 asynchronous APs) at BSL, -10 mmHg LBNP, -40 mmHg LBNP, and APN, respectively in Experiment One.

Compared with BSL, total integrated MSNA increased due to greater burst occurrence in -10 mmHg LBNP, and due to greater burst occurrence and amplitude during -40 mmHg LBNP and APN (Table 3.1). Compared to BSL, changes in the integrated measures of MSNA with -10 mmHg LBNP, -40 mmHg LBNP, and APN were attributed to the increased occurrence of synchronously firing APs and the number of synchronous APs per burst. In this study, the total number of synchronously firing AP clusters was unchanged, but the number of unique AP clusters firing synchronously in bursts was

increased in all experimental conditions, relative to BSL (Table 3.1). While there was a main effect of experimental condition (both RM ANOVA $P < 0.05$) for both integrated burst and synchronous AP latencies, post-hoc tests revealed no differences on going from BSL to -10 mmHg LBNP, -40 mmHg LBNP, and APN (Table 3.1). Hemodynamic variables across conditions are presented in Table 3.1.

At BSL ($R^2 = 0.42$, $P < 0.05$), -10 mmHg LBNP ($R^2 = 0.54$, $P < 0.05$), -40 mmHg LBNP ($R^2 = 0.74$, $P < 0.05$), and APN ($R^2 = 0.47$, $P < 0.05$) synchronous AP cluster latency was related to cluster size, as modelled by an exponential decay function. Consistent with previous work (37), these data support the concept that the synchronous AP clusters detected here scaled to the diameter of the sympathetic c-fibres within the microneurographic recording field.

The representative data from one participant presented in Figure 3.2 demonstrate the between-burst asynchronous sympathetic AP discharge that exhibited weak cardiac-rhythmicity across all experimental conditions. During BSL, 33 ± 12 % of total APs fired asynchronously. Compared to BSL, the probability of asynchronous AP activity decreased with -10 mmHg LBNP (26 ± 10 %), -40 mmHg LBNP (15 ± 7 %), and APN (14 ± 7 %) (Condition Main Effect: $P < 0.05$; all $P_{Post-hoc} < 0.05$) (Fig. 3.3). However, these changes were attributed to greater synchronous discharge (i.e., increased burst frequency) as asynchronous AP frequency (i.e., APs observed in the absence of bursts) was not different from BSL (67 ± 37 AP/min) to -10 mmHg LBNP (69 ± 33 AP/min), -40 mmHg LBNP (83 ± 68 AP/min), or APN (62 ± 39 AP/min) (Condition Main Effect: $P > 0.05$) (Fig. 3.3). Compared to baseline (11 ± 5 clusters), the total number of asynchronous clusters was similar at -10 mmHg LBNP (12 ± 5 clusters, $P_{Post-hoc} > 0.05$) and -40 mmHg

LBNP (12 ± 5 clusters, $P_{Post-hoc} > 0.05$), but reduced with APN (6 ± 2 clusters; $P_{Post-hoc} < 0.05$) (Condition Main Effect: $P < 0.05$). Males and females exhibited similar asynchronous behaviour across experimental conditions. As depicted in Figure 3.4, when APs were arranged by peak-to-peak amplitude and clusters were normalized across conditions, asynchronous APs exhibited similar morphologies to the synchronously firing APs within the same cluster, across all conditions.

When asynchronous APs were sorted by peak-to-peak amplitude and assigned to 10 normalized clusters, a pattern emerged whereby the asynchronous probability decreased as a logarithmic function of AP cluster size (i.e., smaller APs were more likely to fire asynchronously) across all conditions (BSL: $R^2 = 0.90$, $P < 0.05$; -10 mmHg LBNP: $R^2 = 0.82$, $P < 0.05$; -40 mmHg LBNP: $R^2 = 0.74$, $P < 0.05$; APN: $R^2 = 0.84$, $P < 0.05$) (Fig. 3.5). A similar logarithmic relationship was observed for asynchronous AP frequency. Examining the size-distribution of normalized AP clusters demonstrated that AP frequency was consistent for all clusters across the experimental conditions (Fig. 3.5).

Experiment Two: Exploring ganglionic mechanisms contributing to AP synchronicity

This results section describes the role of the sympathetic paravertebral ganglia in AP synchronicity. In our previous study (24) examining synchronous AP discharge during ganglionic blockade, we identified that trimethaphan infusion produced an ordered de-recruitment of synchronous APs beginning with the larger APs active at BSL, followed by reductions in the occurrence of smaller synchronous APs. After several minutes of the trimethaphan infusion, integrated bursts of MSNA were no longer visible, yet we recorded a population of smaller, trimethaphan-resistant APs. As reported previously

(24), HR increased and mean arterial pressure decreased from BSL (57 ± 11 bpm, 97 ± 7 mmHg) to the last minute of trimethaphan with visible bursts (66 ± 12 bpm, 90 ± 7 mmHg) and the period of the trimethaphan infusion where bursts were abolished but trimethaphan-resistant APs persisted to fire (80 ± 6 bpm, 87 ± 12 mmHg) (Condition Effect for both HR and BP: $P < 0.05$, all $P_{Post-hoc} < 0.05$).

Analyses for Experiment Two were performed on a total of 620 ± 311 APs (148 ± 43 asynchronous APs), 88 ± 52 APs (70 ± 50 asynchronous APs), and 76 ± 63 APs (all APs were deemed asynchronous) at BSL, the last minute of the trimethaphan condition with visible bursts, and the period of the trimethaphan condition where bursts had been abolished, respectively.

As highlighted by one participant's data in Figure 3.6, the present study tracked and quantified both synchronous and asynchronous AP discharge from BSL to the last minute of the trimethaphan condition with visible integrated bursts, and the period of the trimethaphan infusion where visible bursts had been blocked but a population of smaller APs persisted to fire asynchronously. In the current analysis, trimethaphan infusion was associated with de-recruitment of larger asynchronous APs. Compared to BSL (11 ± 4 AP clusters), the total number of asynchronous clusters was reduced in the final minute of the trimethaphan infusion with visible bursts (7 ± 2 AP clusters), and during the period of the trimethaphan infusion where bursts were no longer visible (6 ± 2 AP clusters) (Condition Main Effect $P < 0.05$; both $P_{Post-hoc} < 0.05$). Relative to BSL (29 ± 16 %), the total probability of asynchronous AP firing increased in the final minute of the trimethaphan infusion with visible bursts (76 ± 13 %; $P_{Post-hoc} < 0.05$) and further

increased to $100 \pm 0 \%$ ($P_{Post-hoc} < 0.05$) during the period of the trimethaphan infusion where smaller APs persisted to fire without visible bursting (Condition Main Effect $P < 0.05$). However, these changes were attributed to reductions in synchronous AP firing in bursts with trimethaphan as asynchronous AP frequency did not change from BSL (53 ± 15 AP/min) to the last minute of the trimethaphan infusion with visible bursts (47 ± 23 AP/min), or the period of the trimethaphan infusion without visible bursts [38 ± 31 AP/min; (24)] (Condition Main Effect: $P > 0.05$).

When asynchronous APs were sorted by peak-to-peak amplitude and assigned to 10 normalized clusters, asynchronous AP probability decreased as a logarithmic function of cluster size at BSL ($R^2 = 0.93$, $P < 0.05$) and this relationship was maintained but shifted upwards for the smaller asynchronous APs continuing to fire during the last minute of the trimethaphan condition with visible bursts ($R^2 = 0.70$, $P < 0.05$) (Fig. 3.7). When visible bursts had been abolished by trimethaphan, the smallest APs that expressed the greatest asynchronous probability at BSL continued to fire asynchronously without producing bursts (Fig. 3.7). Trimethaphan de-recruited the largest asynchronous APs but did not alter the firing rate across the size-distribution of the smaller asynchronous APs (Fig. 3.7).

Repeatability Analysis

Bland-Altman plots (not shown) constructed with data from two BSL periods (BSL Period One: 199 ± 20 s, BSL Period Two: 176 ± 54 s) from a sub-sample of 8 individuals ($n = 4$ participants from Experiment Two; $n = 5$ females) revealed strong agreement for the probability of asynchronous APs (BSL Period One: $30 \pm 15 \%$, BSL Period Two: $30 \pm 13 \%$; mean difference: $1 \pm 5 \%$, mean absolute difference: $4 \pm 3 \%$) and asynchronous

AP frequency (BSL Period One: 45 ± 15 AP/min, BSL Period Two: 43 ± 19 AP/min; mean difference: -1 ± 8 AP/min, mean absolute difference: 6 ± 8 AP/min). For both variables, all data points fell within two standard deviations of the mean difference. Neither variable exhibited fixed bias (both $P > 0.67$). When differences between baseline periods were regressed against the mean of the baseline periods, asynchronous AP probability and asynchronous AP frequency did not express proportional bias (both $P > 0.14$).

Table 3.1 Hemodynamic, integrated muscle sympathetic nerve activity, and synchronous sympathetic action potential indices during BSL, -10 mmHg LBNP, -40 mmHg LBNP, and APN.

	BSL	-10 mmHg LBNP	-40 mmHg LBNP	APN
<i>Hemodynamic indices</i>				
HR, bpm*	60 (7)	61 (6)	75 (9)†	68 (6)†
MAP, mmHg*	89 (6)	94 (4)†	93 (6)†	100 (8)†
PP, mmHg*	52 (6)	54 (6)	46 (8)	53 (8)
SBP, mmHg*	124 (9)	130 (6)†	123 (10)	135 (13)†
DBP, mmHg*	72 (6)	76 (4)†	78 (5)†	83 (6)†
SV, mL*	89 (20)	88 (20)	65 (19) †	85 (19)
Q, L/min*	5.3 (1.1)	5.3 (1.2)	4.9 (1.2)	5.7 (1.1)
TPR, mmHg/L/min	18 (4)	19 (5)	20 (5)	18 (4)
<i>Integrated indices</i>				
Burst Frequency, bursts/min*	20 (6)	24 (6)†	35 (8)†	35 (9)†
Burst Incidence, bursts/100beats*	33 (11)	40 (11)‡	48 (14)†	52 (14)†
Burst Amplitude, AU*	42 (7)	45 (8)	57 (8)†	64 (13)†
Total MSNA, AU/min*	801 (192)	1069 (202)†	1994 (523)†	2189 (596)†
Burst Latency, s*	1.32 (0.04)	1.33 (0.04)	1.32 (0.04)	1.29 (0.05)
<i>Synchronous AP indices</i>				
AP Frequency, AP/min*	144 (69)	211 (87)†	410 (207)†	397 (160)†
AP Incidence, AP/100beats*	246 (121)	351 (142)†	568 (325)†	593 (241)†
APs/burst*	7 (2)	8 (3)†	11 (4)†	11 (3)†
AP Clusters/burst*	4 (1)	4 (1)†	5 (2)†	5 (1)†
Total AP clusters*	14 (4)	15 (4)	18 (7)	16 (6)
AP Latency, s*	1.24 (0.04)	1.26 (0.03)	1.26 (0.04)	1.23 (0.01)

Values are mean (SD). BSL, baseline; LBNP, lower body negative pressure, APN, end-expiratory apnea; HR, heart rate; MAP, mean arterial pressure; PP, pulse pressure; SBP, systolic blood pressure; DBP, diastolic blood pressure; SV, stroke volume; Q, cardiac output; TPR, total peripheral resistance; MSNA, muscle sympathetic nerve activity; AP, action potential.

*, indicates condition main effect $P < 0.05$.

†, indicates $P_{Post-hoc} < 0.05$ vs. BSL

‡, indicates $P_{Post-hoc} = 0.08$ vs. BSL

□

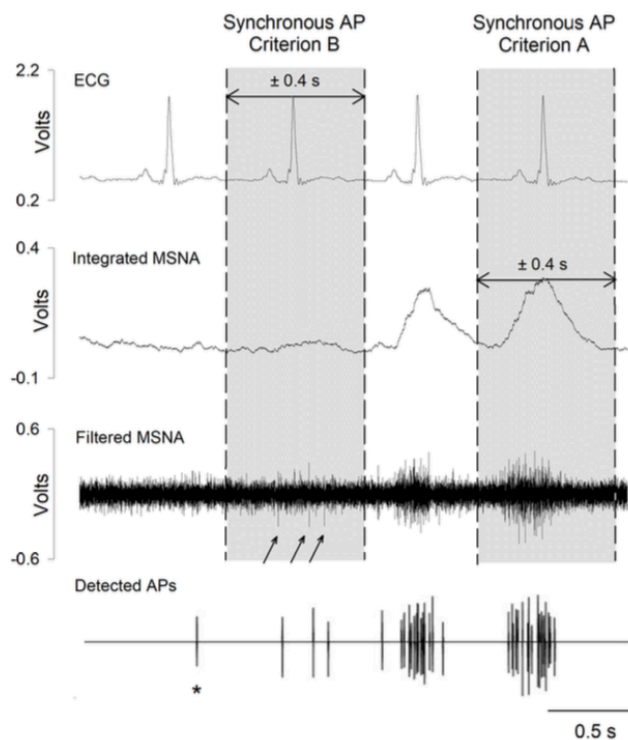


Figure 3.1 Criteria employed to discriminate between synchronous and asynchronous action potentials (AP) during analysis. Electrocardiogram (ECG), integrated muscle sympathetic nerve activity (MSNA), filtered MSNA, and detected APs from one individual. Synchronous AP criterion A: APs were considered to fire synchronously if their occurrence corresponded with ± 0.4 s from the peak of an integrated MSNA burst. Synchronous AP criterion B: When no integrated burst was apparent, APs were considered to fire synchronously if *at least 2 APs were visible* in the filtered neurogram and occurred within ± 0.4 s of an ECG R-wave. For HRs ≥ 75 bpm the window for synchronous APs was reduced to one-half of the R-R interval for that beat. The neurogram was corrected for the conduction delay. Arrows indicate three APs visible within the filtered neurogram. APs that did not satisfy these two criteria were deemed asynchronous. An asterisk (*) indicates the one asynchronous AP detected in this section of data.

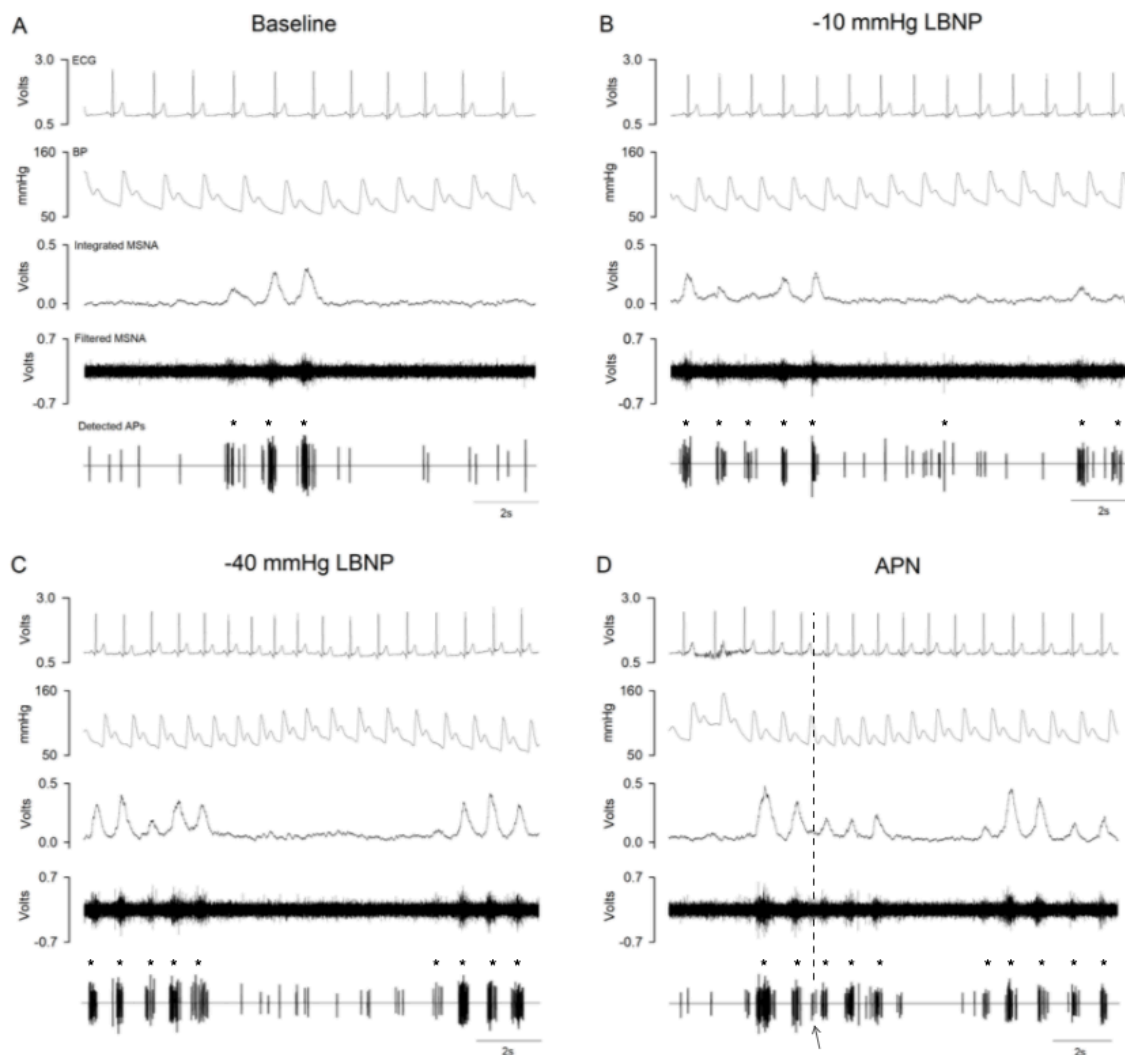


Figure 3.2 Representative data from one participant depicting the electrocardiogram (ECG), blood pressure (BP), integrated muscle sympathetic nerve activity (MSNA), filtered MSNA, and detected action potentials (AP) at baseline (BSL) (A), -10 mmHg lower body negative pressure (LBNP) (B), -40 mmHg LBNP (C), and the onset of end-expiratory apnea (APN). Data selections illustrate synchronous AP discharge [indicated by asterisks (*)] often forming bursts and asynchronous APs firing between bursts for each study condition. Notice in the APN data selection, as indicated by the arrow and dashed line, that some asynchronous APs fired without cardiac rhythmicity between two adjacent bursts of synchronous APs. All neurograms were corrected for the conduction delay.

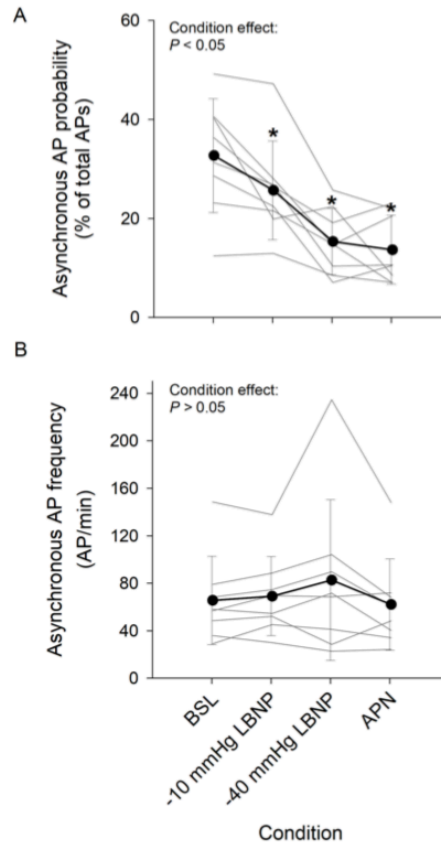


Figure 3.3 Probability (A) and frequency (B) of asynchronous action potential (AP) discharge at BSL (BSL), -10 mmHg lower body negative pressure (LBNP), -40 mmHg LBNP, and end-expiratory apnea (APN). Mean \pm SD for each condition are represented by filled circles and error bars. Individual data are represented by thin grey lines. P values for main effect of condition obtained with RM ANOVA are reported. *, indicate $P_{\text{post-hoc}} < 0.05$ vs. BSL.

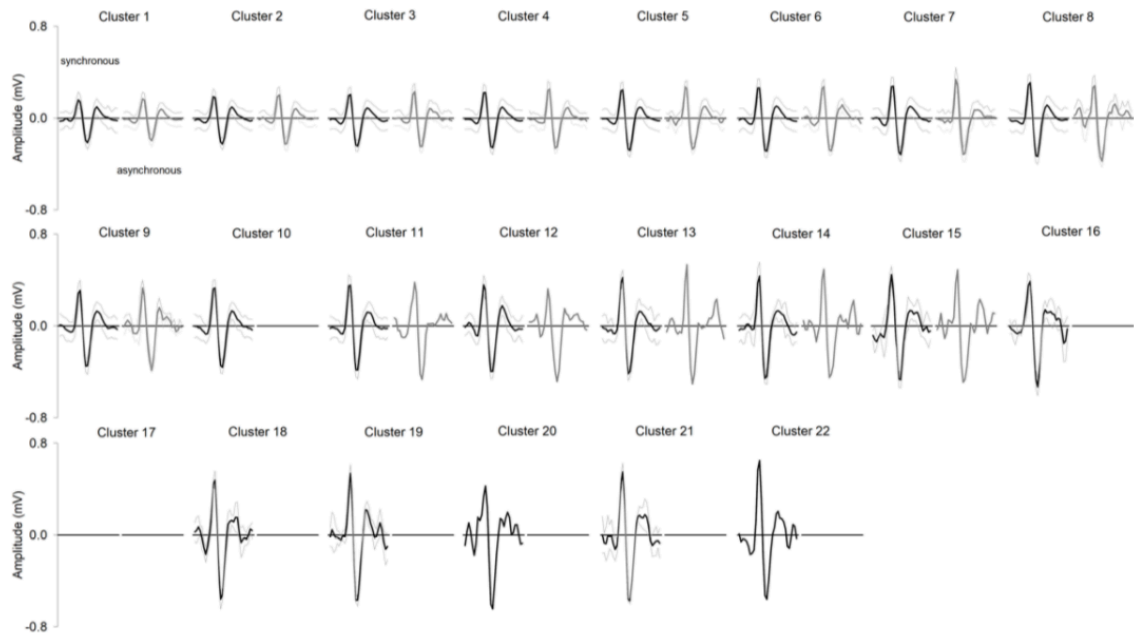


Figure 3.4 Representative morphologies of synchronously (left black tracing within each panel) and asynchronously (right grey tracing within each panel) discharging action potential (AP) clusters, detected in one participant during BSL (BSL), -10 mmHg lower body negative pressure (LBNP), -40 mmHg LBNP, and end-expiratory apnea (APN). AP clusters were binned based on peak-to-peak amplitude. $n = 1986$ synchronous and $n = 454$ asynchronous APs fired across all conditions. Thick and thin lines represent means and standard deviations of cluster amplitude, respectively. Clusters without a mean AP tracing indicate no AP activity across all study conditions.

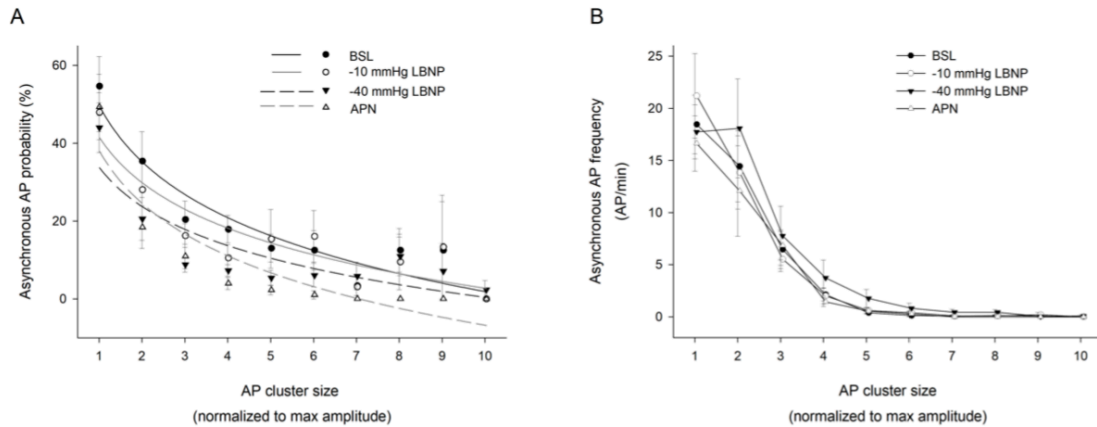


Figure 3.5 Asynchronous AP probability (A) and asynchronous AP frequency (B) versus normalized AP cluster (normalized to 10 clusters; e.g., cluster 1 represents 0-10% of largest cluster detected across all conditions) at baseline (BSL), -10 mmHg lower body negative pressure (LBNP), -40 mmHg LBNP, and end-expiratory apnea (APN). A and B: Mean \pm SE for each cluster are represented by filled circles and error bars. A: data from each condition were fitted with a logarithmic function.

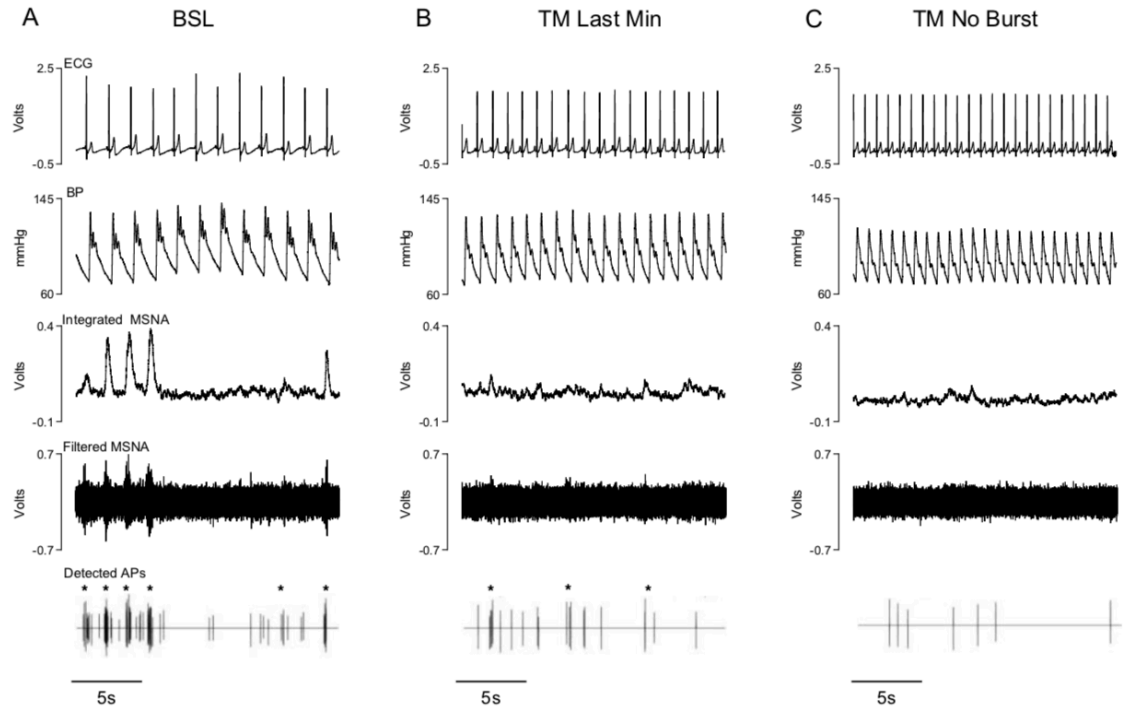


Figure 3.6 Representative data from one participant depicting the electrocardiogram (ECG), blood pressure (BP), integrated muscle sympathetic nerve activity (MSNA), filtered MSNA, and detected action potentials (AP) at baseline (BSL), the last minute of the trimethaphan infusion with visible bursts (TM Last Min), and the period of the trimethaphan infusion with no visible bursts (TM No Burst). Data selections illustrate synchronous AP discharge [indicated by asterisks (*)] often forming bursts and asynchronous APs firing between bursts for BSL and TM Last Min and without bursts in the TM No Burst condition. All neurograms were corrected for the conduction delay.

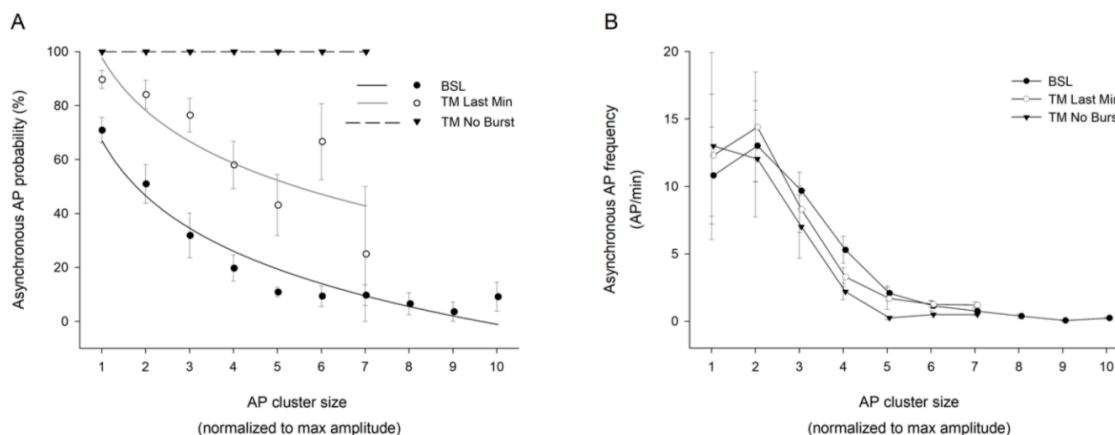


Figure 3.7 Asynchronous AP probability (A) and asynchronous AP frequency (B) versus normalized AP cluster (normalized to 10 clusters; e.g., cluster 1 represents 0-10% of largest cluster detected across all conditions) at BSL (BSL), the last minute of trimethaphan with visible bursts (TM Last Min), and the period of the trimethaphan infusion with no visible bursts (TM No Burst). A and B: Mean \pm SE for each cluster are represented by filled circles and error bars. A: data from BSL and TM Last Min were fitted with logarithmic functions. No error bars are visible for TM No Burst as all clusters expressed 100% asynchronous probability ($n = 7$). B: No error bars are visible for the BSL firing frequency of larger clusters due to small variability ($n = 7$). Notice that at BSL all sized APs fired asynchronously but smaller APs expressed the greatest probability of asynchronous activity. Trimethaphan de-recruited larger asynchronous APs but had no impact on the overall firing frequency of asynchronous APs.

3.4 Discussion

The present study provides novel insight to the fundamental behaviour of sympathetic discharge directed towards the circulation in humans. Specifically, we report asynchronous AP discharge during periods conventionally thought to represent ‘neural silence’ between bursts of synchronously firing sympathetic APs. At BSL, asynchronous AP discharge accounted for approximately 30% of total sympathetic AP activity in each of two separate experiments where data were obtained from two different laboratories. Asynchronous AP frequency (measured between bursts) remained constant across varying degrees of stress. However, the probability of asynchronous APs decreased with physiological stress due to increased synchronous AP discharge and burst frequency. Importantly, asynchronous discharge was not uniform across differently-sized APs, as the probability of asynchronous firing was reduced as cluster size increased. Through trimethaphan infusion in a group of females, we observed that the trimethaphan-resistance property of smaller APs, which we hypothesized earlier (24) to represent non-nicotinic ganglionic mechanisms, contributes to asynchronous discharge of smaller APs in humans.

Previous investigations employing single- (26) and multi-fibre microneurography (37) have exposed the fundamental AP patterns contributing to the variability in integrated burst size and frequency in humans. By studying all active APs in the current analysis, rather than just those that are found within identified bursts, we observed asynchronous, between-burst AP activity in healthy individuals and replicated this finding during BSL conditions in a separate group tested in a different laboratory. To our knowledge, this study describes the first quantification of synchronicity and report of asynchronous

discharge within the human sympathetic nervous system. Nonetheless, several studies in felines have documented asynchronous behaviour in the sympathetic neurogram (10, 11, 19, 22) (discussed in detail below). Asynchronously discharging APs have also appeared in figures from microneurographic recordings made in humans by multiple laboratories (25, 30, 34) but have remained unquantified. Of note, in the present study, asynchronous behaviour was heterogenous, with proportions decreasing logarithmically with increasing cluster size, in both experiments. This observation aligns with previous evidence indicating non-uniform discharge, recruitment, and regulation across the size distribution of recorded APs (33, 34, 38). Asynchronous AP size likely scaled to sympathetic axon diameter as these APs were similar in morphology to the synchronous APs which expressed an exponential decay relationship between cluster latency and size. In fact, this observation suggests that asynchronous APs were also present within the burst periods. Whether this synchronization process was due to a time-varying synchronization mechanism, or simply, to random patterns of AP firing, sometimes falling at the time of a synchronized burst, remains unknown. Unfortunately, our approach to AP detection does not allow determination of whether the AP clusters that are observed between bursts (i.e., asynchronous) and within a burst (i.e., synchronized) arise from the same axon.

The physiological relevance of asynchronous APs remains a compelling question. During stress (e.g., orthostatic, apneic, chemical, etc.) the sympathetic nervous system increases the firing rate of previously active synchronous APs and recruits in a synchronized fashion a subpopulation of previously silent, larger APs increasing integrated burst size along with burst occurrence (4–7, 27). In contrast, under the conditions of physiological stress imposed here, the asynchronous APs do not appear to follow the same rules. It is

clear that bursty patterns of postganglionic sympathetic APs provide the most robust vasoconstrictor response (2, 3). Therefore, one explanation could be that asynchronous AP discharge represents an additional sympathetic communication strategy for maintenance of baseline vasomotor control and have less impact on stress-related vasoactive outcomes. During times of stress, this subpopulation of asynchronously firing APs may contribute to vasomotor regulation by firing within bursts through coincidental capture or some active AP synchronization mechanism. For example, the observation of unchanged asynchronous firing rate but greater burst frequency on going from BSL to baroreflex and apneic stress suggests a greater probability of coincidental incorporation of asynchronous APs in bursts. The finding that fewer asynchronous AP clusters fired during APN compared to BSL may point towards a stress-specific AP synchronization process. Both hypotheses represent additional mechanisms for increasing within-burst AP content during stress, beyond the recruitment of larger axons or increasing the firing rate of previously active synchronous axons.

Complex neural mechanisms likely govern synchronicity among human muscle sympathetic c-fibres. Here, in a group of women, we identified that trimethaphan de-recruited the largest asynchronously firing APs. However, smaller APs, which expressed the greatest asynchronous discharge at BSL (and across all conditions in Experiment One) persisted to fire throughout the trimethaphan infusion, demonstrating resistance to trimethaphan, as synchronous discharge dissipated. We interpret these data to suggest that nicotinic ganglionic mechanisms participate in the regulation of synchronous and asynchronous neuronal discharge and burst production, and that non-nicotinic mechanisms contribute to the regulation of a subpopulation of small diameter

asynchronously discharging postganglionic axons. The notion that the ganglia affect the synchronicity among sympathetic neurons has been tested in cats. These earlier studies noted that stimulation of preganglionic fibres or hypothalamic nuclei elicited a bimodal postganglionic response characterized by a rapid-onset synchronous discharge, followed by a delayed, longer-lasting asynchronous discharge (10, 11, 19). Furthermore, the rapid-onset burst of activity to preganglionic stimulation in these experimental models was consistently abolished by nicotinic receptor antagonists, whereas muscarinic antagonists eliminated asynchronous firing (10, 11, 19, 22). In canines, a nicotinic-muscarinic interaction mediated the firing of a discrete subpopulation of postganglionic vasoconstrictor fibres that were activated by chemical stress and resistant to nicotinic blockade (18). Peptidergic and purinergic ganglionic co-transmission may also contribute to asynchronous AP firing (14, 21).

Additional factors beyond ganglionic mechanisms may contribute to asynchronous AP discharge. We base this conjecture on the finding that asynchronous firing was observed across all AP clusters, not just the smaller APs expressing trimethaphan-resistance. One possibility is the baroreflex effect that exerts considerable influence over the cardiac-gated bursty pattern of MSNA (12, 29). Our previous study examining only synchronously firing APs revealed that small-to-moderate sized APs received considerable baroreflex influence whereas the larger APs did not (34). This may be attributed to sympathetic neurons projecting directly from supra-medullary sites (e.g., paraventricular hypothalamus or pons) to spinal neurons, as documented in rats (39). Specifically, the current analysis revealed that asynchronous APs did not always exhibit cardiac rhythmicity and asynchronous AP frequency remained constant in both

experiments across a range of HRs and BPs, suggesting that features of baroreflex or cardiac afferent inputs do not modulate completely this population of sympathetic neurons. Also, the rhythmicity – due to intrinsic pacemaker behaviour and/or neural inputs – of extra-baroreflex supra-medullary and spinal nuclei likely exert additional control over AP synchronization, but how these sites interact with the baroreflex to shape postganglionic discharge requires investigation (1, 8, 15, 28). Combined, our two experiments suggest that compared to synchronously discharging axons, the postganglionic c-fibres generating asynchronous APs are governed differently at the central and/or peripheral level of the sympathetic organization.

We are confident that all APs reflected sympathetic postganglionic axonal firing for the following reasons. First, the continuous wavelet technique used here extracts APs matching real human muscle sympathetic APs (32). Inspection of all extracted AP clusters revealed the prototypical extracellular sympathetic c-fibre morphology as obtained by the hardware and signal processing employed by our laboratory (38) and others (13). Second, the microneurographic recordings were made from muscle sympathetic bundles only, as in each participant the neural signal expressed spontaneous pulse-rhythmic bursting that increased during apnea but not with arousal to a loud noise or when stroking the skin (16). Third, based on the high-quality nerve recordings our AP detection software operates with a false detection rate of less than 3% (32). While the possibility remains, the abovementioned lines of evidence minimize the likelihood that our analysis included sympathetic APs other than those originating from muscle sympathetic nerves.

3.4.1 Conclusion

This study advances our knowledge of the sympathetic neural communication strategies contributing to circulatory regulation. Particularly, we identified that asynchronous AP discharge, rather than complete ‘neural silence’, exists between bursts of synchronously firing sympathetic APs, and the degree of asynchronous discharge scales inversely to AP size, such that smaller APs express the greatest probability of asynchronous firing. Thus, approaches to MSNA quantification that rely on signal integration (16), or focusing on within-burst AP discharge using single- (27) or multi-unit (38) techniques, appear to underestimate and conceal a fundamental element of muscle sympathetic AP discharge. During a physiological challenge, the inclusion of previously asynchronous APs into bursts may represent an additional strategy to increase burst size. Based on patterns of AP behaviour during the trimethaphan infusion, we propose that non-nicotinic receptors at the ganglia underlie asynchronous behaviour, at least for the smaller AP clusters. However, central sympathetic mechanisms such as reduced baroreflex control of discrete AP subpopulations may also generate asynchronous firing. The current findings represent an additional layer of intricacy contained within the neural language of the sympathetic nervous system as well as a component of the neural organization subserving this communication strategy.

3.5 References

1. **Al-Khazraji BK, Shoemaker JK.** The human cortical autonomic network and volitional exercise in health and disease. *Appl Physiol Nutr Metab* 43: 1122–1130, 2018.
2. **Andersson PO.** Comparative vascular effects of stimulation continuously and in bursts of the sympathetic nerves to cat skeletal muscle. *Acta Physiol Scand* 118: 343–348, 1983.
3. **Ando S, Imaizumi T, Takeshita A.** Effects of patterns of sympathetic nerve stimulation on vasoconstricting responses in the hindquarter of rabbits. *J Auton Nerv Syst* 45: 225–233, 1993.
4. **Badrov MB, Barak OF, Mijacika T, Shoemaker LN, Borrell LJ, Lojpur M, Drvis I, Dujic Z, Shoemaker JK.** 50 Years of Microneurography: Insights into Neural Mechanisms in Humans: Ventilation inhibits sympathetic action potential recruitment even during severe chemoreflex stress. *J Neurophysiol* 118: 2914, 2017.
5. **Badrov MB, Lalande S, Olver TD, Suskin N, Shoemaker JK.** Effects of aging and coronary artery disease on sympathetic neural recruitment strategies during end-inspiratory and end-expiratory apnea. *Am J Physiol Circ Physiol* 311: H1040–H1050, 2016.
6. **Badrov MB, Olver TD, Shoemaker JK.** Central vs. peripheral determinants of sympathetic neural recruitment: insights from static handgrip exercise and postexercise circulatory occlusion. *Am J Physiol Integr Comp Physiol* 311: R1013–R1021, 2016.
7. **Badrov MB, Usselman CW, Shoemaker JK.** Sympathetic neural recruitment strategies: responses to severe chemoreflex and baroreflex stress [Online]. *Am J Physiol Integr Comp Physiol* 309: R160–R168, 2015.
8. **Barman SM, Yates BJ.** Deciphering the Neural Control of Sympathetic Nerve Activity: Status Report and Directions for Future Research. *Front Neurosci* 11: 730, 2017.
9. **Bronk DW, Ferguson LK, Margaria R, Solandt DY.** The activity of the cardiac sympathetic centers. *Am J Physiol Content* 117: 237–249, 1936.
10. **Brown AM.** Cardiac sympathetic adrenergic pathways in which synaptic transmission is blocked by atropine sulfate. *J Physiol* 191: 271–288, 1967.
11. **Brown AM.** Sympathetic ganglionic transmission and the cardiovascular changes of the defense reaction in the cat. *Circ Res* 24: 843–849, 1969.
12. **Delius W, Hagbarth K, Hongell A, Wallin BG.** General characteristics of

- sympathetic activity in human muscle nerves [Online]. *Acta Physiol Scand* 84: 65–81, 1972.
13. **Diedrich A, Charoensuk W, Brychta RJ, Ertl AC, Shiavi R.** Analysis of raw microneurographic recordings based on wavelet de-noising technique and classification algorithm: wavelet analysis in microneurography. *IEEE Trans Biomed Eng* 50: 41–50, 2003.
 14. **Gibbins IL, Jobling P, Messenger JP, Teo EH, Morris JL.** Neuronal morphology and the synaptic organisation of sympathetic ganglia. *J Auton Nerv Syst* 81: 104–109, 2000.
 15. **Gilbey MP.** Sympathetic rhythms and nervous integration. *Clin Exp Pharmacol Physiol* 34: 356–361, 2007.
 16. **Hagbarth K, Vallbo ÅB.** Pulse and respiratory grouping of sympathetic impulses in human muscle nerves. *Acta Physiol Scand* 74: 96–108, 1968.
 17. **Hart ECJ, Head GA, Carter JR, Wallin G, May CN, Hamza SM, Hall JE, Charkoudian N, Osborn JW.** Recording sympathetic nerve activity in conscious humans and other mammals: guidelines and the road to standardization. *Am J Physiol Circ Physiol* 312: H1031–H1051, 2017.
 18. **Henderson CG, Ungar A.** Effect of cholinergic antagonists on sympathetic ganglionic transmission of vasomotor reflexes from the carotid baroreceptors and chemoreceptors of the dog. *J Physiol* 277: 379–385, 1978.
 19. **Hoffmeister B, Hussels W, Jänig W.** Long-lasting discharge of postganglionic neurones to skin and muscle of the cat's hindlimb after repetitive activation of preganglionic axons in the lumbar sympathetic trunk. *Pflügers Arch* 376: 15–20, 1978.
 20. **Holm S.** A simple sequentially rejective multiple test procedure. *Scand J Stat* 6: 65–70, 1979.
 21. **Jan LY, Jan YN.** Peptidergic transmission in sympathetic ganglia of the frog. *J Physiol* 327: 219–246, 1982.
 22. **Jänig W, Krauspe R, Wiedersatz G.** Reflex activation of postganglionic vasoconstrictor neurones supplying skeletal muscle by stimulation of arterial chemoreceptors via non-nicotinic synaptic mechanisms in sympathetic ganglia. *Pflügers Arch* 396: 95–100, 1983.
 23. **Klassen SA, De Abreu S, Greaves DK, Kimmerly DS, Arbeille P, Denise P, Hughson RL, Normand H, Shoemaker JK.** Long-duration bed rest modifies sympathetic neural recruitment strategies in males and females. *J Appl Physiol* 124: 769–779, 2017.

24. **Klassen SA, Limberg JK, Baker SE, Nicholson WT, Curry TB, Joyner MJ, Shoemaker JK.** The role of the paravertebral ganglia in human sympathetic neural discharge patterns. *J Physiol* 596: 4497–4510, 2018.
25. **Macefield VG, Elam M, Wallin BG.** Firing properties of single postganglionic sympathetic neurones recorded in awake human subjects. *Auton Neurosci* 95: 146–159, 2002.
26. **Macefield VG, Wallin BG.** Physiological and pathophysiological firing properties of single postganglionic sympathetic neurons in humans. *J Neurophysiol* 119: 944–956, 2017.
27. **Macefield VG, Wallin BG, Vallbo AB.** The discharge behaviour of single vasoconstrictor motoneurons in human muscle nerves. *J Physiol* 481: 799–809, 1994.
28. **Malpas SC.** The rhythmicity of sympathetic nerve activity. *Prog Neurobiol* 56: 65–96, 1998.
29. **McAllen RM, Malpas SC.** Sympathetic burst activity: characteristics and significance. *Clin Exp Pharmacol Physiol* 24: 791–799, 1997.
30. **Millar PJ, Murai H, Morris BL, Floras JS.** Microneurographic evidence in healthy middle-aged humans for a sympathoexcitatory reflex activated by atrial pressure. *Am J Physiol Circ Physiol* 305: H931–H938, 2013.
31. **Mueller PJ, Clifford PS, Crandall CG, Smith SA, Fadel PJ.** Integration of central and peripheral regulation of the circulation during exercise: acute and chronic adaptations. *Compr Physiol* 8: 103–151, 2011.
32. **Salmanpour A, Brown LJ, Shoemaker JK.** Spike detection in human muscle sympathetic nerve activity using a matched wavelet approach [Online]. *J Neurosci Methods* 193: 343–355, 2010.
33. **Salmanpour A, Brown LJ, Steinback CD, Usselman CW, Goswami R, Shoemaker JK.** Relationship between size and latency of action potentials in human muscle sympathetic nerve activity [Online]. *J Neurophysiol* 105: 2830–2842, 2011.
34. **Salmanpour A, Shoemaker JK.** Baroreflex mechanisms regulating the occurrence of neural spikes in human muscle sympathetic nerve activity [Online]. *J Neurophysiol* 107: 3409–3416, 2012.
35. **Scott DW.** On optimal and data-based histograms. *Biometrika* 66: 605–610, 1979.
36. **Shoemaker JK, Badrov MB, Al-Khazraji BK, Jackson DN.** Neural Control of Vascular Function in Skeletal Muscle. *Compr Physiol* 6: 303–329, 2016.

37. **Shoemaker JK, Klassen SA, Badrov MB, Fadel PJ.** Fifty years of microneurography: learning the language of the peripheral sympathetic nervous system in humans. *J Neurophysiol* 119: 1731–1744, 2018.
38. **Steinback CD, Salmanpour A, Breskovic T, Dujic Z, Shoemaker JK.** Sympathetic neural activation: an ordered affair. *J Physiol* 588: 4825–4836, 2010.
39. **Strack AM, Sawyer WB, Platt KB, Loewy AD.** CNS cell groups regulating the sympathetic outflow to adrenal gland as revealed by transneuronal cell body labelling with pseudorabies virus. *Brain Res* 491: 274–296, 1989.
40. **Vallbo ÅB, Hagbarth K-E, Wallin BG.** Microneurography: how the technique developed and its role in the investigation of the sympathetic nervous system [Online]. *J Appl Physiol* 96: 1262–1269, 2004.
41. **Van Lieshout JJ, Toska K, van Lieshout EJ, Eriksen M, Walløe L, Wesseling KH.** Beat-to-beat noninvasive stroke volume from arterial pressure and Doppler ultrasound. *Eur J Appl Physiol* 90: 131–137, 2003.

Chapter 4

4 Baroreflex control of sympathetic action potential subpopulations during orthostatic stress

4.1 Introduction

Pulse-rhythmic feedback from arterial baroreceptors synchronizes action potential (AP) discharge to produce the characteristic bursty pattern of muscle sympathetic nerve activity (MSNA) (5, 7, 35). While the baroreflex imposes strong regulation over the frequency of these bursts, burst amplitude — a function of the size and number of synchronously firing APs — exhibits only weak baroreflex control (14, 24, 37). This stems from the baroreflex exerting differential control over the varying-sized sympathetic APs (representing different sized axons) synchronized to fire in bursts (31). Specifically, under baseline conditions, the arterial baroreflex strongly governs medium-sized APs, which fire in most bursts, but minimally governs larger AP clusters, which fire with low probability and contribute proportionately more to larger bursts (31, 35). Also, small APs may not be governed strongly by the arterial baroreflex. In fact, we reported that 30% of total APs fired *asynchronously* outside baroreflex-gated bursts at baseline, with smaller APs expressing the greatest proportion of asynchronous discharge (17).

Arterial baroreflex-mediated sympathetic arousal represents a critical mechanism for blood pressure regulation during orthostatic stress (8, 33). Unlike other forms of stress (e.g., chemical, metabolic, or apneic) (15, 20, 34), baroreflex unloading represents a weak reflex when it comes to recruiting larger, latent AP clusters (i.e., high-threshold axons) until severe levels, such as -80 mmHg lower body negative pressure (LBNP), with some

inter-individual variability (2, 29). Thus, the baroreflex relies primarily on increasing the firing probability of previously-active APs (i.e., low-threshold axons) to elicit sympathoexcitation during orthostatic stress (29). Yet, the precise mechanisms subserving the enhanced firing rate remain unclear. Based on the observation that medium AP clusters express strong baroreflex regulation under baseline conditions (31) we reasoned that the upward shift in baroreflex control over integrated bursts of MSNA during orthostatic stress (11, 12, 29) might be related to specific control over these medium AP clusters along with relocation of the operating points to positions of greater gain to facilitate enhanced discharge. However, observations made during the hypotensive phase of a modified Oxford test of reduced firing probability of the cluster of the smallest APs (18) suggest that this subpopulation may express reductions in baroreflex control during orthostatic stress.

Therefore, this study aimed to examine the heterogeneity of baroreflex control over AP discharge by measuring the baroreflex gain of all AP clusters. This research tested the hypothesis that during orthostatic stress the baroreflex confers its greatest effect on the gain of medium AP clusters that fire normally with high probability. If so, then the change in position and slope of each AP cluster's baroreflex curve should vary across the distribution of recorded APs.

4.2 Methods

4.2.1 Ethical Approval

This study received approval from the Health Sciences Research Ethics Board at the University of Western Ontario (No. 108026). This study conforms to the *Declaration of*

Helsinki, except for registration in a database. Each participant provided informed written consent to the study following verbal and written explanations of study procedures

4.2.2 Sample

Six healthy young individuals (3 females) participated in this study (26 ± 1 years, 170 ± 2 cm, 70 ± 6 kg). Participants were normotensive and were free of cardiovascular or neurological disease. This study did not control for oral contraceptive use or stage of the menstrual cycle in females (39).

4.2.3 Experimental Procedures and Protocol.

Participants arrived at the *Laboratory for Brain and Heart Health* at the University of Western Ontario after a 4-hr fast and avoiding alcohol and caffeine consumption, and vigorous physical exercise for 12 hours. Participants were instructed to empty their bladder after which they assumed the supine position with their lower body sealed below the iliac crest in a LBNP chamber for the duration of the study. Participants were familiarized with a bout of LBNP prior to commencing the experimental protocol.

Data collection began following at least 30 minutes in the supine position. The experimental protocol consisted of: 1) at least 5 minutes under baseline (BSL) conditions, 2) 3 – 5 mins exposure to -40 mmHg LBNP, and 3) 3 – 5 mins exposure to -80 mmHg. The order of tests was not randomized or varied due to the greater risk of signal loss at the higher level of lower body suction. The maximal LBNP level that provided high quality microneurographic data was analyzed for each participant. LBNP -40 mmHg was used for two participants (1 female) and LBNP -80 was used for four participants. Similar

changes in baroreflex gain were observed on going from BSL to either -40 mmHg or -80 mmHg LBNP so these levels were collapsed into a single LBNP condition.

4.2.4 Experimental Measures and Analysis.

A 3-lead ECG measured heart rate (BioAmp FE132, ADInstruments; Bella Vista, New South Wales, Australia). Beat-by-beat blood pressure was measured by finger photoplethysmography (Finometer; Finapres Medical Systems, Amsterdam, The Netherlands) with the Modelflow algorithm providing stroke volume and cardiac output (40). Reconstructed brachial blood pressures were calculated and used for analysis. Total peripheral resistance was calculated as the quotient of mean arterial pressure and cardiac output. A calibrated pressure sensor measured chamber pressure (MLT0670, ADInstruments; Castle Hill, New South Wales, Australia).

Continuous muscle sympathetic postganglionic c-fibre discharge was measured from the common peroneal nerve as described originally by Hagbarth and Vallbo (9), and recently by our laboratory (16, 17). Postganglionic sympathetic activity was recorded with a nerve traffic analyzer (662C-3; Bioengineering University of Iowa, Iowa City, IA). The neural signal was pre-amplified with a gain of 1,000 (using preamplifier and isolation amplifier; gains of 100 and 10, respectively), then further amplified with a gain of 75 (using a variable gain amplifier). Neural activity was then band-pass filtered (bandwidth of 700–2,000 Hz) before being rectified and integrated (using a leaky integrator; 0.1-s time constant). Muscle sympathetic nerve activity (MSNA) was confirmed by the absence of skin paresthesia and the observation of an increase in bursting during a volitional apnea, but not arousal to a loud noise. Filtered and integrated MSNA signals were sampled at 10,000 Hz, while all other signals were sampled at 1,000 Hz. LabChart 8 and PowerLab

systems (ADInstruments; Bella Vista, New South Wales, Australia) enabled data collection, storage, and analysis.

Integrated MSNA bursts were analyzed if they aligned with an R-wave and exhibited a 2:1 ratio relative to the previous period of between-burst signal. Burst frequency (bursts/min), burst incidence (bursts/100beats), and burst amplitude (AU) normalized to the largest burst at BSL, provided metrics of the integrated MSNA.

As described previously (28), sympathetic APs were extracted from the filtered neurogram using a continuous wavelet transform. Based on our previous finding that a considerable amount of AP discharge occurs asynchronously *between bursts* (17), any AP that was detected during BSL and LBNP was extracted regardless of whether or not it occurred within an identified burst of MSNA. APs were ordered based on peak-to-peak amplitude and sorted into bins (i.e., clusters) using Scott's rule. Within each participant, AP bin properties were normalized to ensure that bin width, bin number, and maximum bin centre were identical between BSL and LBNP. This strategy enables quantification of the number of AP clusters that were recruited from BSL to LBNP and the change in firing probability for each cluster. Moreover, to enable between-participant comparisons of AP cluster activity, data were normalized to the largest AP cluster (which fired during LBNP in all participants) and assigned to 15 clusters. The signal-to-noise ratio (SNR) was determined as the amplitude of the negative peak of the mean AP over the standard deviation of the background noise around each AP at BSL (3.9 ± 0.1) and LBNP (4.1 ± 0.1). These values of SNR will ensure a correct detection rate of ~95% and a false positive rate of <3% (28).

During each condition, AP behaviour was quantified by AP frequency (AP/min), incidence (AP/100beats), and the total number of AP clusters (total bins). In heartbeats with AP discharge, AP behaviour was also quantified by the number of APs per heartbeat (spikes/beat) and the number of unique clusters per heartbeat (bins/beat). The firing probability (%) of each cluster was calculated as the quotient of the total number of times each cluster fired and the total number of heartbeats, multiplied by 100%.

4.2.5 Integrated baroreflex threshold and sensitivity

For both experimental conditions, baroreflex threshold and sensitivity analyses were performed for integrated bursts and AP clusters following the nomenclature employed previously (10, 14, 31). Baroreflex threshold analysis for integrated bursts involved grouping the diastolic blood pressures (DBP) of individual heartbeats into 2-mmHg bins and calculating the burst probability (%) for each DBP bin: that is, the percentage (%) of heartbeats per DBP bin that were associated with an integrated burst. Integrated baroreflex threshold gain for burst occurrence was measured as the slope of the linear relationship between burst probability versus the mean DBP for each bin. Baroreflex sensitivity gain for integrated burst size was measured as the slope of the relationship between individual normalized burst amplitude versus the corresponding DBP. For all regressions, Pearson's correlation coefficients were recorded. For both experimental conditions, the operating point was determined for integrated baroreflex threshold and sensitivity diagrams by plotting the point of intersection of mean burst probability or amplitude, respectively, and mean DBP.

4.2.6 Action potential baroreflex threshold and sensitivity

Baroreflex threshold analysis for AP occurrence was performed for each AP cluster based on a previously described method (31). Consistent with above, DBPs were grouped into 2-mmHg bins and AP probability (%) for each bin was calculated. For each cluster, baroreflex threshold gain was measured as the slope of the linear relationship between AP probability versus the mean DBP for each bin. AP baroreflex sensitivity gain was calculated as the slope of the linear relationship between the number of unique AP clusters that fired in each heartbeat versus the DBP for that beat. Pearson's correlation coefficients were recorded for each regression. For both experimental conditions, the operating point was determined for AP cluster baroreflex threshold diagrams by plotting the point of intersection for mean cluster probability and mean DBP. The operating point for AP baroreflex sensitivity was determined by plotting the point of intersection for the mean number of unique AP clusters per heartbeat and the mean DBP.

4.2.7 Statistical Analysis

A two-way repeated measures analysis of variance (RM ANOVA) assessed the impact of experimental condition and AP cluster on the slope of the AP level baroreflex threshold relationship. Main effects (i.e., condition, AP cluster) and interactions (i.e., condition-by-AP cluster) were tested. Hypothesis-driven planned contrasts were executed using one-tailed paired t-tests to inspect significant interactions. Paired sample t-tests examined the impact of condition on hemodynamic, integrated burst and AP indices, and baroreflex variables. Values are mean \pm SE. Tests were two-tailed unless otherwise specified, with $\alpha = 0.05$. Statistical analyses were performed with SPSS Statistics (v 25, IBM Corp., Armonk, NY, USA).

4.3 Results

Fig. 4.1 depicts the representative hemodynamic and sympathetic neural emissions at BSL and LBNP. Compared to baseline, burst occurrence and amplitude increased with LBNP (Table 4.1). Augmented integrated bursting behaviour during LBNP was associated with an increase in AP occurrence and AP content per heartbeat compared to BSL, which was attributed to an increase in the firing probability of previously active APs and the recruitment of larger latent APs (Table 4.1). Fig 4.2 illustrates AP discharge by cluster over time as a function of DBP in a single individual at BSL and LBNP. A total of 254 ± 22 s of data were analyzed at BSL and 182 ± 22 s during LBNP.

Fig. 4.3 illustrates the mean regression outcomes calculated for the baroreflex threshold and sensitivity diagrams for integrated sympathetic bursts during BSL and LBNP. Under BSL conditions, the baroreflex strongly regulated burst occurrence [slope (β): -3.8 ± 0.4 %/mmHg, y-intercept (y-int): 302 ± 31 %, $r = -0.89 \pm 0.03$], but exhibited weaker control (P value for b comparison: < 0.05) over normalized burst amplitude (β : -1.4 ± 0.4 AU/mmHg, y-int: 144 ± 29 AU, $r = -0.21 \pm 0.1$). Compared to BSL, neither the slope of the baroreflex threshold (β : -4.1 ± 0.8 %/mmHg, y-int: 357 ± 75 %, $r = 0.89 \pm 0.02$) or sensitivity (β : -0.7 ± 0.5 AU/mmHg, y-int: 125 ± 38 AU, $r = -0.04 \pm 0.1$) relationships were altered with LBNP (both $P > 0.05$). However, the operating points for both baroreflex threshold [BSL (DBP, probability): 71 ± 3 mmHg, 31 ± 3 %; LBNP (DBP, probability): 75 ± 2 mmHg, 51 ± 4 %] and sensitivity relationships [BSL (DBP, normalized amplitude): 71 ± 3 mmHg, 44 ± 3 AU; LBNP (DBP, normalized amplitude): 75 ± 2 mmHg, 73 ± 8 AU] were reset rightwards ($P < 0.05$) and upwards ($P < 0.05$) from BSL to LBNP.

Fig. 4.4 shows the mean baroreflex threshold relationships calculated for 15 normalized clusters at BSL and LBNP. At BSL, the strength of baroreflex control over AP occurrence varied by AP size, such that medium APs expressed the greatest threshold slopes, while the smallest (BSL normalized cluster 3 vs. BSL normalized cluster 1: $P < 0.05$) and largest (BSL normalized cluster 3 vs. BSL normalized cluster 7: $P < 0.05$) active clusters exhibited lesser threshold slopes. The change in baroreflex threshold slope from BSL to LBNP varied by AP cluster size (Condition: $P < 0.05$, Cluster: $P < 0.05$, Condition-by-Cluster: $P < 0.05$). Specifically, medium AP slopes increased with LBNP, while the slopes for the smallest and largest APs present at BSL exhibited a reduction and no change respectively, compared to BSL. The larger AP clusters which were silent at BSL and recruited with LBNP fired with low probabilities at LBNP and expressed weak baroreflex threshold slopes (LBNP normalized cluster 4 vs. LBNP normalized cluster 14: $P < 0.05$). Fig. 4.5 illustrates the interactive effects of condition and cluster on the slope of AP baroreflex threshold relationship. At BSL and LBNP, the mean Pearson's correlation statistics for the threshold relationships were stronger than $r = -0.50$ for all normalized clusters, with the exception of cluster 1 ($r = -0.49 \pm 0.10$), cluster 2 ($r = -0.36 \pm 0.10$), and cluster 15 ($r = -0.45 \pm 0.13$) firing during LBNP. Males and females expressed similar changes in baroreflex control of AP discharge from BSL to LBNP.

Inspection of operating points by cluster (Fig. 4.4) demonstrated that the AP clusters expressed non-uniform firing probabilities, where the medium APs exhibited the greatest probabilities and the smallest (BSL normalized cluster 3 vs. BSL normalized cluster 1: $P < 0.05$) and largest APs (BSL normalized cluster 3 vs. BSL normalized cluster 7: $P < 0.05$) present at BSL fired less often. The operating points of medium clusters (e.g.,

normalized clusters 3 to 8) were reset upwards ($P < 0.05$) and rightwards with LBNP ($P < 0.05$), while the operating points of smaller and larger clusters active at BSL were only shifted rightwards (Condition: $P < 0.05$, Cluster: $P < 0.05$, Condition-by-Cluster: $P < 0.05$).

Last, Fig. 4.6 highlights the mean baroreflex sensitivity relationships for AP cluster behaviour at BSL (β : -0.12 ± 0.03 AP clusters/beat/mmHg, y-int: 12 ± 3 AP clusters/beat) and LBNP (β : -0.22 ± 0.1 AP clusters/beat/mmHg, y-int: 21 ± 4 AP clusters/beat). A weak slope was observed for the baroreflex sensitivity relationship at BSL and was unchanged, but the operating point was reset rightwards ($P < 0.05$) and upwards ($P < 0.05$) with LBNP [BSL (DBP, AP clusters/beat): 71 ± 3 mmHg, 3 ± 0.3 AP clusters/beat; LBNP (DBP, AP clusters/beat): 75 ± 2 mmHg, 5 ± 1 AP clusters/beat]. Weak Pearson correlation coefficients were observed for the AP cluster baroreflex sensitivity relationships under both conditions (BSL: $r = -0.25 \pm 0.1$, LBNP: $r = -0.37 \pm 0.1$).

Table 4.1 Hemodynamic variables, integrated, and action potential level indices of muscle sympathetic nerve activity at baseline and lower body negative pressure.

	BSL	LBNP
<i>Hemodynamics</i>		
HR, bpm	60 (2)	92 (11)*
SBP, mmHg	124 (4)	116 (6)*
DBP, mmHg	71 (3)	75 (2)*
MAP, mmHg	89 (3)	89 (3)
PP, mmHg	53 (3)	41 (4)*
CO, L/min	6 (0.4)	5 (0.4)*
SV, mL	92 (7)	54 (7)*
TPR, mmHg/L/min	17 (2)	19 (2)*
<i>MSNA: Integrated Indices</i>		
Burst Frequency, bursts/min	19 (2)	45 (4)*
Burst Incidence, bursts/100beats	31 (3)	51 (4)*
Burst amplitude, AU	44 (3)	73 (8)*
<i>MSNA: AP indices</i>		
AP Frequency, AP/min	212 (41)	720 (117)*
AP Incidence, AP/100beats	356 (68)	859 (187)*
AP/beat	4 (1)	8 (2)*
Clusters/beat	3 (0.3)	5 (1)*
Total Clusters	18 (2)	29 (3)*

BSL, baseline; LBNP, lower body negative pressure; HR, heart rate; SBP, systolic blood pressure; DBP, diastolic blood pressure; MAP, mean arterial pressure; PP, pulse pressure; CO, cardiac output; SV, stroke volume; TPR, total peripheral resistance; MSNA, muscle sympathetic nerve activity; AP, action potential.

*, indicates $P < 0.05$ vs. BSL (paired t-test).

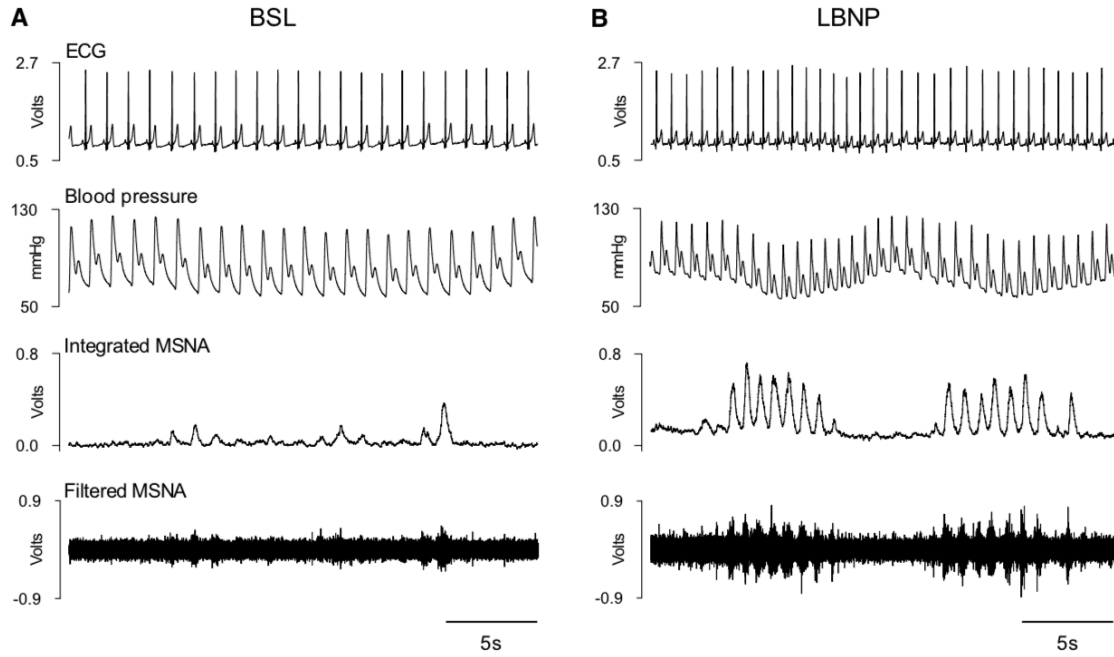


Figure 4.1 Data from a single individual illustrating hemodynamic data, integrated muscle sympathetic nerve activity (MSNA) and filtered MSNA at baseline (BSL) and lower body negative pressure (LBNP; -80 mmHg in this example).

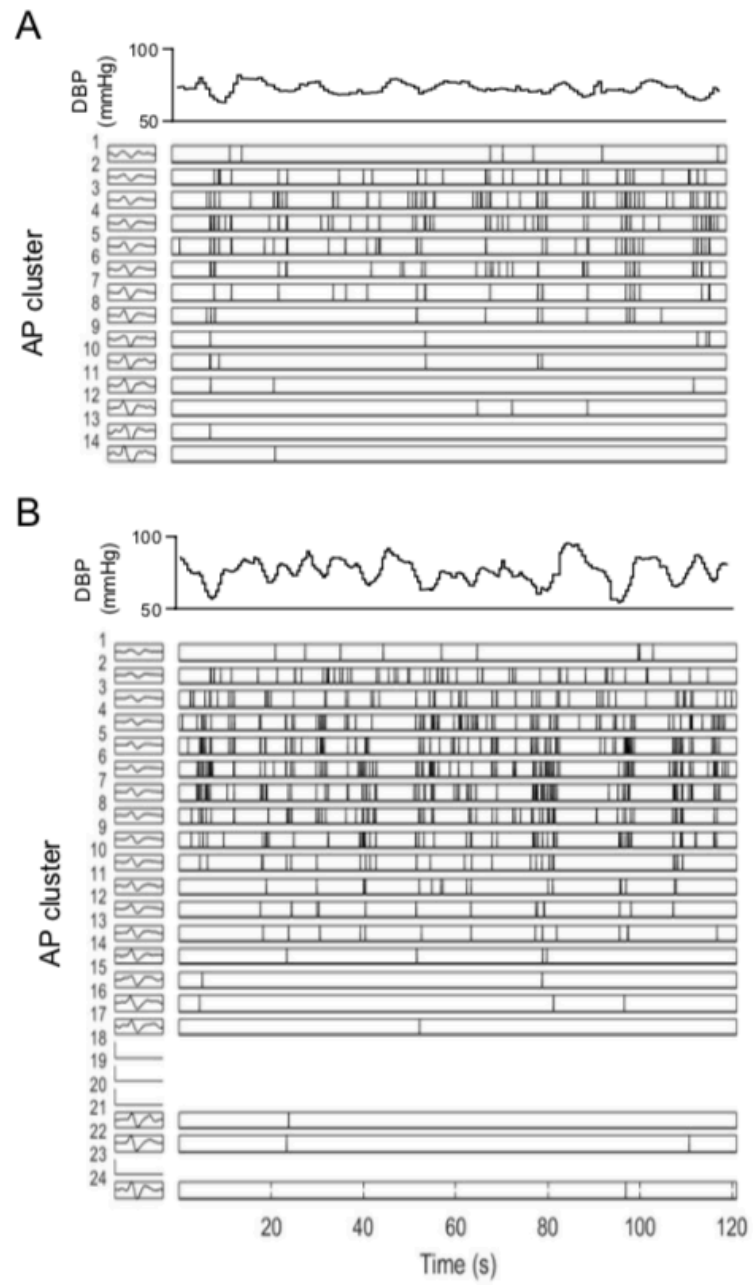


Figure 4.2 Data from a single individual illustrating the pattern of action potential (AP) discharge over time as a function of their diastolic blood pressure (DBP; top) and cluster (left) at baseline (BSL) (A) and lower body negative pressure (LBNP; -80 mmHg in this example) (B). AP cluster refers to all APs of similar morphology and are normalized between conditions to ensure within-participant comparisons (e.g., cluster 1 represents the same-sized APs at BSL and LBNP). (Previous page).

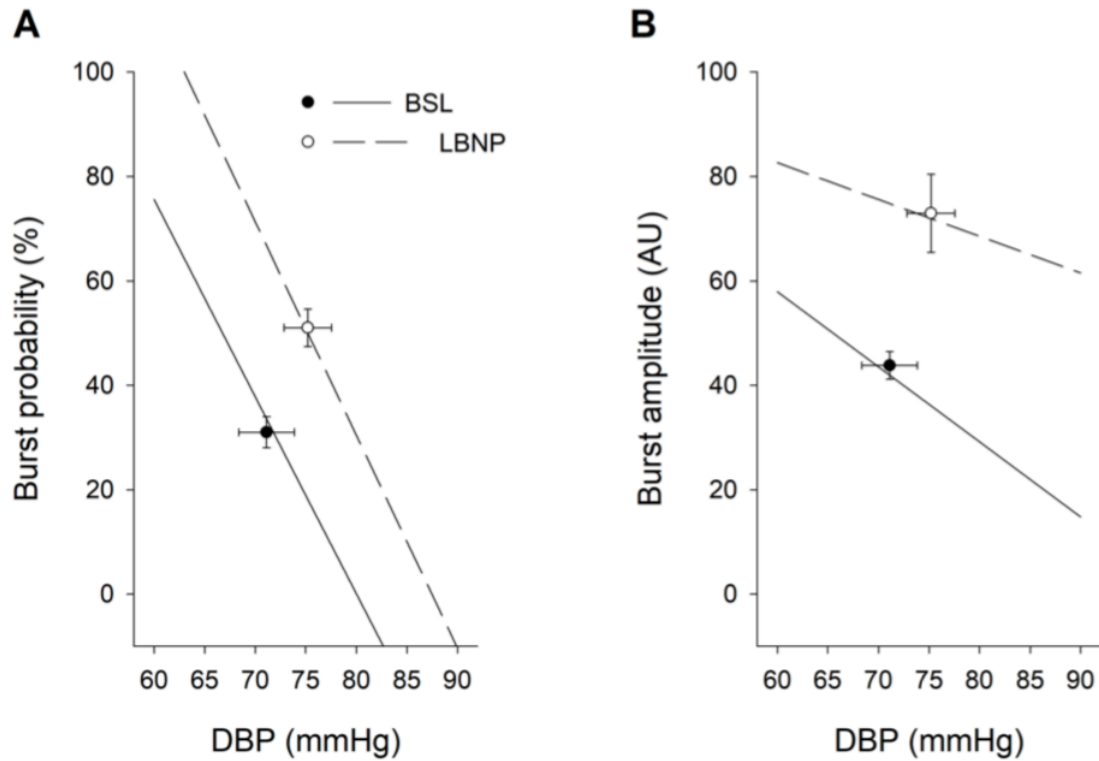


Figure 4.3 Mean baroreflex threshold relationships for the integrated muscle sympathetic nerve activity (MSNA) burst occurrence (A) and mean baroreflex sensitivity relationships for normalized integrated MSNA burst size at baseline (BSL) and lower body negative pressure (LBNP) (B). Filled and empty circles with error bars (SE) represent the operating points at BSL and LBNP, respectively.

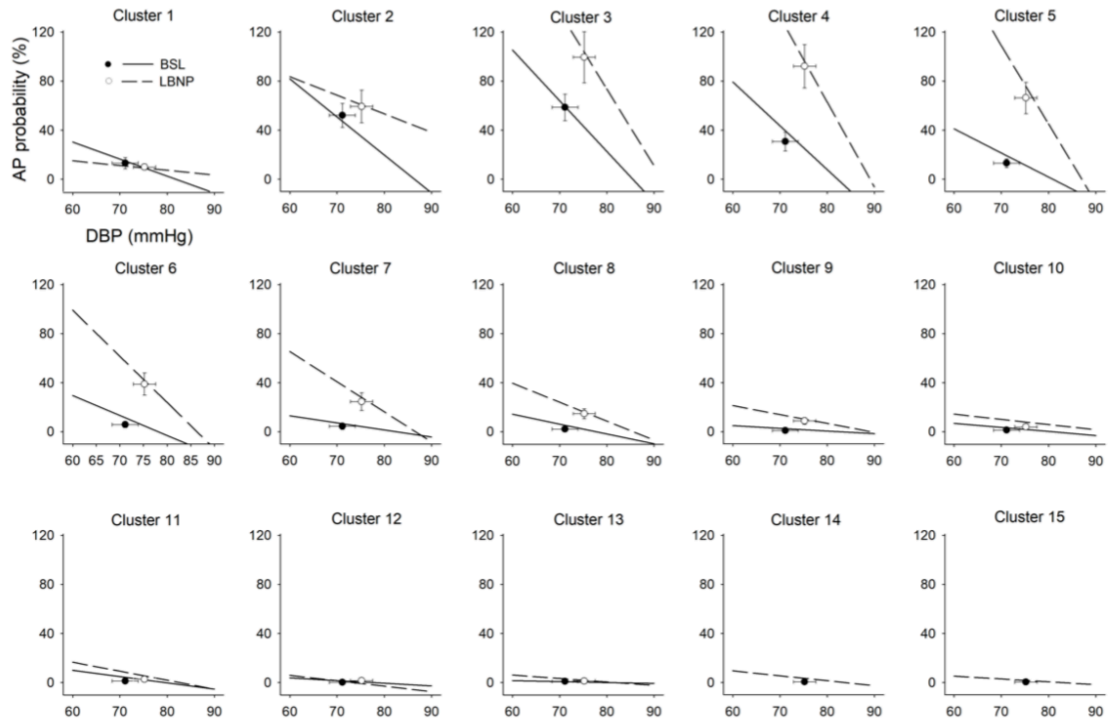


Figure 4.4 Mean baroreflex threshold relationships between action potential (AP) discharge probability and diastolic blood pressure (DBP) for 15 normalized clusters at baseline (BSL) and lower body negative pressure (LBNP). Filled and open circles with error bars (SE) represent the operating point for each cluster at BSL and LBNP, respectively.

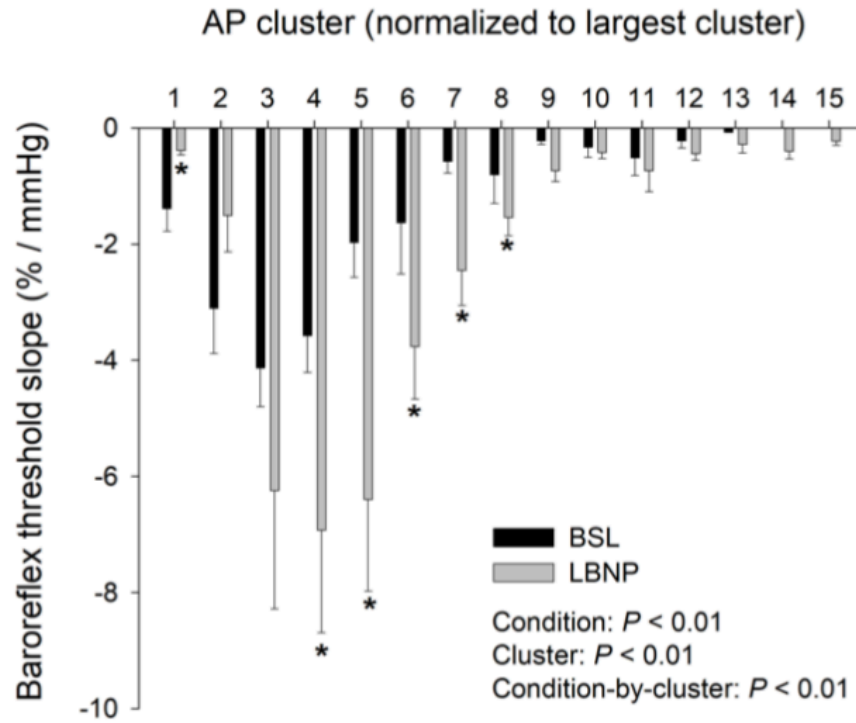


Figure 4.5 Mean baroreflex threshold slopes for 15 normalized action potential (AP) clusters at baseline (BSL) and lower body negative pressure (LBNP). Means and SE are presented. This figure represents the slopes of the baroreflex threshold relationships depicted in Fig. 4. *, indicates $P < 0.05$ (one-tailed, planned contrast).

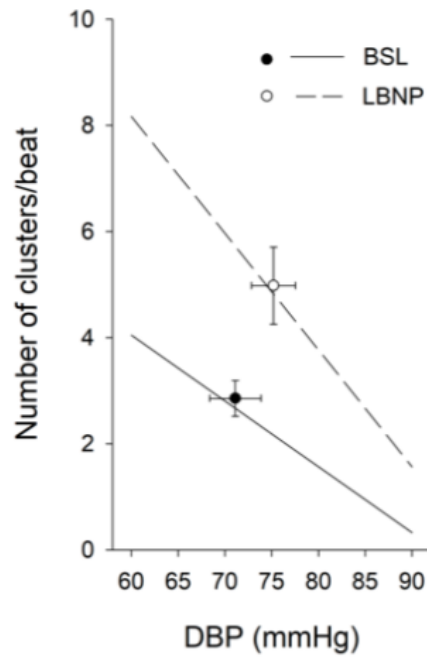


Figure 4.6 Mean baroreflex sensitivity relationship between the number of action potential (AP) clusters per beat and diastolic blood pressure (DBP) at baseline (BSL) and lower body negative pressure (LBNP). Filled and open circles with error bars (SE) represent the operating point at BSL and LBNP.

4.4 Discussion

The present study exposed new knowledge regarding the baroreflex mechanisms contributing to elevated sympathetic AP discharge during orthostatic stress. First, we identified that the baroreflex gain for APs active at BSL becomes modified during LBNP. However, LBNP-mediated modifications to baroreflex gain varied by AP cluster size such that the slopes for medium-sized APs increased with LBNP, while the slopes for the smallest and largest APs active at BSL exhibited a reduction and no change, respectively, compared to BSL. Also, new and larger APs that were silent at BSL and recruited with LBNP expressed weak baroreflex control. Examining baroreflex control of MSNA using integrated measures concealed the impact of LBNP as the strength of baroreflex control over burst occurrence and burst size was unchanged from BSL to LBNP. We interpret these findings to suggest that when defending blood pressure during orthostatic stress, baroreflex control of a discrete group of medium-sized sympathetic APs active at baseline becomes enhanced concurrent with an increase in firing rate. Also, the findings suggest further that the recruitment process that leads to the appearance of larger AP clusters during LBNP that were not present at baseline, is not due to a baroreflex mechanism.

In the present study, a collection of medium clusters (e.g., normalized clusters 4 to 8) exhibited augmented baroreflex gain concomitant with a relocation of the baroreflex slopes to greater firing probabilities and elevated DBP from BSL to LBNP. Some of these AP clusters expressed strong baroreflex slopes and fired with high probabilities at BSL (i.e., normalized clusters 4 and 5). This observation replicates findings from our previous investigation with a different group of participants (31). Of note, however, both

the gain and operating point of these high probability AP clusters were reset during LBNP. Thus, it appears that the baroreflex strongly controls the behaviour of most medium APs. Fundamentally, enhanced baroreflex control during LBNP enables greater inhibitory control to prevent exaggerated sympathetic arousal during orthostatic stress (41) but also greater AP firing for a given change in DBP.

Unlike medium AP clusters, the largest AP clusters active during BSL expressed weak baroreflex control that was unchanged with LBNP (i.e., normalized clusters 9 to 13). Whether greater levels of baroreflex stress than those imposed here could have augmented the baroreflex gain for these APs remains to be tested but we suspect that the likelihood remains low as these APs appear to be governed primarily by other neural inputs (1, 35). Similarly, we found the largest APs that were previously silent at BSL and recruited during LBNP express weak baroreflex slopes in all participants (i.e., normalized clusters 14 and 15). This finding aligns with our previous observation that this AP subpopulation was only recruited during severe levels of baroreflex stress (29). Here, even during baroreflex stimuli sufficient for recruitment, the baroreflex only weakly governed the moment-to-moment discharge of these APs. We suspect that either a threshold of baroreflex unloading must be reached to withdraw baroreflex-inhibition over the central neural region(s) primarily governing this subpopulation or some other non-baroreflex mechanism recruited these APs. Indeed, many forms of physiological stress recruit previously silent larger and faster conducting APs including those activating the arterial chemoreflex and muscle metaboreflex along with manoeuvres involving volitional effort or perceptual stress (e.g., Valsalva's Manoeuvre, voluntary apnea) (1, 15, 30, 32, 34, 35). In these other manoeuvres, it remains possible that baroreflex resetting is

responsible for the recruitment of previously silent APs. However, the current data argue against that mechanism. Rather, the present results support the hypothesis that large AP clusters, including those firing infrequently at BSL and the subpopulation of latent, high-threshold APs receive a variety of neural inputs, but baroreflex afferents do not represent the dominant source (19, 22). The organization of baroreflex inputs within medullary brainstem nuclei and/or direct projections from supra-medullary sites (e.g., paraventricular nucleus of the hypothalamus, caudal raphe nuclei, pons) to spinal preganglionic neurons may contribute to reduced baroreflex control of larger sympathetic axons (4, 21, 36).

In the current study, the cluster of the smallest APs (i.e., normalized cluster 1) expressed intriguing baroreflex control. In the BSL condition, the small APs demonstrated lesser baroreflex gain compared to medium-sized clusters. Previously our laboratory reported reduced baroreflex control as AP size increased, yet individual data figures presented in this earlier study do hint at the BSL behaviour illustrated here (31). This pattern was likely exposed more clearly in the present study by cluster normalization and because we extracted all detected APs regardless of if they fired within or between bursts, whereas our previous study focused solely on the synchronized APs forming integrated bursts (31). This analysis strategy was based on a recent observation that about 30% of sympathetic APs at BSL fire asynchronously *between* MSNA bursts in healthy young individuals, with the smallest APs expressing the greatest proportion of asynchronous activity (17). While we did not examine the baroreflex gain of synchronous and asynchronous APs separately here, reduced baroreflex control of small APs may

represent an additional mechanism contributing to asynchronous behaviour of this subpopulation in our previous study.

Compared to BSL, the cluster of the smallest APs (e.g., normalized cluster 1) showed reductions in baroreflex gain but no change in firing probability during LBNP, pointing to diminished baroreflex regulation during orthostatic stress. No previous study has investigated baroreflex control of AP occurrence during physiological stress, but some insight may be gained from earlier investigations of multi-unit AP discharge during baroreflex stress. Using the wavelet approach to extract APs firing within bursts, Limberg and colleagues (18) observed a paradoxical reduction in the smallest AP cluster firing probability during orthostatic stress imposed by sodium nitroprusside infusion. Also, the single-unit technique has exposed a subpopulation of APs that display paradoxical reductions in firing frequency during modest LBNP (13, 23). Overall, these data indicate that the small APs are regulated primarily by non-baroreflex processes and/or may be inhibited by baroreflex unloading.

The mechanisms underlying modifications in baroreflex control across the size-range of AP subpopulations remain unclear. Baroreflex slopes were calculated from spontaneous pressure fluctuations that were not large enough to estimate the complete baroreflex sigmoid for the various AP clusters this study. While the baroreflex sigmoid relationship (6, 27) remains to be derived for sympathetic discharge at the AP level, we speculate that for medium AP clusters, the baroreflex functions are shifted to higher levels of activity and greater DBPs, and that the operating points relocate to regions of greater gain during orthostatic stress. Based on the variability in baroreflex slope and operating point among medium clusters at BSL and LBNP, we hypothesize that of the medium-sized APs under

strong baroreflex control, the position of the operating point and/or morphology of the baroreflex sigmoid may depend on AP size. The alterations in baroreflex function from BSL to LBNP observed here may be linked to reductions in pulse pressure detected by arterial baroreceptors, or relocation of venous blood detected by cardiopulmonary baroreceptors and/or venous mechanoreceptors (3, 25). Also, descending neural signals related to the perception of effort accompanying the muscular contraction required to resist suction during LBNP may have shaped baroreflex behaviour in this study (26).

Historically, baroreflex control of MSNA has been quantified by relying on the integrated signal to examine the relationship between burst occurrence or burst size and DBP (14, 38). In the present study, we replicated findings from our laboratory and others indicating that under BSL conditions, the arterial baroreflex strongly governs burst occurrence and only weakly controls burst size (12, 14, 20, 31). Consistent with previous research (11, 12), we observed no change in the strength of baroreflex control over integrated burst probability or burst size from BSL to LBNP, but the operating points were shifted to higher levels of activity and greater DBP. The finding that LBNP did not impact the weak baroreflex regulation of burst size can be explained by the following: 1) Burst size is a function of the number and size of APs, with larger APs contributing mainly to larger bursts (35), and 2) LBNP did not impact the strength of baroreflex control over the number of unique clusters per beat or the occurrence of the largest APs. Why baroreflex control of integrated burst occurrence remained unchanged from BSL to LBNP despite enhanced baro-control of medium APs (which fire in most bursts) remains unclear. Only the upward and rightward shifts in medium AP operating points were mirrored in the integrated baroreflex threshold operating point. Perhaps the heterogeneous changes in

baroreflex control of differently AP subpopulations rendered the slope of the integrated baroreflex threshold relationship unchanged due to the averaging impact of the integration process.

4.4.1 Conclusion

The present study discovered that the baroreflex gain of the subpopulation of medium-sized sympathetic APs that were active under BSL conditions becomes enhanced and reset to higher levels of activity to facilitate elevated sympathetic discharge during LBNP. The large APs present under BSL conditions and the subpopulation of larger APs that were silent at BSL but recruited during LBNP were under weak, if any, baroreflex control. Clusters of small APs, which express weak baroreflex control under baseline conditions exhibit paradoxical reductions in gain during LBNP. Also, the baroreflex expressed minimal control over the number of unique AP clusters firing per beat under both conditions. Thus, baroreflex control represents only one input to sympathetic activation during orthostatic stress. Baroreflex control appears to form a modifiable mechanism — at least for a discrete subpopulation of medium-sized APs — enabling precise regulation of sympathetic outflow during orthostatic stress in healthy young individuals.

4.5 References

1. **Badrov MB, Olver TD, Shoemaker JK.** Central vs. peripheral determinants of sympathetic neural recruitment: insights from static handgrip exercise and postexercise circulatory occlusion. *Am J Physiol Integr Comp Physiol* 311: R1013–R1021, 2016.
2. **Badrov MB, Usselman CW, Shoemaker JK.** Sympathetic neural recruitment strategies: responses to severe chemoreflex and baroreflex stress [Online]. *Am J Physiol Integr Comp Physiol* 309: R160–R168, 2015.
3. **Cui J, McQuillan PM, Blaha C, Kunselman AR, Sinoway LI.** Limb venous distension evokes sympathetic activation via stimulation of the limb afferents in humans. *Am J Physiol Circ Physiol* 303: H457–H463, 2012.
4. **Dampney RA.** Functional organization of central pathways regulating the cardiovascular system. *Physiol Rev* 74: 323–364, 1994.
5. **Delius W, Hagbarth K, Hongell A, Wallin BG.** General characteristics of sympathetic activity in human muscle nerves [Online]. *Acta Physiol Scand* 84: 65–81, 1972.
6. **Fadel PJ, Ogoh S, Watenpaugh DE, Wasmund W, Olivencia-Yurvati A, Smith ML, Raven PB.** Carotid baroreflex regulation of sympathetic nerve activity during dynamic exercise in humans. *Am J Physiol Circ Physiol* 280: H1383–H1390, 2001.
7. **Fagius JAN, Wallin BG, Sundlof G, Christer N, Englesson S.** Sympathetic outflow in man after anaesthesia of the glossopharyngeal and vagus nerves. *Brain* 108: 423–438, 1985.
8. **Fisher JP, Young CN, Fadel PJ.** Autonomic adjustments to exercise in humans. *Compr Physiol* 5: 475–512, 2011.
9. **Hagbarth K-E, Vallbo ÅB.** Discharge characteristics of human muscle afferents during muscle stretch and contraction. *Exp Neurol* 22: 674–694, 1968.
10. **Hart EC, Joyner MJ, Wallin BG, Karlsson T, Curry TB, Charkoudian N.** Baroreflex control of muscle sympathetic nerve activity: a nonpharmacological measure of baroreflex sensitivity [Online]. *Am J Physiol Circ Physiol* 298: H816–H822, 2010.
11. **Ichinose M, Saito M, Fujii N, Kondo N, Nishiyasu T.** Modulation of the control of muscle sympathetic nerve activity during severe orthostatic stress. *J Physiol* 576: 947–958, 2006.
12. **Ichinose M, Saito M, Ogawa T, Hayashi K, Kondo N, Nishiyasu T.** Modulation of control of muscle sympathetic nerve activity during orthostatic stress in humans.

Am J Physiol Circ Physiol 287: H2147–H2153, 2004.

13. **Incognito A V, Doherty CJ, Nardone M, Lee JB, Notay K, Seed JD, Millar PJ.** Evidence for differential control of muscle sympathetic single units during mild sympathoexcitation in young healthy humans. *Am J Physiol Circ Physiol* 316: H13–H23, 2018.
14. **Kienbaum P, Karlsson T, Sverrisdottir YB, Elam M, Wallin BG.** Two sites for modulation of human sympathetic activity by arterial baroreceptors? *J Physiol* 531: 861–869, 2001.
15. **Klassen SA, De Abreu S, Greaves DK, Kimmerly DS, Arbeille P, Denise P, Hughson RL, Normand H, Shoemaker JK.** Long-duration bed rest modifies sympathetic neural recruitment strategies in males and females. *J Appl Physiol* 124: 769–779, 2017.
16. **Klassen SA, Limberg JK, Baker SE, Nicholson WT, Curry TB, Joyner MJ, Shoemaker JK.** The role of the paravertebral ganglia in human sympathetic neural discharge patterns. *J Physiol* 596: 4497–4510, 2018.
17. **Klassen SA, Moir ME, Limberg JK, Baker SE, Nicholson WT, Curry TB, Joyner MJ, Shoemaker JK.** Asynchronous action potential discharge in human muscle sympathetic nerve activity [Online]. *Am. J. Physiol. Circ. Physiol.* doi: 10.1152/ajpheart.00258.2019, 2019.
18. **Limberg JK, Ott EP, Holbein WW, Baker SE, Curry TB, Nicholson WT, Joyner MJ, Shoemaker JK.** Pharmacological Assessment of the Contribution of the Arterial Baroreflex to Sympathetic Discharge Patterns in Healthy Humans. *J. Neurophysiol* 119: 2166–2175, 2018.
19. **Malpas SC.** A new model for the generation of sympathetic nerve activity [Online]. *Clin Exp Pharmacol Physiol* 22: 11–16, 1995.
20. **Malpas SC, Bendle RD, Head GA, Ricketts JH.** Frequency and amplitude of sympathetic discharges by baroreflexes during hypoxia in conscious rabbits. *Am J Physiol Circ Physiol* 271: H2563–H2574, 1996.
21. **Malpas SC, Coote JH.** Role of vasopressin in sympathetic response to paraventricular nucleus stimulation in anesthetized rats. *Am J Physiol Integr Comp Physiol* 266: R228–R236, 1994.
22. **Malpas SC, Ninomiya I.** Effect of chemoreceptor stimulation on the periodicity of renal sympathetic nerve activity in anesthetized cats. *J Auton Nerv Syst* 37: 19–28, 1992.
23. **Millar PJ, Murai H, Morris BL, Floras JS.** Microneurographic evidence in healthy middle-aged humans for a sympathoexcitatory reflex activated by atrial pressure. *Am J Physiol Circ Physiol* 305: H931–H938, 2013.

24. **Ninomiya I, Malpas SC, Matsukawa K, Shindo T, Akiyama T.** The amplitude of synchronized cardiac sympathetic nerve activity reflects the number of activated pre-and postganglionic fibers in anesthetized cats. *J Auton Nerv Syst* 45: 139–147, 1993.
25. **Pawelczyk JA, Raven PB.** Reductions in central venous pressure improve carotid baroreflex responses in conscious men. *Am J Physiol Circ Physiol* 257: H1389–H1395, 1989.
26. **Raven PB, Young BE, Fadel PJ.** Arterial Baroreflex Resetting During Exercise in Humans: Underlying Signaling Mechanisms. *Exerc Sport Sci Rev* 47: 129–141, 2019.
27. **Rea RF, Eckberg DL.** Carotid baroreceptor-muscle sympathetic relation in humans. *Am J Physiol Integr Comp Physiol* 253: R929–R934, 1987.
28. **Salmanpour A, Brown LJ, Shoemaker JK.** Spike detection in human muscle sympathetic nerve activity using a matched wavelet approach [Online]. *J Neurosci Methods* 193: 343–355, 2010.
29. **Salmanpour A, Brown LJ, Steinback CD, Usselman CW, Goswami R, Shoemaker JK.** Relationship between size and latency of action potentials in human muscle sympathetic nerve activity [Online]. *J Neurophysiol* 105: 2830–2842, 2011.
30. **Salmanpour A, Frances MF, Goswami R, Shoemaker JK.** Sympathetic neural recruitment patterns during the Valsalva maneuver. In: *2011 Annual International Conference of the IEEE Engineering in Medicine and Biology Society*. IEEE, 2011, p. 6951–6954.
31. **Salmanpour A, Shoemaker JK.** Baroreflex mechanisms regulating the occurrence of neural spikes in human muscle sympathetic nerve activity [Online]. *J Neurophysiol* 107: 3409–3416, 2012.
32. **Shoemaker JK.** Recruitment strategies in efferent sympathetic nerve activity. *Clin Auton Res* 27: 369–378, 2017.
33. **Shoemaker JK, Badrov MB, Al-Khazraji BK, Jackson DN.** Neural Control of Vascular Function in Skeletal Muscle. *Compr Physiol* 6: 303–329, 2016.
34. **Shoemaker JK, Klassen SA, Badrov MB, Fadel PJ.** Fifty years of microneurography: learning the language of the peripheral sympathetic nervous system in humans. *J Neurophysiol* 119: 1731–1744, 2018.
35. **Steinback CD, Salmanpour A, Breskovic T, Dujic Z, Shoemaker JK.** Sympathetic neural activation: an ordered affair. *J Physiol* 588: 4825–4836, 2010.
36. **Strack AM, Sawyer WB, Hughes JH, Platt KB, Loewy AD.** A general pattern

- of CNS innervation of the sympathetic outflow demonstrated by transneuronal pseudorabies viral infections. *Brain Res* 491: 156–162, 1989.
37. **Sundlöf G, Wallin BG.** Effect of lower body negative pressure on human muscle nerve sympathetic activity. *J Physiol* 278: 525–532, 1978.
 38. **Sundlöf G, Wallin BG.** Human muscle nerve sympathetic activity at rest. Relationship to blood pressure and age. *J Physiol* 274: 621–637, 1978.
 39. **Usselman CW, Gimon TI, Nielson CA, Luchyshyn TA, Coverdale NS, Van Uum SHM, Shoemaker JK.** Menstrual cycle and sex effects on sympathetic responses to acute chemoreflex stress. *Am J Physiol Circ Physiol* 308: H664–H671, 2015.
 40. **VanLieshout JJ, Toska K, van Lieshout EJ, Eriksen M, Walløe L, Wesseling KH.** Beat-to-beat noninvasive stroke volume from arterial pressure and Doppler ultrasound. *Eur J Appl Physiol* 90: 131–137, 2003.
 41. **Wallin BG, Eckberg DL.** Sympathetic transients caused by abrupt alterations of carotid baroreceptor activity in humans. *Am J Physiol Circ Physiol* 242: H185–H190, 1982.

Chapter 5

5 General Discussion

The studies comprising the present dissertation provide new knowledge regarding the behaviour of, and mechanisms governing, low-threshold sympathetic APs: APs that are active during baseline conditions and some of which exhibit augmented firing during physiological stress. We illustrated that sympathetic c-fibre discharge results from the integration of arterial baroreflex and yet unknown non-baroreflex inputs within the central sympathetic circuitry, and contributions from the paravertebral ganglia, where interactions between nicotinic and non-nicotinic neurotransmission along with varying patterns of pre-to-postganglionic innervation exist. Consequently, low-threshold APs do not express uniform behaviour, but rather function as discrete subpopulations related to postganglionic AP size (reflecting different sized axons) that receive differential regulation and express varying firing properties, during baseline conditions and physiological stress. Consistently, the discharge probability among low-threshold APs relates to AP cluster size in a manner that resembles an inverted “U” distribution.

Collectively, the data generated by these studies indicate that the subpopulation of medium APs fires synchronously within most bursts of MSNA [Study One (10), Study Two (11), and Study Three] as a result of upstream neurons linked to this postganglionic subpopulation receiving strong baroreflex regulation (Study Three) and predominantly nicotinic mechanisms at the ganglia (Study One). During baroreflex stress imposed by mild to severe LBNP, the firing probability of medium APs becomes increased (i.e., rate-coding mechanism) as a result of an upward resetting in the baroreflex control and relocation of the operating point to a position of enhanced gain (Study Three). It should

be noted however, that even within the subpopulation of medium APs under baroreflex control some variability exists in baseline firing probabilities, baroreflex gain, and the responses to baroreflex stress, which we hypothesize stems from baroreflex sigmoid morphology and characteristics (e.g., operating point location) varying by AP size (21). Based on these observations we suspect that this subpopulation of APs aligns with those recorded using the single-unit technique, particularly the seminal investigations by Macefield and colleagues (15, 16). These studies observed most APs to fire once per burst during periods of baroreceptor unloading accompanying transient reductions in blood pressure under baseline conditions and express the capacity to increase firing probability during physiological stress (15, 16). Also, the consistent finding that integrated bursts are abolished by trimethaphan (1, 2, 5) aligns with the conclusion that medium APs contribute to most bursts and are primarily governed by nicotinic ganglionic neurotransmission.

Combined, the present findings suggest that the regulatory mechanisms governing the subpopulation of small sympathetic APs are fundamentally different than those regulating medium APs, both within the central circuitry and at the ganglia. This dissertation highlights that non-baroreflex mechanisms form the primary input to the upstream nerves linked to this subpopulation of smaller APs. For example, under baseline conditions, the small APs expressed low firing probabilities (Study One) and when we examined all APs rather than just those within integrated bursts, this subpopulation exhibited the greatest proportion of asynchronous discharge, indicating that their firing was not initiated in diastole or terminated in systole by baroreflex mechanisms (Study Two). Also, the clusters of the small APs did not respond to baroreflex stress imposed by Valsalva's

Manoeuvre performed during the trimethaphan infusion — where only this subpopulation persisted to fire (Study One) — or during varying levels of LBNP (Studies Two and Three). Also, small APs exhibited weak baroreflex slopes during baseline conditions, then demonstrated *paradoxical* reductions in baroreflex gain on going from baseline to LBNP (Study Three). Likewise, Limberg and colleagues (12) observed that the smallest APs fired with reduced probability (less often) during the hypotensive phase of a modified Oxford protocol performed in healthy participants. The collective evidence also suggests that non-nicotinic mechanisms at the paravertebral ganglia primarily initiate the depolarization of this subpopulation of small APs. Indeed, trimethaphan infusion under baseline conditions blocked medium and larger AP subpopulations thereby abolishing integrated bursts of MSNA, but the small APs persisted to fire in an asynchronous manner (Study One). Upon retrospective analysis of these data focusing on between-burst AP emissions (Study Two), we identified that small APs firing asynchronously also survived trimethaphan. Thus, small APs may arise from postganglionic nerves activated by muscarinic or non-cholinergic receptors, which have been found to contribute to ganglionic neurotransmission in lower animals (7–9). In addition to weak baroreflex control centrally, non-nicotinic ganglionic mechanisms may contribute to asynchronous firing of small APs (3, 4).

In contrast to the medium sized AP clusters, large APs are observed to fire infrequently during baseline conditions. The present studies highlight new information that this subpopulation of large APs active under baseline conditions represent a subpopulation of postganglionic axons regulated primarily by non-baroreflex inputs within the central sympathetic organization and nicotinic mechanisms at the ganglia. We infer minimal

baroreflex regulation of this subpopulation based on the finding that under baseline conditions large APs fired infrequently (Studies One, Two, and Three) and expressed weak baroreflex slopes (Study Three), then exhibited no change in discharge rate or baroreflex gain during baroreflex unloading with LBNP (Study Three). However, we speculate that the central non-baroreflex mechanisms governing larger low-threshold APs may differ from those regulating the smallest APs as these subpopulations express incongruent responses in baroreflex gain during LBNP (Study Three). Specifically, while the smallest APs expressed reductions in baroreflex gain, the large APs demonstrated no change in baroreflex control from baseline to LBNP (Study Three). Both previously active APs and the subpopulation of larger latent APs may be regulated by other peripheral reflexes other than the baroreflex. For example, studies in humans and animals illustrate that chemoreflex stress preferentially augments burst amplitude, reflecting higher probability of larger AP discharge (17, 23). The PVN hypothalamus and periaqueductal gray may also contribute to the regulation of larger APs as animal and human studies found that activation of these sites (chemical or electrical stimulation) to increase burst size (18, 24). At the ganglia, the finding that larger APs active under baseline conditions were de-recruited first by trimethaphan suggests that the postganglionic axons generating these APs are activated primarily by nicotinic receptors (Study One). However, we suspect that the patterns of pre-to-postganglionic innervation vary by sympathetic c-fibre size given the progressive AP blockade (with the exception of the smallest APs) by trimethaphan from largest to smallest (19, 20).

5.1 Perspectives

The present studies further our understanding of the sympathetic emissions directed towards the vasculature supplying skeletal muscle and the mechanisms affecting these neural patterns. However, this series of studies generated several key questions regarding the neural processes shaping sympathetic outflow. Specifically, the central networks (i.e., supra-spinal and spinal) shaping the behaviour of varying-sized low-threshold APs along with the recruitment of previously-silent larger APs remain unclear. Techniques involving simultaneous multi-fibre microneurography and functional magnetic resonance imaging or stimulation of implanted electrodes may yield new information in this area (13, 24). For example, by performing microneurography at the same time as functional imaging in healthy humans, Macefield and colleagues (13, 14) found baseline sympathetic burst amplitude to relate to the activation of a functional network of nuclei comprised by the insula, hypothalamus, periaqueductal gray, and RVLM. Consistent with this finding, stimulation of the dorsolateral periaqueductal gray via implanted deep brain electrodes produced larger sympathetic bursts compared to pre-stimulation conditions (24). Although inferences may be drawn regarding the impact of these regions on AP discharge and/or recruitment, microneurographic studies examining AP behaviour within these experimental paradigms remain to be conducted. Continued use of pharmacological agents will also reveal intricacies within the sympathetic organization (10, 25). For example, pharmacological blockade and activation of the widely centrally distributed GABA receptors (25) and α_2R (26), respectively, have demonstrated sympathoinhibitory effects, but the influence of the underlying AP patterns remain concealed by signal integration. Basic studies of this sort are paramount to identifying the

critical elements of the sympathetic system that contribute to aberrant and overactive discharge patterns which are hallmark of cardiovascular and neurological pathologies (6, 22).

5.2 Conclusion

The present studies nuanced the complexity of the sympathetic discharge patterns employed to communicate the appropriate circulatory adjustments for homeostatic maintenance and the mechanisms subserving these neural behaviours in healthy humans. Indeed, the arterial baroreflex does not exert strong control over all sympathetic AP subpopulations and extra-baroreflex processes, both centrally and peripherally, govern AP discharge. At the paravertebral ganglia, both nicotinic and non-nicotinic mechanisms, as well as varying degrees of pre-to-postganglionic innervation affect sympathetic AP discharge. The sympathetic neural architecture produces heterogeneous firing properties that vary by AP size, such that the distribution of within-burst firing probabilities resembles an inverted “U” shape under baseline conditions: medium APs fire in most bursts and the small and large APs discharge infrequently. However, as a result of weak baroreflex control and non-nicotinic ganglionic neurotransmission, not all AP discharge occurs synchronously within bursts, as ~30% of total APs fire asynchronously between bursts of activity at baseline, with the smallest APs expressing the greatest proportion of asynchronous activity. During baroreflex stress, the sympathetic system increases total MSNA by increasing the firing probabilities of previously-active low-threshold APs, and recruiting a subpopulation of larger latent APs. However, not all low-threshold APs participate in the rate-coding strategy for increasing total MSNA, as only the medium APs under strong baroreflex control at baseline are reset upwards with operating points

relocated to positions of enhanced gain to augment firing probability during baroreflex stress.

5.3 References

1. **Baker SE, Limberg JK, Dillon GA, Curry TB, Joyner MJ, Nicholson WT.** Aging Alters the Relative Contributions of the Sympathetic and Parasympathetic Nervous System to Blood Pressure Control in Women. *Hypertension* 72: 1236–1242, 2018.
2. **Barnes JN, Hart EC, Curry TB, Nicholson WT, Eisenach JH, Wallin BG, Charkoudian N, Joyner MJ.** Aging enhances autonomic support of blood pressure in women. *Hypertension* 63: 303–308, 2014.
3. **Brown AM.** Cardiac sympathetic adrenergic pathways in which synaptic transmission is blocked by atropine sulfate. *J Physiol* 191: 271–288, 1967.
4. **Brown AM.** Sympathetic ganglionic transmission and the cardiovascular changes of the defense reaction in the cat. *Circ Res* 24: 843–849, 1969.
5. **Delius W, Hagbarth K, Hongell A, Wallin BG.** General characteristics of sympathetic activity in human muscle nerves [Online]. *Acta Physiol Scand* 84: 65–81, 1972.
6. **Goldstein DS, Kopin IJ.** Homeostatic systems, biocybernetics, and autonomic neuroscience. *Auton Neurosci* 208: 15–28, 2017.
7. **Henderson CG, Ungar A.** Effect of cholinergic antagonists on sympathetic ganglionic transmission of vasomotor reflexes from the carotid baroreceptors and chemoreceptors of the dog. *J Physiol* 277: 379–385, 1978.
8. **Jan LY, Jan YN.** Peptidergic transmission in sympathetic ganglia of the frog. *J Physiol* 327: 219–246, 1982.
9. **Jänig W, Krauspe R, Wiedersatz G.** Reflex activation of postganglionic vasoconstrictor neurones supplying skeletal muscle by stimulation of arterial chemoreceptors via non-nicotinic synaptic mechanisms in sympathetic ganglia. *Pflügers Arch* 396: 95–100, 1983.
10. **Klassen SA, Limberg JK, Baker SE, Nicholson WT, Curry TB, Joyner MJ, Shoemaker JK.** The role of the paravertebral ganglia in human sympathetic neural discharge patterns. *J Physiol* 596: 4497–4510, 2018.
11. **Klassen SA, Moir ME, Limberg JK, Baker SE, Nicholson WT, Curry TB, Joyner MJ, Shoemaker JK.** Asynchronous action potential discharge in human muscle sympathetic nerve activity [Online]. *Am. J. Physiol. Circ. Physiol.* <https://doi.org/10.1152/ajpheart.00258.2019>.
12. **Limberg JK, Ott EP, Holbein WW, Baker SE, Curry TB, Nicholson WT, Joyner MJ, Shoemaker JK.** Pharmacological Assessment of the Contribution of the Arterial Baroreflex to Sympathetic Discharge Patterns in Healthy Humans. *J*


Neurophysiol. 119: 2166-2175, 2018.

13. **Macefield VG, Henderson LA.** “Real-time” imaging of cortical and subcortical sites of cardiovascular control: concurrent recordings of sympathetic nerve activity and fMRI in awake subjects. *J Neurophysiol* 116: 1199–1207, 2016.
14. **Macefield VG, Henderson LA.** Identification of the human sympathetic connectome involved in blood pressure regulation. *Neuroimage* 1116119, 2019.
15. **Macefield VG, Wallin BG.** Firing properties of single vasoconstrictor neurones in human subjects with high levels of muscle sympathetic activity. *J Physiol* 516: 293–301, 1999.
16. **Macefield VG, Wallin BG, Vallbo AB.** The discharge behaviour of single vasoconstrictor motoneurons in human muscle nerves. *J Physiol* 481: 799–809, 1994.
17. **Malpas SC, Bendle RD, Head GA, Ricketts JH.** Frequency and amplitude of sympathetic discharges by baroreflexes during hypoxia in conscious rabbits. *Am J Physiol Circ Physiol* 271: H2563–H2574, 1996.
18. **Malpas SC, Coote JH.** Role of vasopressin in sympathetic response to paraventricular nucleus stimulation in anesthetized rats. *Am J Physiol Integr Comp Physiol* 266: R228–R236, 1994.
19. **Purves D, Lichtman JW.** Geometrical differences among homologous neurons in mammals. *Science (80-)* 228: 298–302, 1985.
20. **Purves D, Rubin E, Snider WD, Lichtman J.** Relation of animal size to convergence, divergence, and neuronal number in peripheral sympathetic pathways. *J Neurosci* 6: 158–163, 1986.
21. **Rea RF, Eckberg DL.** Carotid baroreceptor-muscle sympathetic relation in humans. *Am J Physiol Integr Comp Physiol* 253: R929–R934, 1987.
22. **Shoemaker JK, Badrov MB, Al-Khazraji BK, Jackson DN.** Neural Control of Vascular Function in Skeletal Muscle. *Compr Physiol* 6: 303–329, 2016.
23. **Steinback CD, Salzer D, Medeiros PJ, Kowalchuk J, Shoemaker JK.** Hypercapnic vs. hypoxic control of cardiovascular, cardiovagal, and sympathetic function. *Am J Physiol Integr Comp Physiol* 296: R402–R410, 2009.
24. **Sverrisdóttir YB, Green AL, Aziz TZ, Bahuri NFA, Hyam J, Basnayake SD, Paterson DJ.** Differentiated baroreflex modulation of sympathetic nerve activity during deep brain stimulation in humans. *Hypertension* 63: 1000–1010, 2014.
25. **Teixeira AL, Fernandes IA, Vianna LC.** GABAA receptors modulate sympathetic vasomotor outflow and the pressor response to skeletal muscle

metaboreflex activation in humans. *J Physiol* 597: 4139–4150, 2019.

26. **Wilkins BW, Hesse C, Charkoudian N, Nicholson WT, Sviggum HP, Moyer TP, Joyner MJ, Eisenach JH.** Autonomic cardiovascular control during a novel pharmacologic alternative to ganglionic blockade. *Clin Pharmacol Ther* 83: 692–701, 2008.

Appendix: Ethics Approval



**Western
Research**

**Western University Health Science Research Ethics Board
HSREB Full Board Initial Approval Notice**

Research Ethics

Principal Investigator: Dr. Kevin Shoemaker
Department & Institution: Health Sciences/Kinesiology, Western University

Review Type: Full Board
HSREB File Number: 108026
Study Title: Exploring the Impact of Somatosensory Nerve Stimulation on Autonomic Regulation

HSREB Initial Approval Date: July 13, 2016
HSREB Expiry Date: July 13, 2017

Documents Approved and/or Received for Information:

Document Name	Comments	Version Date
Recruitment Items	Phone Script	2016/05/24
Recruitment Items	Handout	2016/05/24
Recruitment Items	Classroom Script	2016/05/24
Recruitment Items	Poster	2016/05/24
Other	NSERC Approval Form	2013/04/02
Data Collection Form/Case Report Form	MRI Screening (Received 27Apr16)	
Recruitment Items	Email	2016/05/24
Data Collection Form/Case Report Form	Health History	2016/05/24
Data Collection Form/Case Report Form	Participant Contact Info	2016/05/24
Data Collection Form/Case Report Form	Screening Form	2016/05/24
Data Collection Form/Case Report Form	MoCA	2016/05/24
Data Collection Form/Case Report Form	Trail Making Test	2016/05/24
Letter of Information & Consent		2016/05/24
Recruitment Items	Newspaper ad	2016/05/24
Western University Protocol	Received 5Jul16	

The Western University Health Science Research Ethics Board (HSREB) has reviewed and approved the above named study, as of the HSREB Initial Approval Date noted above.

HSREB approval for this study remains valid until the HSREB Expiry Date noted above, conditional to timely submission and acceptance of HSREB Continuing Ethics Review.

The Western University HSREB operates in compliance with the Tri-Council Policy Statement Ethical Conduct for Research Involving Humans (TCPS2), the International Conference on Harmonization of Technical Requirements for Registration of Pharmaceuticals for Human Use Guideline for Good Clinical Practice Practices (ICH E6 R1), the Ontario Personal Health Information Protection Act (PHIPA, 2004), Part 4 of the Natural Health Product Regulations, Health Canada Medical Device Regulations and Part C, Division 5, of the Food and Drug Regulations of Health Canada.

Members of the HSREB who are named as Investigators in research studies do not participate in discussions related to, nor vote on such studies when they are presented to the REB.

The HSREB is registered with the U.S. Department of Health & Human Services under the IRB registration number IRB 00000000

Ethics Officer, on behalf of Dr. Marcelo Kremenchutzky, HSREB Vice Chair

Ethics Officer: Erika Basile ___ Nicole Kaniki ___ Grace Kelly ___ Kaitlyn Harris ___ Vikki Trank ___ Karen Gopal ___

Western University, Research, Support Services Bldg., Rm. 5150
London, ON, Canada N6G 1G9 t. 519.661.3036 f. 519.850.2466 www.uwo.ca/research/ethics



Date: 20 November 2017

To: Kevin Shoemaker

Project ID: 108026

Study Title: Exploring the Impact of Somatosensory Nerve Stimulation on Autonomic Regulation (SSNS)

Application Type: HSREB Amendment Form

Review Type: Delegated

Meeting Date / Full Board Reporting Date: 05/Dec/2017

Date Approval Issued: 20/Nov/2017

REB Approval Expiry Date: 13/Jul/2018

Dear Kevin Shoemaker,

The Western University Health Sciences Research Ethics Board (HSREB) has reviewed and approved the WREM application form for the amendment, as of the date noted above.

Documents Approved:

Document Name	Document Type	Document Date	Document Version
HSREB_108026_SSNS_Screening_Form_19_09_2016_clean	Recruitment Materials	19/Sep/2017	2
REB_108026_SSNS_LOI_6_11_2017_clean	Consent Form	06/Nov/2017	3
REB_108026_SSNS_Newspaper_Advertisement_9_09_2017_clean	Recruitment Materials	19/Sep/2017	2
REB_108026_SSNS_Recruitment_Classroom_Script_6_11_2017_clean	Recruitment Materials	06/Nov/2017	3
REB_108026_SSNS_Recruitment_Email_6_11_2017_clean	Recruitment Materials	06/Nov/2017	3
REB_108026_SSNS_Recruitment_Handout_9_09_2017_clean	Recruitment Materials	19/Sep/2017	2
REB_108026_SSNS_Recruitment_Phone_Script_9_09_2017_clean	Recruitment Materials	19/Sep/2017	2
REB_108026_SSNS_Recruitment_Poster_9_09_2017_clean	Recruitment Materials	19/Sep/2017	2
REB_108026_Western_Protocol_Edited_6_11_2017_clean	Protocol	06/Nov/2017	3

REB members involved in the research project do not participate in the review, discussion or decision.

The Western University HSREB operates in compliance with, and is constituted in accordance with, the requirements of the TriCouncil Policy Statement: Ethical Conduct for Research Involving Humans (TCPS 2); the International Conference on Harmonisation Good Clinical Practice Consolidated Guideline (ICH GCP); Part C, Division 5 of the Food and Drug Regulations; Part 4 of the Natural Health Products Regulations; Part 3 of the Medical Devices Regulations and the provisions of the Ontario Personal Health Information Protection Act (PHIPA 2004) and its applicable regulations. The HSREB is registered with the U.S. Department of Health & Human Services under the IRB registration number IRB 00000940.

Please do not hesitate to contact us if you have any questions.

Sincerely,

Patricia Sargeant, Ethics Officer on behalf of Dr. Marcelo Kremenchutzky, HSREB Vice-Chair



Date: 27 September 2018

To: Kevin Shoemaker

Project ID: 108026

Study Title: Exploring the Impact of Somatosensory Nerve Stimulation on Autonomic Regulation

Application Type: HSREB Amendment Form

Review Type: Delegated

Meeting Date / Full Board Reporting Date: 16/Oct/2018

Date Approval Issued: 27/Sep/2018

REB Approval Expiry Date: 13/Jul/2019

Dear Kevin Shoemaker,

The Western University Health Sciences Research Ethics Board (HSREB) has reviewed and approved the WREM application form for the amendment, as of the date noted above.

Documents Approved:

Document Name	Document Type	Document Date
1_REB_108026_SSNS_LOI_27_09_2018_CLEAN	Letter of Information/Consent	27/Sep/2018
REB_108026_Westem_Protocol_Edited_27_09_2018_CLEAN	Protocol	27/Sep/2018

REB members involved in the research project do not participate in the review, discussion or decision.

The Western University HSREB operates in compliance with, and is constituted in accordance with, the requirements of the TriCouncil Policy Statement: Ethical Conduct for Research Involving Humans (TCPS 2); the International Conference on Harmonisation Good Clinical Practice Consolidated Guideline (ICH GCP); Part C, Division 5 of the Food and Drug Regulations; Part 4 of the Natural Health Products Regulations; Part 3 of the Medical Devices Regulations and the provisions of the Ontario Personal Health Information Protection Act (PHIPA 2004) and its applicable regulations. The HSREB is registered with the U.S. Department of Health & Human Services under the IRB registration number IRB 00000940.

Please do not hesitate to contact us if you have any questions.

Sincerely,

Patricia Sargeant, Ethics Officer (ex) on behalf of Dr. Joseph Gilbert, HSREB Chair

Note: This correspondence includes an electronic signature (validation and approval via an online system that is compliant with all regulations).

From: IRBe
Sent: Monday, April 19, 2010 2:53 PM
To: Roberts, Shelly K., R.N.
Subject: IRB Application has been Approved

Principal Investigator Notification:

From: Mayo Clinic IRB
To: Michael Joyner
CC: Pamela Engrav
 Emma Hart
 Shirley Kingsley-berg
 Jean Knutson
 Karen Krucker
 Nancy Meyer
 Shelly Roberts
Re: IRB Application # [09-008584](#)

Study Title: Autonomic support of blood pressure in postmenopausal women

Please note that all correspondence (modifications, continuing reviews, reportable events) related to this application must be submitted electronically in the IRBe system.

The following is an excerpt from the minutes of the Mayo Clinic Institutional Review Boards (IRB-C) meeting dated 4/16/2010:

DECISION: The Committee reviewed and approved the above referenced application and noted that all requirements for approval of research (21CFR56.111 and 45CFR46.111) were met. This approval is valid for one year unless during that time the IRB determines that it is appropriate to halt or suspend the study earlier. IRB approval will expire on April 15, 2011. The Committee approved the accrual of 30 female adult subjects from a screening population of 40. The Committee approved the following sites to conduct this study: Mayo Clinic Rochester.

REVIEW: The Committee noted receipt of the protocol dated December 29, 2009. The Committee noted that the Data Safety Monitoring Plan was appropriate for the study. Funding for the study is provided by NIH. The Committee noted the IND# 70,082 for the study drug, Trimetaphan camsylate, dated July 16, 2004. Based on the investigator's justification, the Committee determined that the proposed study meets the requirements for exemption from IND regulations as outlined at 21 CFR 312.2(b). The Committee approved remuneration up to \$200.00.

CONSENT: The Committee approved the consent form (00) as written. The final approved consent form will be provided under the Documents tab of the main study workspace in IRBe.

REMINDERS: The Committee:

- Reminds the investigator to contact the CTSA Service Center at (77)5-7101 for communications review and approval prior to posting all advertisements for use in this study.
- Reminds the investigator that, per HIPAA regulations, protected health information collected during the screening of prospective subjects who do not subsequently sign the consent form and/or HIPAA authorization form must be discarded or de-identified.
- Reminds the investigator to submit a continuing review report prior to the expiration date (reminder will be sent prior to expiration).

Charlton, Michael R. M.D., Chair
 Tamyra Dull, Correspondent
 Mayo Clinic Institutional Review Boards

IRB-C

Appendix: Manuscript Permissions

JOHN WILEY AND SONS LICENSE TERMS AND CONDITIONS

Aug 28, 2019

This Agreement between Mr. Stephen Klassen ("You") and John Wiley and Sons ("John Wiley and Sons") consists of your license details and the terms and conditions provided by John Wiley and Sons and Copyright Clearance Center.

License Number	4657830695930
License date	Aug 28, 2019
Licensed Content Publisher	John Wiley and Sons
Licensed Content Publication	Journal of Physiology
Licensed Content Title	The role of the paravertebral ganglia in human sympathetic neural discharge patterns
Licensed Content Author	J. Kevin Shoemaker, Michael J. Joyner, Timothy B. Curry, et al
Licensed Content Date	Aug 19, 2018
Licensed Content Volume	596
Licensed Content Issue	18
Licensed Content Pages	14
Type of use	Dissertation/Thesis
Requestor type	Author of this Wiley article
Format	Electronic
Portion	Full article
Will you be translating?	No
Title of your thesis / dissertation	Action potential subpopulations in human muscle sympathetic nerve activity: discharge properties and governing mechanisms
Expected completion date	Sep 2019
Expected size (number of pages)	170
Requestor Location	Mr. Stephen Klassen
	<div style="border: 1px solid black; height: 40px; width: 100%;"></div>
	Canada
	Attn: Mr. Stephen Klassen
Publisher Tax ID	EU826007151
Total	0.00 CAD
Terms and Conditions	

Reuse by Authors of Their Work Published by APS

The APS Journals are copyrighted for the protection of authors and the Society. The Mandatory Submission Form serves as the Society's official copyright transfer form. Author's rights to reuse their APS-published work are described below:

Republishing in New Works	Authors may republish parts of their final-published work (e.g., figures, tables), without charge and without requesting permission, provided that full citation of the source is given in the new work.
Meeting Presentations and Conferences	Authors may use their work (in whole or in part) for presentations (e.g., at meetings and conferences). These presentations may be reproduced on any type of media in materials arising from the meeting or conference such as the proceedings of a meeting or conference. A copyright fee will apply if there is a charge to the user or if the materials arising are directly or indirectly commercially supported ¹ . Full citation is required.
Theses and Dissertations	Authors may reproduce whole published articles in dissertations and post to thesis repositories without charge and without requesting permission. Full citation is required.
Open Courseware	Authors may post articles, chapters or parts thereof to a public access courseware website. Permission must be requested from the APS ¹ . A copyright fee will apply to a book chapter and during the first 12 months of a journal article's publication. Full citation is required.
Websites	Authors may not post a PDF of the accepted or final version of their published work to any website including social and research networking platforms; instead, links may be posted to the APS or publisher partner website where the work is published ¹ (see exception to authors' own institution's repository, as note below).
Institutional Repositories (non-theses)	Authors may deposit their accepted, peer-reviewed journal manuscripts into an institutional repository providing: <ul style="list-style-type: none"> ◦ the APS retains copyright to the article¹ ◦ a 12-month embargo period from the date of final publication of the article is observed by the institutional repository and the author ◦ a link to the article published on the APS or publisher-partner website is prominently displayed alongside the article in the institutional repository ◦ the article is not used for commercial purposes ◦ self-archived articles posted to repositories are without warranty of any kind
	¹ Unless it is published under the APS Open Access (<i>AuthorChoice</i>) option, which allows for immediate public access under a Creative Commons license (CC BY 4.0) (See also the APS Policy on Depositing Articles in PMC.)

Curriculum Vitae

Stephen A. Klassen

School of Kinesiology, Western University
London, ON, Canada

Education

Doctor of Philosophy (Integrative Biosciences in Kinesiology). Western University. 2015-2019 (expected).

Advisor: Dr. J. Kevin Shoemaker

Master of Science (Applied Health Sciences). Brock University. 2013-2015.

Advisor: Dr. D.D. O'Leary

Bachelor of Science (Honours) in Medical Sciences. Brock University. 2009-2013.

Articles published or accepted in peer-reviewed journals

1. **Klassen, S.A.**, Moir, M.E., Limberg, J.K., Baker, S.E., Nicholson W.T., Curry T.B., Joyner, M.J., Shoemaker, J.K. (2019). Asynchronous action potential discharge in human muscle sympathetic nerve activity. *Am J Physiol Heart Circ Physiol*. doi: 10.1152/ajpheart.00258.2019. Accepted August 2, 2019.
2. Moir, M.E., **Klassen, S.A.**, Al-Khazraji, B., Woerhle, E., Smith, S., Matuszewski, B., Kozić D., Đujić, Ž., Barak O., Shoemaker, J.K. (2019). Impaired dynamic cerebral autoregulation in trained breath-hold divers. *J Appl Physiol*. 126(6), 1694-1700.
3. Balestrini, C.S., Moir, M.E., Abbott K.C., **Klassen S.A.**, Fischer L.K., Fraser D.D., Shoemaker J.K. Autonomic Dysregulation in Adolescent Concussion Is Sex-and-Posture-Dependent. Clinical journal of sport medicine. *Clin J Sport Med*. Doi: 10.1097/JSM.0000000000000734. Accepted March 15, 2019.
4. **Klassen, S.A.**, Limberg, J.K., Baker, S.E., Nicholson W.T., Curry T.B., Joyner, M.J., Shoemaker, J.K. (2018). The role of the paravertebral ganglia in human sympathetic neural discharge patterns. *J. Physiol*, 596.18.
5. **Klassen, S.A.**, Dempster, K.S., Chirico, D., O'Leary, D.D. (2018). Validity and reliability of carotid-toe pulse wave velocity as a measure of arterial stiffness in healthy individuals: comparison to carotid-femoral pulse wave velocity. *Artery Research*, 23.

6. Zamir, M., Moir, M.E., **Klassen S.A.**, Balestrini, C.S., Shoemaker, J.K. (2018). Cerebrovascular compliance within the confines of the skull. *Frontiers in Physiology*, 9, 940.
7. Moir, M.E., Balestrini, C.S., Abbott, K.C., **Klassen, S.A.**, Fischer, L.K., Fraser D.D., Shoemaker, J.K. (2018). Impaired dynamic cerebral autoregulation in adolescent concussion. *Med Sci Sports Exerc*, 50.11.
8. Shoemaker, J. K., **Klassen, S. A.**, Badrov, M. B., & Fadel, P. J. (2018). Fifty years of microneurography: learning the language of the peripheral sympathetic nervous system in humans. *Journal of neurophysiology*, 119(5), 1731-1744.
9. **Klassen, S.A.**, De Abreu, S., Greaves, D.K., Kimmerly D.K., Arbeille, P., Denise, P., Hughson, R.L., Normand, H., Shoemaker, J.K. (2018). Long-duration bed rest modifies sympathetic neural recruitment strategies in males and females. *J Appl Physiol*. 124:796-779.
10. **Klassen, S.A.**, Chirico, D., Dempster, K.S., Shoemaker, J.K., O’Leary, D.D. (2016). The role of aortic arch vascular mechanics in cardiovagal baroreflex sensitivity. *Amer J of Physiol – Regul Integr Comp Physiol*. 311(1), R24-R32.
11. **Klassen, S.A.**, Chirico, D., O’Leary, D.D., Cairney, J., Wade, T.J. (2016). Linking systemic arterial stiffness among adolescents to adverse childhood experiences. *Child abuse & neglect*. 56:1-10.

Conference Abstracts

1. **Klassen, S.A.**, Moir, M.E., Shoemaker, J.K. (2019). Baroreflex control of sympathetic action potential discharge during orthostatic stress. *ISAN*. 19.081.
2. **Klassen, S.A.**, Moir, M.E., Shoemaker, J.K. (2019). Asynchronous Action Potential Discharge in Human Muscle Sympathetic Nerve Activity. *FASEB*. 562.5.
3. Moir, M.E., Woerhle, E., Smith, S.O., **Klassen, S.A.**, Matuszewski, B., Barak, O.F., Dujic, Z., Kozic, D., Shoemaker, J.K. (2018). Cerebrovascular Regulation in Breath-hold Divers Exposed to Long-duration Apneas. *FASEB*. 855.1.
4. Wainman, L.I., Dempster, K.S., Cameron A.J., **Klassen S.A.**, Chirico D., Josse A.R., O’Leary D.D. (2018). High intensity interval training improves central arterial stiffness. *CSEP*. 43.103.
5. **Klassen, S.A.**,* Limberg, J.K, Baker, S.E., Nicholson, W.T., Curry, T.B., Joyner, M.J. Shoemaker, J.K. (2018). The role of the paravertebral ganglia in sympathetic vasoconstrictor neural discharge patterns. *FASEB*. 32.1.

6. Smith, S.O.,* Woerhle, E., **Klassen, S.A.**, Jacobs, K.G., Knetsch, R.J., Shoemaker, J.K. (2018). Effects of Contralateral Forearm Somatosensory Stimulation on Heart Rate Responses to Isometric Hand Grip Exercise. *FASEB*.32.1.
7. Jacobs, K.G.,* **Klassen, S.A.**, Woerhle, E., Smith, S.O., Knetsch, R.J., Barker, A., Shoemaker, J.K. (2018). Sex Differences in Heart Rate Response to Isometric Handgrip Exercise with Concurrent Contralateral Forearm Somatosensory Stimulation. *FASEB*. 32.1.
8. Moir, M.E.,* Zamir, M., **Klassen S.A.**, Balestrini, C.S., Shoemaker, J.K., (2018). Cerebrovascular compliance is affected by posture. *FASEB*. 32.1.
9. Knetsch, R.J.,* **Klassen, S.A.**, Shoemaker, J.K. (2018). Cardiodynamic associations with mental health and resilience in undergraduate students. *FASEB*. 32.1.
10. Jacobs, K.G.,* Woerhle, E., **Klassen, S.A.**, Deck, S., Kouali, D., Humphreys, D., Hall, C., Shoemaker, J.K. (2017). Heart rate variability analysis and mental health outcomes in university female hockey players. *Journal of Exercise, Movement, and Sport*. 49(1), 93.
11. Balestrini, C.S.,* Moir, M.E., Abbott, K.C., **Klassen, S.A.**, Johnson, M., Fischer, L.K., Fraser D.D., Shoemaker, J.K. (2017). Sex-dependent cardiovagal dysregulation in adolescent concussion. *Clin J Sport Med*. 27(3), e42.
12. **Klassen, S.A.**,* De Abreu, S., Denise, P., Shoemaker, J.K., Normand, H. (2016). Sixty Days Head-Down Bed Rest Augments Sympathetic Responses to Apnea. *FASEB*. 31.1.
13. Wade T.J., O’Leary D.D., Cairney J., Pretty C., **Klassen S.A.** (2016). Adverse Childhood Experiences and Cardiovascular Health among Children. *Academy on Violence & Abuse*.
14. **Klassen, S.A.**,* De Abreu, S., Denise, P., Shoemaker, J.K., Normand, H. (2016). Head-down tilt bed rest increases sympathetic burst latency. *Clin Autonomic Research*. 26(5).
15. Dempster, K.S.,* **Klassen, S.A.**, Chirico, D., and O’Leary, D.D. (2015). Carotid-toe pulse wave velocity as an index of central arterial stiffness: Comparison to carotid-femoral pulse wave velocity. *APNM*. 40:s18.
16. **Klassen, S.A.**,* Chirico, D., Dempster, K.S., Shoemaker, J.K., and O’Leary, D.D. (2015). Aortic arch distensibility may contribute to sex differences in cardiovagal baroreflex sensitivity, *APNM*. 40:s33.

17. **Klassen, S.A.,*** Chirico, D., Hood, C.D, Wade T.J., Cairney J., and O’Leary D.D. (2014). Cardiovascular baroreflex sensitivity is improved in children with high blood pressure after a psychosocial intervention. *FASEB*. 28.1.

Non-peer-reviewed contributions

1. Shoemaker J.K., **Klassen, S.A.** (2016). Simulated Microgravity and the Autonomic Nervous System. Oral Presentation. *Computing in Cardiology*. Vancouver, BC, Canada.
2. **Klassen, S.A.**, Chirico, D., Dempster, K.S., Shoemaker, J.K., O’Leary, D.D. (2015). Exploring the contribution of aortic arch and carotid sinus mechanics to cardiovascular baroreflex sensitivity. Oral Presentation. *Saltin International Graduate Conference*. Toronto, ON, Canada.
3. **Klassen, S.A.**, Shoemaker, J.K., O’Leary, D.D. (2015). The role of aortic arch mechanics in cardiovascular baroreflex sensitivity. Oral Presentation. *Michigan Physiological Society Conference*. Detroit, MI, U.S.A..
4. **Klassen, S.A.**, O’Leary, D.D., (2013). Sex differences in arterial mechanics and cardiovascular baroreflex sensitivity. Oral Presentation. *Mapping the New Knowledge Conference*. Niagara, ON, Canada.

Teaching

1. “Baroreflex control of blood pressure”. Physiology of Exercise. Western University. Dr. B. Al-Khazraji. October 5, 2017 and October 23/25, 2018.
2. “Infectious Agents and Chronic Diseases”. Global Issues in Infectious Disease. Brock University. Dr. A. Sanchez October 21, 2014.
3. “Autonomic Pharmacology”. Introduction to pharmacology. Dr. H. Wang. Brock University. October 22, 2013.

Mentorship

1. Emme Lee. Project: Baroreflex control of heart rate during orthostatic stress. Third year university undergraduate-scholars elective student. Western University. September 2018 to April 2019.
2. Hannah Bristow. Project: Central versus peripheral measures of pulse-wave velocity in humans. Secondary School Student. Governor Simcoe Secondary School. September 2014 to January 2015.

Trainee Scholarships/Fellowships

1. Natural Sciences and Engineering Research Council (NSERC) Post-Doctoral Fellowship. \$90,000. Mayo Clinic. December 2019 – December 2021.

2. Natural Sciences and Engineering Research Council (NSERC) Post-graduate Doctoral Scholarship (PGS D). \$42,000. Western University. September 2017-August 2019.
3. Ontario Graduate Scholarship (OGS) Doctoral Award. \$15,000. Western University. September 2017-August 2018. Declined.
4. Ontario Graduate Scholarship (OGS) Doctoral Award. \$15,000. Western University. September 2016-August 2017.
5. Ontario Graduate Scholarship (OGS) Doctoral Award. \$15,000. Western University. September 2015-August 2016.
6. Ontario Graduate Scholarship (OGS) Masters Award. \$15,000. Brock University. September 2014-August 2015.

Honours and Awards

1. School of Kinesiology Graduate Travel Award. \$417. Western University. August 2019.
2. International Society for Autonomic Neuroscience Geoffrey Burnstock Poster Presentation Award. \$ 500 Euros. July 2019.
3. Graduate Student Teaching Assistant Award Nomination. Western University. June 2019.
4. Canadian Institutes of Health Research in partnership with the Institute of Community Support and the Institute for Circulatory and Respiratory Health Travel Award. \$1,000. April 2019
5. American Physiological Society International Early Career Physiologist Travel Award. \$1,000 USD. April 2019.
6. American Physiological Society Neural Control and Autonomic Regulation Section Experimental Biology Trainee Award. \$500 USD. April 2019.
7. School of Kinesiology Graduate Travel Award. \$500. Western University. June 2018.
8. Faculty of Health Sciences (FHS) Graduate Travel Award. \$250. Western University. April 2018.
9. Canadian Institutes of Health Research in partnership with the Institute of Community Support and the Institute for Circulatory and Respiratory Health Travel Award. \$1,000. April 2018.

10. Caroline Tum Suden Professional Opportunity Award. American Physiological Society. \$585 USD. January 2018.
11. School of Kinesiology Graduate Travel Award. \$500. Western University. April 2017.
12. Faculty of Health Sciences (FHS) Graduate Travel Award. \$250. Western University. November 2016.
13. Faculty of Health Sciences (FHS) Tri-council Scholarship Application Review Award. \$1,000. Western University. November 2016.
14. Dean of Graduate Studies Award. \$2,500. Brock University. September 2014-August 2015.
15. Dean of Graduate Studies Award. \$2,000. Brock University. September 2013-August 2014.
16. First Class Standing in Applied Health Sciences. Brock University. June 2013.
17. Dean's Honour List in Applied Health Sciences. Brock University. September 2009-April 2013.
18. Brock University Entrance Scholarship (93+% average). \$14,000. Brock University. September 2009-April 2013.

Service: Community and Committee Involvement

1. Science Outreach Workshop (classroom and laboratory demonstrations) for Grade 7/8 class from Sacred Heart Catholic School. "How the cardiovascular system serves our lives". May 13, 2019.
2. Editorial Activity: American Journal of Physiology – Heart and Circulatory Physiology. Manuscripts reviewed: 1. 2019-present.
3. Abstract Committee Member for the 2017 Western Exercise is Medicine Conference. Exercise is Medicine National Conference at Western University. April-June 2017.
4. Editor of the Brock Health Magazine Issues 10 and 11. Brock University. September 2014-August 2015.
5. "Scientifically Yours" Project Leader-Health and Human Performance Workshop. Brock University. May 2015.

6. Inaugural Elected Executive Member of the Brock University Chapter of the Canadian Coalition for Global Health Research. Brock University. May 2014-August 2015.
7. Congress of the Humanities and Social Sciences Conference. Support Staff. Brock University. 2014.
8. Head Coach for the Bantam Boys St. Catharines Cobras Baseball Team. St. Catharines. 2014.
9. Volunteer exercise-rehabilitation supervisor for the Brock-Niagara Centre for Health and Well-Being. Brock University. 2013-2015.